

ACTA GEO TECHNICA S LOVENICA

2013/2

g. dolinar & s. škrabl
ATTERBERG LIMITS IN RELATION TO OTHER
PROPERTIES OF FINE-GRAINED SOILS

v. jagodnik et al.
ON THE APPLICATION OF A MIXED FINITE-ELEMENT APPROACH TO
BEAM-SOIL INTERACTION

o. sivrikaya et al.
PREDICTION OF THE COMPACTION PARAMETERS FOR COARSE-GRAINED
SOILS WITH FINES CONTENT BY MLR AND GEP

g. ebrahimian & a. nazari
EVOLUTIONARY-BASED PREDICTION OF ϵ_{50} FOR THE LATERAL
LOAD-DISPLACEMENT BEHAVIOR OF PILES IN CLAYS

s. kadali et al.
INVESTIGATIONS TO ESTABLISH THE INFLUENCE OF THE THERMAL
ENERGY FIELD ON SOIL PROPERTIES

ustanovitelji
founders

Univerza v Mariboru, Fakulteta za gradbeništvo
University of Maribor, Faculty of Civil Engineering

Univerza v Ljubljani, Fakulteta za gradbeništvo in geodezijo
University of Ljubljana, Faculty of Civil and Geodetic Engineering

Univerza v Ljubljani, Naravoslovnotehniška fakulteta
University of Ljubljana, Faculty of Natural Sciences and Engineering

Slovensko geotehniško društvo
Slovenian Geotechnical Society

Društvo za podzemne in geotehniške konstrukcije
Society for Underground and Geotechnical Constructions

izdajatelj
publisher

Univerza v Mariboru, Fakulteta za gradbeništvo
University of Maribor, Faculty of Civil Engineering

odgovorni urednik
editor-in-chief

Ludvik Trauner University of Maribor

uredniki
co-editors

Bojana Dolinar	University of Maribor
Borut Macuh	University of Maribor
Stanislav Škrabl	University of Maribor
Helena Vrecl Kojc	University of Maribor
Damijana Zlatolas	University of Maribor
Bojan Žlender	University of Maribor

posvetovalni uredniki
advisory editors

Darinka Battelino	University of Trieste
Heinz Brandl	Vienna University of Technology
Chandrakant. S. Desai	University of Arizona
Pedro Seco e Pinto	National Laboratory of Civil Engineering

lektor
proof-reader

Paul McGuinness

naklada
circulation

300 izvodov - issues

cena
price

25 EUR/izvod - 25 EUR/issue; (50 EUR for institutions/za institucije)

tisk
print

ROLGRAF tiskarna Medvode d.o.o.

Revija redno izhaja dvakrat letno. Članki v reviji so recenzirani s strani priznanih mednarodnih strokovnjakov. Baze podatkov v katerih je revija indeksirana: SCIE - Science Citation Index Expanded, JCR - Journal Citation Reports / Science Edition, ICONDA - The international Construction database, GeoRef. Izid publikacije je finančno podprla Javna agencija za knjigo Republike Slovenije iz naslova razpisa za sofinanciranje domačih periodičnih publikacij.

uredniški odbor
editorial board

Amin Barari	Aalborg University
Theodoros Hatzigogos	Aristotle University of Thessaloniki
Vojkan Jovičić	IRGO - Ljubljana, President of the SloGeD
Rolf Katzenbach	Technical University Darmstadt
Nasser Khalili	The University of New South Wales, Sydney
Jakob Likar	University of Ljubljana
Janko Logar	University of Ljubljana
Bojan Majes	University of Ljubljana
Milan Maksimović	University of Belgrade
Borut Petkovšek	Slovenian National Building and Civil Engineering Institute
Mihael Ribičič	University of Ljubljana
César Sagaseta	University of Cantabria
Patrick Selvadurai	McGill University
Stephan Semprich	University of Technology Graz
Devendra Narain Singh	Indian Institute of Technology, Bombay
Abdul-Hamid Soubra	University of Nantes
Kiirchi Suzuki	Saitama University
Antun Szavits-Nossan	University of Zagreb
Ivan Vaniček	Czech Technical University in Prague
Jianhua Yin	The Hong Kong Polytechnic University

naslov uredništva
address

ACTA GEOTECHNICA SLOVENICA
Univerza v Mariboru, Fakulteta za gradbeništvo
Smetanova ulica 17, 2000 Maribor, Slovenija
Telefon / Telephone: +386 (0)2 22 94 300
Faks / Fax: +386 (0)2 25 24 179
E-pošta / E-mail: ags@uni-mb.si

spletni naslov
web address

<http://www.fg.uni-mb.si/journal-ags/>

The journal is published twice a year. Papers are peer reviewed by renowned international experts. Indexation data bases of the journal: SCIE - Science Citation Index Expanded, JCR - Journal Citation Reports / Science Edition, ICONDA - The international Construction database, GeoRef. The publication was financially supported by Slovenian Book Agency according to the Tender for co-financing of domestic periodicals.

VSEBINA

2	Ludvik Trauner UVODNIK
4	Ivan Vaníček POMEMBNOST NATEZNE TRDNOSTI V GEOTEHNIČNEM INŽENIRSTVU
19	Mojtaba Movahedifari & J. Bolouri Bazaz OCENA PASIVNEGA PRITISKA NA KRAJNO PODPORO INTEGRALNEGA MOSTU OB UPOŠTEVANJU VPLIVA USLOČENJA
33	Ender Basari & Gurkan Ozden SPREMEMBA VOLUMNA SLJUDASTIH PEŠČENIH TAL IZ STARE DELTE REKE GEDIZ PO LIKVIFAKCIJI
42	Nihat Kaya & Murat Ornek EKSPERIMENTALNE IN NUMERIČNE ŠTUDIJE T-OBLIKOVANIH TEMELJEV
60	Primož Jelušič & Bojan Žlender UPORABA ANFIS-A PRI STABILNOSTNIH ANALIZAH STEN Z ŽEBLJANO ZEMLJINO
74	NAVODILA AVTORJEM

CONTENTS

Ludvik Trauner EDITORIAL	3
Ivan Vaníček THE IMPORTANCE OF TENSILE STRENGTH IN GEOTECHNICAL ENGINEERING	5
Mojtaba Movahedifari & J. Bolouri Bazaz AN ESTIMATION OF THE PASSIVE PRESSURE AGAINST INTEGRAL BRIDGE ABUTMENTS CONSIDERING ARCHING EFFECTS	20
Ender Basari & Gurkan Ozden POST-LIQUEFACTION VOLUME CHANGE IN MICA- CEOUS SANDY SOILS OF OLD GEDIZ RIVER DELTA	34
Nihat Kaya & Murat Ornek EXPERIMENTAL AND NUMERICAL STUDIES OF T-SHAPED FOOTINGS	43
Primož Jelušič & Bojan Žlender SOIL-NAIL WALL STABILITY ANALYSIS USING ANFIS	61
INSTRUCTIONS FOR AUTHORS	75

UVODNIK

Letos bomo izdali dve številki revije AGS z oznako Vol.10 (2013/1 in 2013/2), kar pomeni 10. jubilejno leto rednega izhajanja te revije pod pokroviteljstvom uglednega mednarodnega uredniškega odbora. Članom uredniškega odbora in vsem mednarodnim recenzentom se zahvaljujem za odlično opravljeno dosedanje delo. Posebej bi se rad zahvalil uredniku: prof. dr. Jozsefu Farkasu (Budimpešta) in prof. dr. Zlatku Langofu (Sarajevo) za plemenito desetletno sodelovanje. Njihovo pomembno strokovno delo bosta nadaljevala nova uredniška člana prof. dr. Amin Barrari (Aalborg University, Denmark) in prof. dr. Vojko Jovičič (IRGO - Inštitut za rudarstvo, geotehnologijo in okolje, predsednik Slovenskega geotehniškega društva SloGeD), ki jima kličem dobrodošlico.

V tej številki objavljamo pregledni članek in štiri znanstvene prispevke:

prof. dr. Ivan Vaniček s češke tehniške univerze v Pragi in podpredsednik ISSMGE za Evropo podaja zanimiv pregledni članek z naslovom »Pomembnost natezne trdnosti v geotehničnem inženirstvu«, ki povzema njegovo bogato znanje in izjemne prispevke v bazičnih in aplikativnih raziskavah na področju natezne in upogibne trdnosti v zemljinah. Na temo tega prispeka je dr. Vaniček imel vabljen predavanje na 13. Šukljegovih dnevih (Lipica, 15. Junij 2012), kjer je za sodelovanje in odlično predstavitev prejel najvišje priznanje Slovenskega geotehniškega društva.

V drugem članku avtorja, Ender Basari in Gurkan Ozden, pojasnjujeta posedanje sljudastega peska po likvifikaciji. Članek preučuje vpliv vsebnosti sljude na volumenski raztezek zmesi peska in sljude. Ugotovljeno je, da ima povečanje vsebnosti sljude pri določeni relativni gostoti posledično višji volumenski raztezek v primerjavi s čistim peskom po likvifikaciji.

V tretjem članku avtorja, Mojtaba Movahedifar in Jafar Bolouri Bazaz, prikazujeta raziskavo preučevanja nastalega pasivnega zemeljskega pritiska na integralni most z uporabo laboratorijskega modela in analitičnega pristopa. Integralni mostovi so brezstični mostovi, pri katerih je prekladna konstrukcija povezana s podporami brez dilatacijskih stikov. Rezultati kažejo, da je porazdelitev pasivnega pritiska nelinearna in da je njegova maksimalna vrednost vzdolž podporne stene odvisna od veličine rotacije stene in števila cikličnih horizontalnih premikov.

V četrtem članku avtorja, Nihat Kaya in Murat Ornek, predstavljata številne eksperimentalne in numerične rezultate posedanja T- oblikovanih plitkih temeljev zaradi ekscentričnih obremenitev. Rezultati dokazujejo, da se lahko nosilnost temelja pri skrajnih ekscentričnih obremenitvah izboljša z vstavljenjem vertikalnega centralnega dela, ki se togo pritrdi na dno temelja.

V petem članku avtorja, Primož Jelušič in Bojan Žlender, predstavljata optimiranje varnostnega faktorja sidrane stene. Optimiranje sta izvedla s pristopom nelinearnega programiranja in v ta namen razvila optimizacijski model OPTINC. Razvila sta tudi model ANFIS-SF za napovedovanje varnostnega faktorja za različne nagibe sten, kota nagiba brežine, dolžine sider in premera vrtine, kar omogoča obsežno analizo geotehničnih problemov.

Ludvik Trauner
Glavni urednik



EDITORIAL

Volume 10 of AGS will have two issues this year (2013/1 and 2013/2) and will celebrate its 10th anniversary of publishing under the auspices of the prestigious international editorial board. I use this occasion to thank the members of the editorial board as well as the outstanding international reviewers for their excellent work up to now. Special thanks are due to the editors Prof. Dr. József Farkas (Budapest) and Prof. Dr. Zlatko Langof (Sarajevo) for their precious collaboration during all ten years. Their important professional work will be continued by dr. Amin Barrari (Aalborg University, Denmark) and dr. Vojko Jovičič (IRGO - Institute for Mining, Geotechnology and Environment, President of the Slovenian Geotechnical Society SloGeD), whom I welcome as the new members of the Editorial Board.

In this issue, one review article and four scientific articles are published:

Prof. Dr. Ivan Vaniček, Professor at the Czech Technical University in Prague and Vice President of ISSMGE for Europe, presents an interesting review article entitled "The importance of tensile strength in geotechnical engineering" which summarizes his extensive knowledge and outstanding contributions in basic and applied research in the field of tensile and bending strength of soils. Dr. Vaniček presented this topic in his invited lecture at the 13th Šuklje memorial days, held in Lipica on June 15, 2012. On this occasion he was awarded the highest Slovenian Geotechnical Society award for his cooperation and excellent presentation.

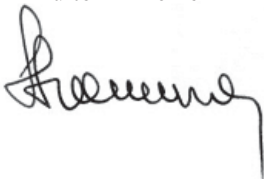
In the second article, the authors Ender Basar and Gurkan Ozden explain post-liquefaction settlement characteristics of micaceous sands. This paper examines the influence of mica content on post-liquefaction volumetric strain of sand-mica mixtures. It was found that increasing mica content at a certain relative density resulted in higher volumetric strains as compared with the data on clean sands.

In the third article, the authors Mojtaba Movahedifar and Jafar Bolouri Bazaz examine passive soil pressure against integral bridge abutments using a laboratory model and an analytical approach. Integral bridges are joint-less bridges where the superstructure is connected with the abutments without expansion joints. The results indicate that the passive pressure distribution is non-linear and its maximum value along the wall is dependent on the magnitude of the wall rotation and number of horizontal cyclic displacements.

In the fourth article, the authors Nihat Kaya and Murat Ornek present numerous experimental and numerical results of settlement of T-shaped shallow foundations due to eccentric loads. The results show that the ultimate bearing capacity of a footing under eccentric loads could be improved by inserting a vertical central cut-off rigidly connected to the footing bottom.

In the fifth article, the authors Primož Jelušič and Bojan Žlender present the safety-factor optimization for a soil-nail wall. The optimization was performed using the non-linear programming approach for which purpose the NLP optimization model OPTINC was developed. Additionally, an ANFIS-SF model was developed to predict the safety factor for different inclinations of the wall, the slope angle of the terrain, the length of the nails and the hole diameter allowing a comprehensive analysis of geotechnical problems.

Ludvik Trauner
Editor-in-chief



POMEMBNOST NATEZNE TRDNOSTI V GEOTEH- NIČNEM INŽENIRSTVU

IVAN VANÍČEK

o avtorju

Ivan Vaníček
Czech Technical University in Prague,
Geotechnical Department
Thakurova 7, 166 29 Praga 6, Češka Republika
E-pošta: vaniceki@fsv.cvut.cz

izvleček

Večina učbenikov o mehaniki tal zajema le malo podatkov o nateznih lastnostih zemljin. Izjema je Šukljetov učbenik "Reološki vidiki mehanike tal" [1], ki ta problem obravnava v poglavju "Natezna in upogibna trdnost zemljin". Zato tudi ni presenetljivo, da so 13. Šukljetovi dnevi posvečeni temi obnašanju tal v nateznih pogojih. Članek opisuje natezne preizkuse in podaja rezultate preizkusov v nedreniranem in dreniranem okolju. Podana je praktična uporaba rezultatov, zlasti za primere, ko pričakujemo razvoj nateznih razpok. Ker dajejo rezultati nateznih testov v dreniranih pogojih več podatkov o vezeh med posameznimi delci, so obravnavani tudi teoretski vidiki teh preizkusov.

ključne besede

natezne razpoke, natezna trdnost, upogibanje, triaksialni natezni testi v suhem okolju

THE IMPORTANCE OF TENSILE STRENGTH IN GEOTECHNICAL ENGINEERING

IVAN VANÍČEK

about the author

Ivan Vaníček
Czech Technical University in Prague,
Geotechnical Department
Thakurova 7, 166 29 Praha 6, Czech Republic
E-mail: vaniceki@fsv.cvut.cz

abstract

Many Soil mechanics textbooks contain only limited information about tensile characteristics. Šuklje's "Rheological aspects of soil mechanics" [1] is an exception, as he devoted a special chapter to this problem "Tensile and Bending Strength of Soils". Therefore, it is not a great surprise that the subject of the 13th Šuklje's Lecture is devoted to soil behaviour in tension. Tensile tests are briefly described, some results as well, with a distinction between undrained and drained tests. Practical examples of the application of the results are discussed, firstly in cases where the development of tensile cracks can be expected. Because the results of the drained tests give more information about the bonds between individual particles, some theoretical aspects of these tests are discussed as well.

keywords

tensile cracks, tensile strength, bending, triaxial drained tensile test

1 INTRODUCTION

The behaviour of soils in tension is a subject of great interest, not only for geotechnical engineers, but also for other branches of engineering, such as agricultural or mining, where the main object is connected with tillage or with resistance during soil excavation.

From the geotechnical engineering point of view, the interest with respect to the tensile strength of soils is very often connected with the different tensile cracks that

can develop in earth structures, such as embankment dams, slopes, retaining walls from reinforced soil, or with a capping clay sealing system of sanitary landfills, e.g., Vaníček [2]. Some examples are presented in the following figures. Fig. 1 shows a tensile crack that developed close to a rockfill dam crest parallel to its longitudinal axis.



Figure 1. Longitudinal crack on the surface of the clay core – Jirkov dam.

Very often, a tensile crack can be observed at the top of the slope as a first sign of the potential danger of a slope stability problem, Fig. 2.

A large tensile crack was also observed for a high retaining wall made from reinforced soil, very close behind the zone of reinforcement, Fig. 3. The water flowing into this crack started the process of wall overturning, as was observed from the shape of the quasi-homogeneous reinforced part of the wall.



Figure 2. Tensile crack at the upper part of a slope.

In the 1990s a great deal of attention was devoted to the possibility of tensile crack development in the capping sealing system of landfills, e.g., Jessberger and Stone [3], Daniel [4]. Due to the differential settlement of the deposited waste, local depression can develop there with a strong possibility of tensile crack development. These tensile cracks can influence, in a negative sense, the sealing function of this capping sealing system, Fig. 4, Vaníček [5].

The tensile tests and the obtained results are very useful tools for recognising the probability of tensile crack development, either from the view of the tensile strength or the tensile elongation at which the tensile cracks can be opened. However, these results are also very useful for the numerical modelling of the development of the tensile zone in the earth structure. In particular, the modulus of deformation in tension (or extension) determined from these tests can help to improve our knowledge about the tensile zone widening.

However, tensile tests can also help to improve our knowledge from the theoretical point of view, about which failure criteria are more general or what forces



Figure 3. Retaining wall made from reinforced soil – tensile crack behind the zone of reinforcement.

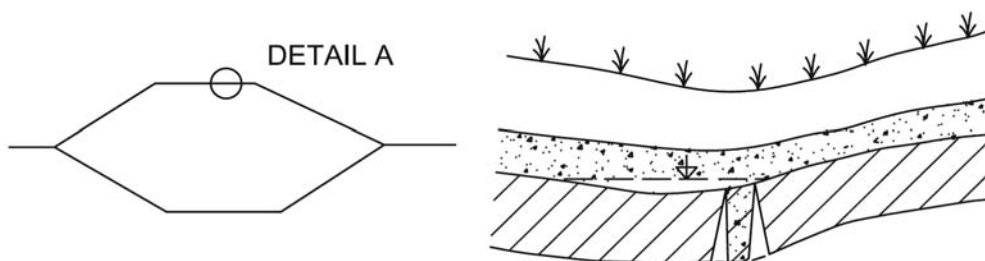


Figure 4. Deformation of the landfill surface – local differential settlements affecting the functionality of the capping clay liner.

between the individual soil particles are affecting the soil structure arrangement, e.g., Rosenquist [6], Bishop and Garga [7], Parry and Nadarajan [8]. This is especially the case with respect to the orientation of soil particles and the nature of the forces between adjacent soil particles. It is obvious that there is a certain relation between the effective tensile strength and the effective cohesion. Very often a negligible, even zero, effective cohesion is attributed to the normally consolidated clayey soils, in spite of the fact that some effective cohesion was measured.

This approach is in certain disagreement with the observation of material on the Moon's surface; where there is supposed to be no water, and so no interparticles forces where the contact is water–mineral, which are very often attributed for the measured effective cohesion. Fig. 5 shows the footprints of an astronaut's boot, where the walls are vertical. The same was observed for the walls of cuts excavated by a small dredging-machine on the Moon's surface.

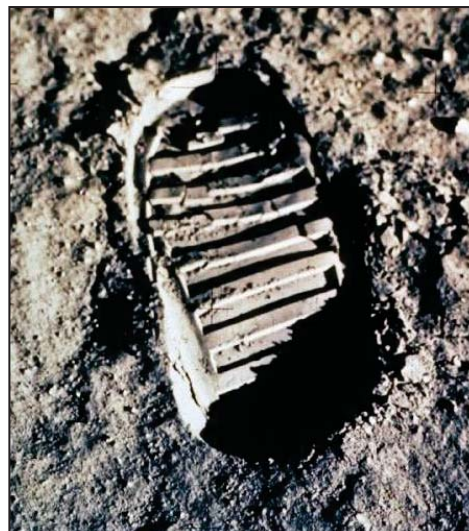


Figure 5. Footprints of an astronaut's boot on the Moon's surface with a vertical wall.

2 TYPES OF TENSILE TESTS

In the literature there are descriptions of the different tensile tests that varied in different ways. There is no unification, like for other soil mechanics tests, like shear or compression tests, see Vaníček [9]. If the dimensions of the tested samples, the manner of the preparation or the time effect are not taken into account, the principal classification can be made by:

- the principle of loading,
- the drainage conditions,
- the opportunity to measure the elongation.

Furthermore, a brief description is provided about the principle of loading with remarks about two other aspects, see Fig. 6

- a) Axial tensile test (direct tension test)
- b) Triaxial tensile test
- c) Bending test
- d) Test on hollow cylinder
- e) Indirect (Brazilian) tensile test.

For the axial tensile test most problems are, according to Šuklje [1], connected with the uniform distribution of the tensile stresses in the test section of the specimen. For the tested samples with a uniform cross section, different types of connection were applied, e.g., freezing, Haefeli [10], or glueing, Zeh and Witt [11].

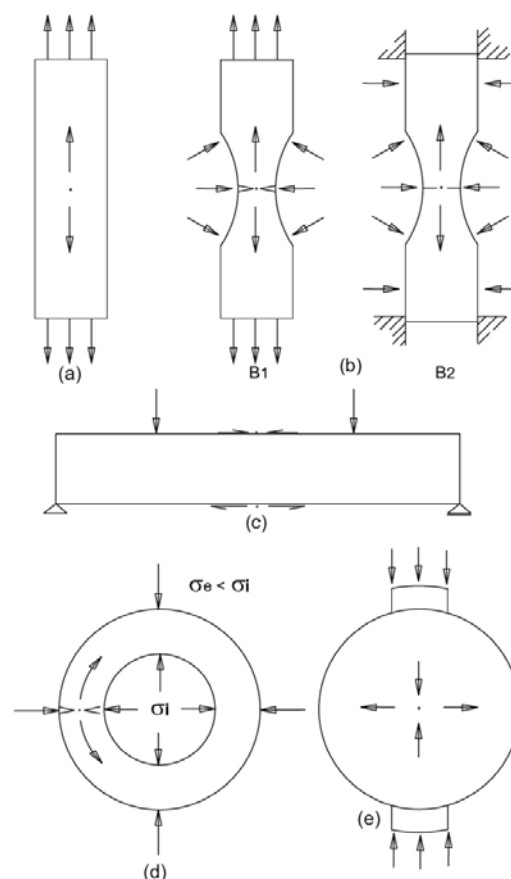


Figure 6. Division of tensile tests according to the principle of loading. a) Axial tensile tests (direct tension test). b) Triaxial tensile test. c) Bending test. d) Test on hollow cylinder. e) Indirect (Brazilian) tensile test.

For samples with wider ends (briquette) some sort of friction via connection clamps was applied. However, as in the first case, the transfer of the tension force from the widened heads to the test section must not cause concentrations of the stresses in the transition part of the specimen. Probably the largest samples were tested by Tšebotariof and De Phillipe [12]. In order to eliminate the unfavourable influence of the self-weight, the specimens are commonly tested in the horizontal position, and the effect of friction is eliminated by ball-bearing rollers, e.g., Tšebotariof and De Phillipe or by Drnovšek and Šubičeva [13]. For the unconfined tests mentioned by Hasegawa and Ikeuti [14], the weight was balanced by testing on a mercury surface. Ajaz and Parry [15] described load controlled and strain controlled direct tension tests, which were carried out by applying the pulling force through rods with universal joints to the brass grips holding the expanded ends of the tension specimen.

A triaxial tension test of type B1 will be described later for the drained tests. A type-B2 test was described by Ter-Martirosjan [16], [17]. The specificity of this test is the possibility to model a different stress state, depending on the ratio of the cross section at the end (A_E) of the sample to the cross section in the centre part of the sample (A_C). When a stiff sleeve is applied to the central part, the unconfined tensile test is modelled.

Some specificity of the tests on samples having the form of hollow cylinders and subjected to various internal and external hydrostatic pressures were described by Šuklje [1] and by Šuklje and Drnovšek [18]:

- well-defined stress states without uncontrolled stress concentration,
- the possibility of investigating the deformability and strength for various stress states,
- the possibility of taking into account the deformation anisotropy,
- the more likely possibility of carrying out long-term and drained tests.

However, up to now, very limited information was published with respect to the tensile soil behaviour.

The principle of the bending test consists of loading the tested soil beam with a pair of forces in the middle part of the sample. The advantage of such loading is the fact that in the central part of the tested beam the shearing force is zero and the bending moment is constant. It is a typical case of pure bending. The outermost fibres are either in tension or in compression.

The indirect (Brazilian) test is more often used in rock mechanics, as the sample is easily prepared from the

obtained core drill and the load transfer is not so difficult. Nevertheless, some results were also published with respect to soil samples, e.g., Narain and Rawat [19] or Krishnaya et al. [20].

In the next sections bending tests will be described in more detail for undrained tests as well the triaxial test for drained tests together with the obtained results.

3 RESULTS OF UNDRAINED TENSILE TESTS (BENDING TESTS)

Undrained tensile tests are usually performed as a very quick test. If the duration of the test is longer, the undrained conditions are satisfied by sample coating, and most often the sample was coated with a layer of petrowax and petrolatum oil.

3.1 BENDING TEST ARRANGEMENT AND EVALUATION

Bending tests were mostly conducted to investigate the state of the compacted horizontal layer in the clay core of the earth and rockfill dams, as during their deflection tensile cracks can develop there, e.g., Leonards and Narain [21], Vaniček [22].

Bending test results can be recalculated in different ways according to the specific theory, see Fig. 7:

- The theory of elasticity assumes that the deformation of the outermost fibres is the same as well the stresses in these outermost fibres are the same. The neutral axis lies in the centre of the sample.
- Navier's hypothesis assumes planar deformation in the cross section of the tested sample (however, the neutral axis is above the centre of gravity of the profile) and also the stresses are linear to the unit deformation.
- The differential method also assumes planar deformation in the cross section of the tested sample; however, this method is not based on any preferred stress-strain law.

The first one was used by Leonards and Narain, the second one by Vaniček and the last one by Ajaz and Parry [2][23]. Vaniček took advantage of the tests performed by Šuklje, who inserted several pairs of measuring pins into the beam, the deformation of which was recorded by photographs and the displacement of the pins determined in photo-comparators. The results of the tests made by Šuklje proved that the strain plots

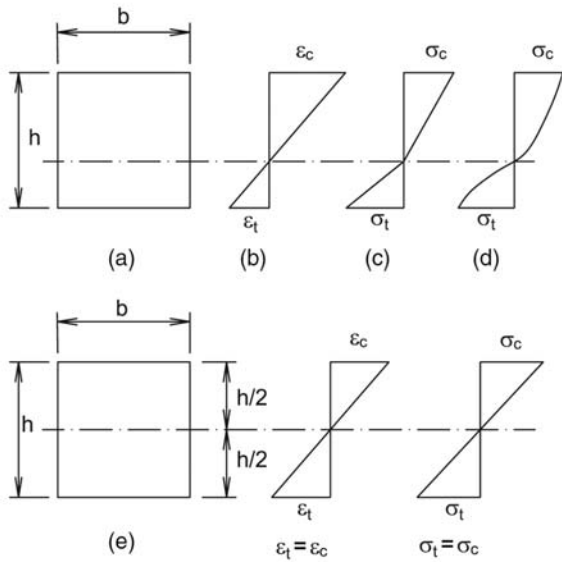


Figure 7. Bending test – fundamental assumptions. a) Beam cross section. b) Strain diagram. c) Stress diagram for Navier's hypothesis (direct method). d) Stress diagram for differential method. e) Elastic bending theory.

are still approximately linear during the appearance of the first tensile cracks. Similar results were obtained by Ajaz and Parry, who applied the Cambridge radiographic technique using an embedded grid of lead shot for monitoring the strains within the beam.

The layout of the measuring device that was used by the author is presented in Fig. 8, see Vaniček [24].

The beam, 300 mm long and 40 × 40 mm in cross-section, is loaded in the horizontal direction. The weight of the beam and the friction are eliminated by means of horizontal ball-bearings. In the central part of the beam, which deforms under a constant bending moment, are fixed with two detectors connected to the beam. The deformation is measured at their ends, with roughly 5× magnification against the deformation of the outermost fibres. The soil-water mix was compressed in four layers in a special mould for the dry density and moisture content determined from the Proctor standard test. The beam was coated with a hot mixture of oil and paraffin. The loading was increased under a constant rate in the direction of the layers.

3.2 FACTORS INFLUENCING THE UNDRAINED TENSILE CHARACTERISTICS

In this section the influence of such factors as the initial moisture content and the compaction energy on the tensile characteristics will be described, together with time effects. This means factors that can be controlled during the construction of the clay core of the earth and rockfill dams.

3.2.1 The influence of moisture content

Generally, the tensile strength of the tested soils decreased with an increase in the moisture content. For small changes around the optimum moisture content this relationship was nearly linear. Fig. 9 shows the influence of the moisture content for a wider range. The result was obtained for the material of the clay core from the Dalešice dam, see Vaniček [25].

The maximum value of the tensile strength is reached for $w = w_{opt} - 3.5\%$. The index of plasticity was used for the comparison of the different tests and soils compacted at the optimum moisture content, Fig. 10, see Vaniček, I. and Vaniček, M. [26].

The increase in the tensile strength with the index of plasticity is not convincing. For most samples with an index of plasticity lower than 30, the maximum tensile strength is in the range 30–80 kN.m⁻². Similar results were obtained

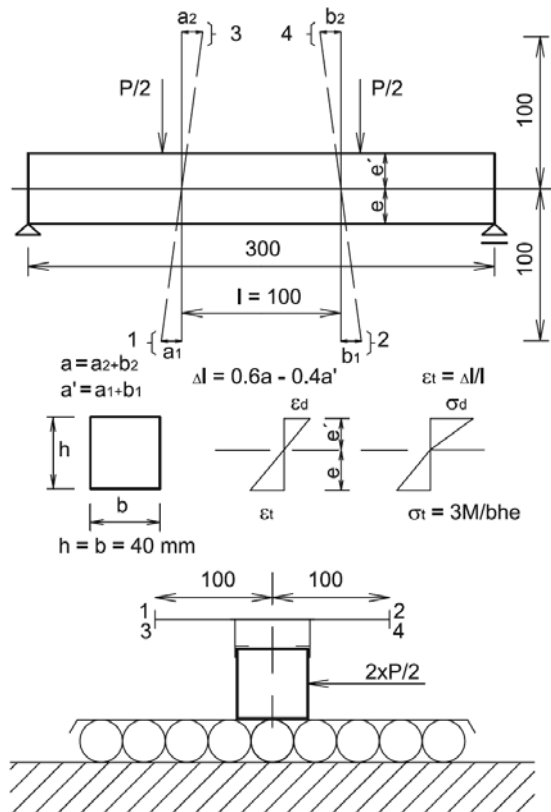


Figure 8. The layout of the arrangement and the evaluation of bending test proposed by the author.

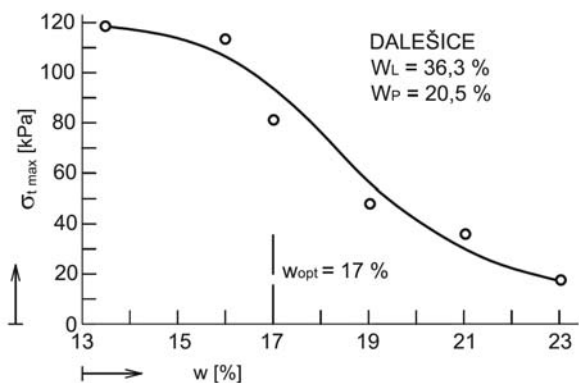


Figure 9. Tensile strength as a function of moisture content for the clay core from the Dalešice dam. Influence of moisture content on the tensile strain at failure.

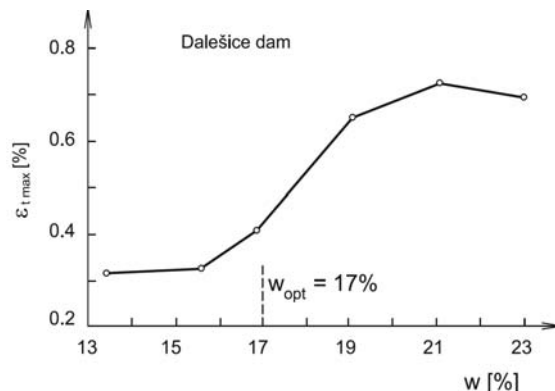


Figure 11. Influence of moisture content on the tensile strain at failure.

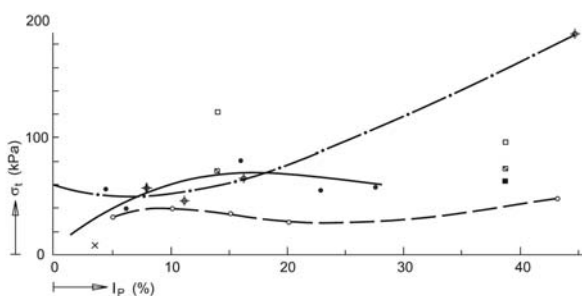


Figure 10. Results of the tensile strength for different tests and soils compacted by the Proctor standard at the optimum moisture content.

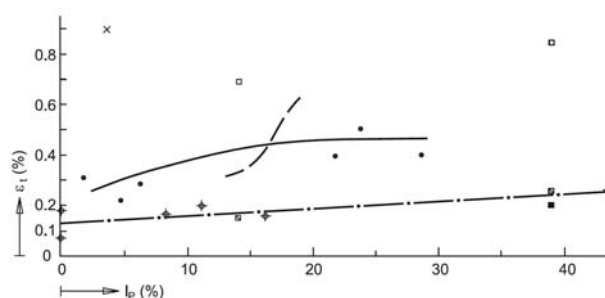


Figure 12. Results of the tensile strain at failure for different tests and soils compacted by the Proctor standard at the optimum moisture content.

by Narain and Rawat [19] and also by Ajaz and Parry [15]. From these results it is clear that the undrained tensile strength is mostly caused by capillary forces.

For small changes of moisture content around the optimum the tensile strain at failure increases linearly with the moisture content. For a wider range of moisture content for Dalešice clay this relation is shown in Fig.11. The increase of the failure tensile strain is relatively steep for a small change in the moisture content from the optimum. The gradient decreases at the end of the observed range and for $w = w_{opt} + 6\%$ first marked the occurrence of the decreasing of the maximum tensile strain.

Again, to compare the results from different authors and for different soils the index of plasticity I_p was used, see Fig.12 – Vaniček [27], Vaniček I. and Vaniček, M. [26].

The individual points represent tests on compacted samples by energy using the Proctor standard with the optimum moisture content. It is clear that the values of the maximum tensile strains are mostly in the range

0.2–0.6 % and increase with the value of the plasticity index. But this increase is not so significant as to unilaterally lead to an application just on plastic materials. The changes in the maximum tensile strain are more affected by the moisture content. It is shown in the same picture for the material from Dalešice dam ($I_p = 15.8$) using a dashed line.

With respect to the possibility of tensile crack development, that the stiffness of the soils stressed by tension is also important. In all cases the tensile modulus of deformation decreases while the moisture content increases. The question is how much the stiffness can be decreased with an acceptable increase in the moisture content. The increasing flexibility and decreasing strength are partly limited to the differences in stresses, which have a tendency to create in the earth structure. Simultaneously, they can be the reason for higher relative and total deformations, which on the other hand can help to create tensile cracks. Therefore, for each particular case there is an optimum value of the flexibility and strength, which will minimize the potential risk of crack development.

3.2.2 The influence of compaction effort

In accordance with the expectation, the higher compaction energy being applied for the optimum moisture content corresponding to this energy, e.g., a comparison of the energy typical for the Proctor standard and the Proctor-modified tests, the material flexibility is substantially reduced. When for the same initial moisture content a higher compaction effort is applied, after that the tensile strength and the tensile strain at failure are increasing. However, the impact on the secant modulus at the failure is negligible. This statement is very important because when the results of the compaction are better from the point of view of the maximum tensile strain, and so after that the shear strength and compression are also better, the shear parameters and the modulus of the deformation are higher.

3.2.3 The influence of time

Tests performed by author for the core of the Bulgarian dam Rosino showed that the influence of time is a complicated problem. On one hand the maximum elongation is increasing with the time of the test's duration, i.e., for very slow tests, from which a justifiable statement can be deduced, the clay core cracking is more probable for quick loading. However, also important is the time of the delay between the sample preparation and the testing, as normally a high pressure is used during the beam's formation. After unloading, a negative pore pressure can reach high values, which can increase the tensile undrained strength.

4 RESULTS OF THE DRAINED TENSILE TESTS

4.1 ARRANGEMENT OF THE DRAINED TESTS

Bishop and Garga [7] described the first triaxial drained tension test without the use of end clamps, type B1 in Fig. 6. A sample with a reduced centre section is enclosed by a rubber membrane. The end caps will only become detached from the ends under the action of an axial tensile force T when the average effective stress at the ends of the sample drops to zero. The axial effective stress throughout the centre section will, at this point, be negative (i.e., in tension), while the magnitude of this tensile stress is dependent on the ratio of the end-section and mid-section areas.

A controlled rate of the strain tension test with a constant cell pressure will thus be a test with $\sigma_1' = \sigma_2' = \text{constant}$, and with σ_3' decreasing (until the peak stress difference $\sigma_1' - \sigma_3'$ is reached).

Bishop and Garga tested London blue clay ($w_L = 75\%$, $w_p = 29\%$) on undisturbed samples, carefully sampled in situ or on a remoulded sample. The differences in the results are clear. For the undisturbed samples, the measured effective tensile strength was in the range 26.3–33.3 kN.m⁻², whereas for remoulded samples it was practically zero. The time to failure for the undisturbed samples was in the range 6.7–55.2 hours and the tensile strain at failure was in the range 2.19–16.7%. Some of the fundamental findings can be briefly summarized as:

- Failure of the sample has the character of a brittle material,
- Tensile stress at failure is almost independent of the value of σ_1' in the range examined,
- The variability of the maximum strain is relatively large.

However, there are some signals that the rate of loading for this type of clay was still insufficient to be fully drained.

The author completed two series of drained triaxial tests using the hydraulic triaxial apparatus described by Bishop and Wesley [28], see Fig.13.

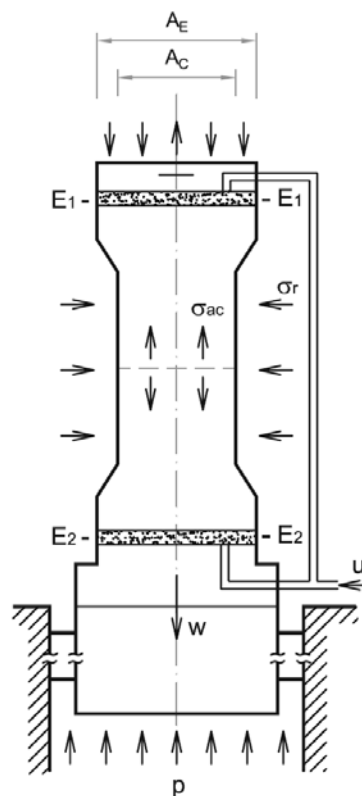


Figure 13. Layout of the drained triaxial tension tests performed in the hydraulic triaxial apparatus. σ_r – radial stress; p – stress in loading cell; u – back pressure applied to the drainage connection; W – weight of piston; σ_{ac} – axial stress on the centre section; A_E – area of end section; A_C – area of centre section.

During the first series, clay from the valley slopes downstream of the Cod Beck Dam was used to study the behaviour of plastic clay material in the range of small compression and tension stresses and to study the influence of the salinity of pore water on this behaviour, see Vaniček [9].

This clay (liquidity limit $w_L = 44.1\%$, plasticity limit $w_p = 18.5\%$, plasticity index $I_p = 25.6\%$) was deposited in a freshwater lake and the minimum of salts was supposed to be in the pore water. The remoulded samples, soil-water mix were compacted by hand into a special mould, with the help of a wooden stick. The samples were consolidated in the triaxial apparatus up to a consolidation pressure of 600 kN.m^{-2} . However, the tests started when the difference between the cell pressure and the back pressure was as low as from 5 to 25 kN.m^{-2} . The load cell was connected to the top cap and the test was started by applying a change in the pressure in the lower pressure cell.

Because the tests were performed as consolidated drained tests, a lot of attention was devoted to the determination rate of the loading, the time to failure, and to ensure that the excess (change) of pore pressures had a chance to dissipate (to equalize). The coefficient of the consolidation was calculated from the consolidation stage. The average value from the three lowest results is $0.07 \text{ cm}^2 \cdot \text{min}^{-1}$ (0.01 m^2 per day). The calculated required time to failure was, in all cases, slightly lower than the real time to failure, which was 30–40 hours.

A second, more extensive, series of tests was performed on Most clay ($w_L = 53.1\%$, $w_p = 25.4\%$, $I_p = 26.7\%$). Dry pulverized clay was mixed with water to form a clay slurry and this clay slurry was consolidated in a large oedometer with a diameter of 250 mm and a height of 150 mm under effective stresses of 100 or 300 kN.m^{-2} . Afterwards, at the end of the consolidation, cylindrical samples were cut out with a diameter of 38.1 mm (1.5").

The test arrangements are described in more detail by Vaniček, I. and Vaniček, M. [26].

4.2 DISCUSSION OF THE OBTAINED RESULTS

The typical result from a drained triaxial tension test is shown in Fig.14. For the presented case (sample No 2) the first peak in the deviator of stresses occurred for a tensile stress in the central part of the sample equal to 3.2 kN/m^2 and for an elongation of 3.6%.

After this first peak, a small neck in the central part was observed, but the deviator of stresses rose again

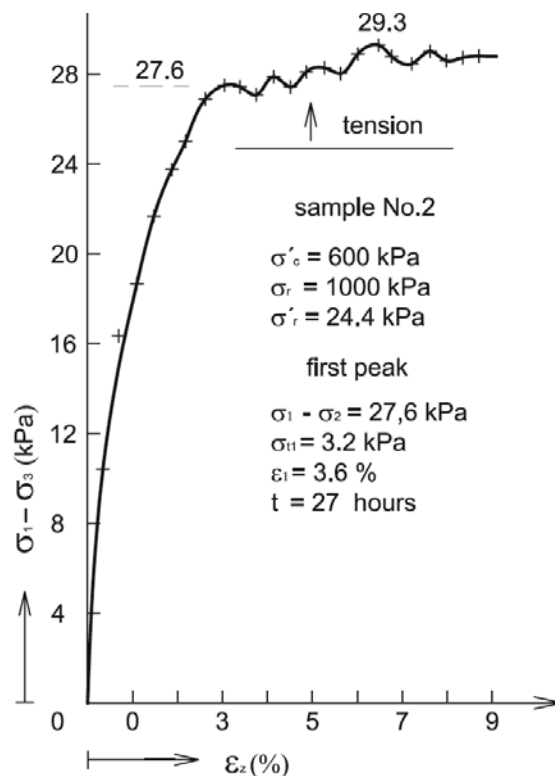


Figure 14. The typical result of drained triaxial tension test.

and a second neck was observed Fig.15. This untypical behaviour – when the failure did not continue in the first neck with the highest concentration of stresses – was observed in soils for the first time.



Figure 15. Photo of tested Most clay with visible two necks.

The character of the stress-strain curve is similar to the stress-strain curve of steel in tension. So, we can speak about a phase of strain hardening. It is rather difficult to explain this special behaviour. But with a high probability, the first failure is due to shear strength. This failure is accompanied by a fall in the deviator of stresses. After that – probably after the rearrangement of the clay particles in this zone – the tensile loading began and the stress-strain work hardening behaviour of the plastic clay was valid for this loading. This makes it possible to develop another shear failure at a different point.

The tests also helped to prove the character of Mohr's circles in the range of small positive (small compression) and negative (tension) stresses. Probably, the Mohr-Coulomb line is not valid for the range of stresses for negative values of the normal pressures, see Fig.16.

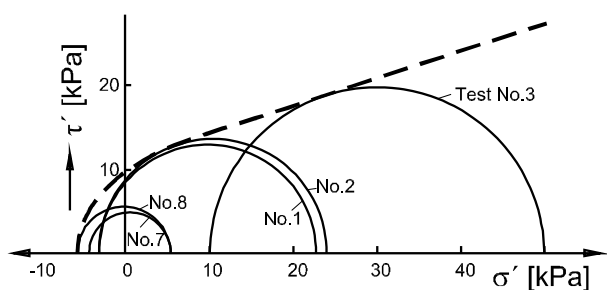


Figure 16. Mohr's circles for tri-axial compression and tension tests (for first failure).

The described sample No 2 was mixed during the phase of preparation only with distilled water. Samples No 4, 5 and 6 were mixed with brine (NaCl and KCl – dissolved in distilled water) so that samples No 4 and 5 contained 2.5 g of salts per litre of pore water and the ratio of the cations K/Na was 0.2 for sample No 4 and 0.8 for sample No 5. The pore water for sample No 6 contained 5 g of salts per litre with the ratio K/Na = 0.2 of potassium (K) and for sodium (Na) it was 0.2. The results indicated a small, positive influence of the water salinity on the tests results, as the effective cohesion was slightly higher (10.5–12.5 kN.m⁻²) than for sample No 2 (9 kN.m⁻²).

However, from the practical point of view the main conclusion is that the character of the drained and undrained tensile tests for the compacted or pre-consolidated samples is very different. The behaviour for the undrained tests is close to the brittle character, while the elongation at failure is rather small compared to the elongation for drained tests, which is roughly 10 times higher, in the range 2–6 %, while the effective tensile

strength is roughly 10 times lower, between 3 and 8 kPa. This means that during drained loading the material is much more flexible and the probability of the development of tensile cracks is significantly lower.

5 APPLICATION OF THE RESULTS ON SPECIFIC EARTH STRUCTURES

In the Introduction some examples were mentioned where the tensile zones and the tensile cracks can be expected and can play a very negative role in the behaviour of these earth structures. The three basic such examples are described in more detail.

5.1 EARTHFILL AND ROCKFILL DAMS

The problem of tensile cracks in the sealing part of fill dams is probably the most sensitive and the most discussed. L. Šuklje in his book mentions "A thorough analysis of the tensile strain states is needed when constructing the clay cores of earth dams. Tensile fissures in such cores can represent a dangerous starting point for the erosive action of seepage water and, therefore, they have to be avoided". However, in the same year, Casagrande [29] expressed his views on the increasing height of dams. He thinks that in the case of high rock dams in valleys with steep sides it is impossible to avoid the tensile zones and transversal cracks in the crest of a dam that is near the sides of a valley. It does not depend on the kind of building material. So it is necessary to protect the dam against the effects of cracks.

Tensile cracks can be initiated either by differential settlement or by hydraulic fracturing. In some cases seismic effects and desiccation also have to be taken into account. Transversal cracks in the direction of the seepage path are the most dangerous. The transversal cracks in a dam crest are usually caused by the differential settlement of the dam body. The advantage is that these cracks are observable, while the internal transversal cracks caused by hydraulic fracturing are not, and therefore they are much more dangerous.

Numerical methods, especially when the results of the tensile tests are utilized, can be a very useful tool for tensile zone prediction and specification. A subsequent parametrical study can give a better view of these zones if different types of soils are used or the selected soil is modified, e.g., with respect to the initial moisture content. In any case, the geometrical profile of the dam body can be rearranged as well.

When tensile crack development cannot be avoided, attention must be concentrated on the crack behaviour when the water starts to seep through it. A high swelling potential plays a positive role, while the high susceptibility to erosion plays a negative one. Therefore, the overall approach to the design of fill dams has been changing over recent decades. The question connected with the possibility of crack development is more important than the problem of slope stability. Therefore, a new, logical scheme for the design of fill dams was proposed by Whitman [30] or in modified form by Vaníček [31].

Vaníček [25] also describes the steps that were performed when the measurement in the Dalešice dam body showed a greater elongation than that measured during the laboratory tensile tests.

From the practical point of view the results from the undrained and drained tests can be used with respect to the dam construction speed or the speed of reservoir filling. For example, transversal cracks at the dam crest are very sensitive to the speed of reservoir filling, as this filling causes deformation of the upstream stabilization zone by its saturation.

5.2 SANITARY LANDFILLS

Due to the different physical, chemical and biological processes inside the deposited material, the settlement of the landfill surface is sometimes very high. In previous times it has very often been pointed out that surface clay sealing systems can embody differential settlement, causing tensile cracks, see Jessberger and Stone [3], and Daniel [4]. As an example, a crater with a diameter $\Delta L = 5$ m with the maximum depression $\Delta s = 0.25$ – 0.5 m is mentioned as a typical case observed on the landfill surface, see Vaníček [5].

This differential settlement corresponds to an elongation of 0.1–1.0 %, which can cause tensile crack development with preferential infiltration into the landfill body. Daniel, for example, indicates that many, if not all, covers for municipal solid waste landfills have areas with a distortion of this magnitude or larger. This is also one of Daniel's arguments for giving preference to a geosynthetic clay liner (GCL) in the capping system.

But on the basis of his own experience with tensile tests, the author is not so sceptical towards the utilization of clay liners in landfills, mainly for the following reasons:

- The maximum tensile elongation for cohesive soils compacted for optimum moisture content according to the Proctor standard test is really in the range 0.1–1.0%, but grows with a moisture-content incre-

ase. Because the compaction of the clay liners is usually performed for a moisture content higher than optimum (due to the decrease of permeability), this aspect is on the positive side.

- Up to now, the mentioned results were obtained for tensile tests that can be labelled as undrained tests. For the real conditions the crater development on the landfill surface is not such a quick process, it is time dependent. For the capping clay liners, partly drained conditions can be expected and therefore also a lower probability of tensile crack development.
- The last chance for improvement is the swelling potential – after the potential opening of the tensile crack and the first water infiltration through it, the crack can be closed by the swelling potential of the clay minerals as was also mentioned for the cracks in the fill dam body.

Therefore, we can conclude that a potential risk of tensile crack development exists, but it is not as high as was believed at the beginning of the last decade.

The possibility of tensile crack development in the capping clay liner by desiccation from the bottom, as mentioned, e.g., by Daniel [4], is still a matter of discussion.

5.3 RETAINING WALLS FROM REINFORCED SOIL

Most geotechnical engineers count on the possibility of tensile-zone development at the top of the slope, which can finally lead to tensile crack opening. Fig.17 shows the results of step-by-step numerical modelling of the pit excavation performed by Dunlop and Duncan (1970) [32], where the first tensile zones were modelled, even for a slope stability that is higher than usually demanded $F = 1.5$.

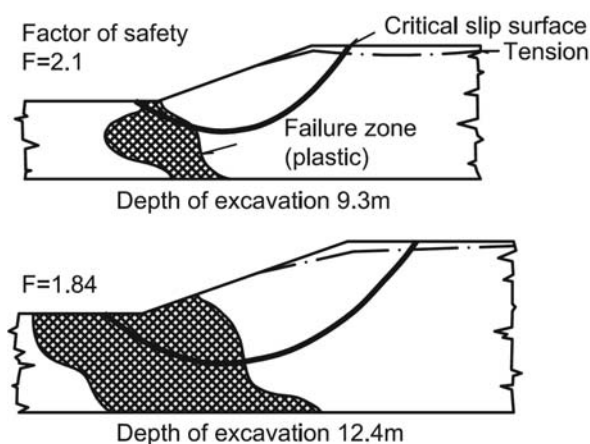


Figure 17. Development of the failure (plastic–tensile) zone during the process of excavation.

However, a similar case was observed for a retaining wall made from reinforced soil, see Fig. 3.

In fact the retaining wall from reinforced soil is a quasi-homogeneous gravity wall, for which different limit states of failure have to be checked. Therefore, a great attention is devoted to the ultimate limit state of failure along slip surfaces passing, not only through the reinforced part (the so-called internal stability) but also behind the zone of reinforcement (external stability). The limit state of overturning is often neglected. Nevertheless, this limit state can be very important, especially in the case that the tensile cracks are opened and filled with water.

For the case shown in Fig. 3 the wall was about 10 m high, the length of the reinforcing elements (geogrids) were in the upper part about 7 m. The soil used for this part was similar to the rest of the embankment; however, this soil was lime stabilized, and therefore the stiffness of this quasi-homogeneous block was much higher than the surrounding soil.

This different stiffness together with the different settlement of the quasi-homogeneous block plays the most

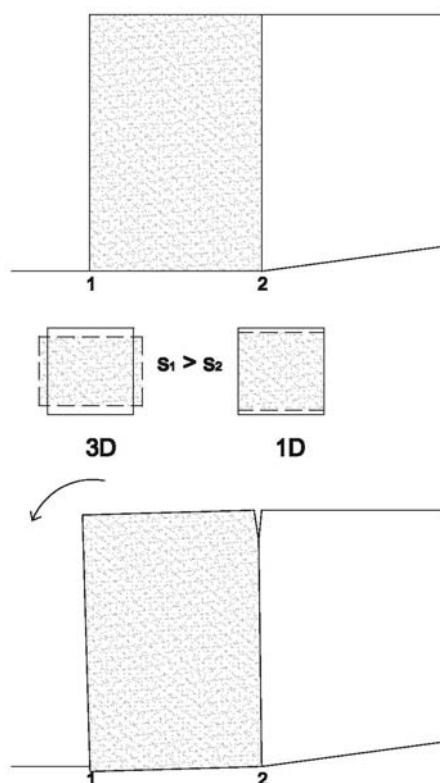


Figure 18. Deformation of the quasi-homogeneous block from the reinforced soil.

important role in crack development just behind the zone of reinforcement. The differential settlement of this block is caused by the different settlement of the block corners. For the outer corner, where the 3D deformation prevails, the settlement is always higher than for the inner corner, where it is roughly a 1D deformation, see Fig. 18. In the given case there were additional factors, the ground behind the outer corner was inclined, and just below this corner some backfilled pipes were situated.

6 CONCLUSION

The main purpose of this paper is to show the importance of the tensile characteristics of soils. The interest in this problem over the last half century has a sinusoidal character, and the peaks of interest were connected with tensile zones or cracks for soil slopes, for cracks in the sealing layers of fill dams, cracks in the capping clay liner of sanitary landfill and, finally, with the cracks behind the zone of reinforcement for the retaining walls from reinforced soil.

The author therefore presented his practical experience, either with tensile tests or with practical applications for the cases mentioned above.

The results of the undrained bending tests performed on compacted clays used for the dam clay core show that the tensile characteristics are strongly influenced by the capillary forces, the tensile strength is in the range 30–80 kPa and the maximum elongation at failure is about 0.2–0.6 % and can be significantly influenced by the moisture content or by the compaction effort. The results of the triaxial drained test show very different behaviour: the effective tensile strength is about 10 times lower and the maximum elongation about 10 times higher. Even if the tensile effective strength is relatively small, this nevertheless shows in the internal forces between the individual clay particles. The salinity of the pore water has a positive effect on the small strength increase. However, the most important factor is the stress-strain curve character (shape), showing in the stress-strain hardening. After the first peak was exceeded (probably as a result of shearing in the weakest point), the stress went up again (probably as the result of resistance against particle separation in this weakest point) causing shear failure at the second weakest point.

The summary shows that tensile tests deserve more attention in the future. There is a lot of opportunity for new findings, especially when the testing devices and monitoring possibilities are rapidly improving with time.

REFERENCES

- [1] Šuklje L. (1969). Rheological aspects of soil mechanics. Wiley-Interscience, London, 1969, 571 p.
- [2] Vaniček I. (2011). Introduction to the Main Session 4: Embankments and Slopes. *15th Euro-pean conference SMGE*, Athens, 2011.
- [3] Jessberger H.L., Stone K. (1991). Subsidence effects on clay barriers. *Géotechnique*, Vol 41, No. 2, pp. 185-194.
- [4] Daniel D.E. (1995). Pollution prevention in landfills using engineered final covers. In: Sarsby (ed) *Green 93 Waste disposal by landfill*. Balkema, Rotterdam, pp 73-92.
- [5] Vaniček I. (2002). Deposition of waste material on the surface. Main Lecture, Session 4: Environmental Protection. In: *Proc. 12th Danube-European Conference Geotechnical Engineering. ISSMGE, Passau*. Verlag Gluckauf GmbH, Essen, pp. 543-554.
- [6] Rosenquist I.T. (1959). Physico-chemical properties of soils. Soil-water system. J. SMFD ASCE, SM2, April.
- [7] Bishop A.W., Garga V.K. (1969). Drained tension tests on London clay. *Géotechnique*, Vol. 19, No. 3, pp. 310-313.
- [8] Parry R.H.G., Nadarajah V. (1974). Anisotropy in a natural soft clayey silt. *Engineering Geology*, Vol. 8, pp. 287-309.
- [9] Vaniček I. (1977c). Some aspects of tension tests. DIC thesis. The University of London.
- [10] Haefeli R. (1951). Investigation and measurements of the shear strength of saturated cohesive soils. *Géotechnique*, Vol. 2, No. 3, pp. 186-208.
- [11] Zeh R.M., Witt, K.J. (2007). The tensile strength of compacted clays as affected by suction and soil structure. *Experimental unsaturated soil mechanics Springer Proceedings in physics*, 2007, Vol. 112, Part III, pp. 219-226.
- [12] Tschebotarioff G.P., Ward E.R., DePhillipe A.A. (1953). The tensile strength of disturbed and recompacted soils. In: *Proc. 3rd ICSMFE*, Zurich, Vol. 1, pp. 207-210.
- [13] Drnovšek J., Šubič I. (1966). Ductility of cohesive soils at uniaxial stress state (In Slovenian). *Gradbeni vestnik*, Ljubljana, pp. 238-241.
- [14] Hasegawa H., Ikeuti M. (1964). On the tensile strength of disturbed soils. IUTAM Symposium Grenoble 1964: Rheology and Soil Mechanics, Springer-Verlag, Berlin, pp. 405-41
- [15] Ajaz A., Parry R.H.G. (1975a). Stress-strain behaviour of two compacted clays in tension and compression. *Géotechnique*, Vol. 25, No. 3, pp. 495-512.
- [16] Ter-Martirosjan Z.G. (1973). Compression-extension as a method of cohesive soil test. In: *Proc. 8th ICSMFE*, Moscow, Vol. 4.2, pp. 20.
- [17] Ter-Martirosjan Z.G. (1977). Certain results of tests on cohesive soils by the compression-extension method. In: *Proc. 5th Danube ECSMFE*, Bratislava, Vol. 4, pp. 159.
- [18] Šuklje L., Drnovšek J. (1965). Investigation of the tensile deformability of soils using hollow cylinders. In: *Proc. 6th ICSMFE*, Montreal, Vol. 1, pp. 368-372.
- [19] Narain J., Rawat P.C. (1970). Tensile strength of compacted soils. *J SMFD, ASCE* 96, SM6, pp. 2185-2190.
- [20] Krisnayya A.V.G., Eisenstein Z., Morgenstern N.R. (1974). Behaviour of compacted soil in tension. *J. Geot. Eng. Div. ASCE* 100, GT9, pp. 1051-1061.
- [21] Leonards G.A., Narain J. (1963). Flexibility of clay and cracking of earth dams. *J. SMFD ASCE* 89, SM2, pp. 47-98.
- [22] Vaniček I. (1975). The stress-strain behaviour of soils in tension. (In Czech). PhD Thesis, Czech Technical University in Prague, pp. 170.
- [23] Ajaz A., Parry R.H.G. (1975b). Analysis of bending stresses in soil beams. *Géotechnique*, Vol. 25, No. 3, pp. 586-591.
- [24] Vaniček I. (1977a). Discussion to Bending test for compacted clays. *JGED, ASCE*, GT 9, pp. 1028-1030.
- [25] Vaniček I. (1982). Simple non-standard laboratory tests before and during construction of Dalešice dam. In: *Proc. 14th ICOLD*, Vol. 1, Rio de Janeiro, pp. 605-609.
- [26] Vaniček I., Vaniček M. (2008). *Earth Structures: in Transport, Water and Environmental Engineering*. Springer, 637 p.
- [27] Vaniček, I. (1977b). Bending tension test on laboratory prepared and in situ taken sample from the core of rockfill dam. In: *Proc. 5th Danube EC SMFE*, Vol1, Bratislava, pp. 415 – 419.
- [28] Bishop A.W., Wesley L.D. (1975). A hydraulic triaxial apparatus for controlled stress path testing. *Géotechnique*, Vol. 25, pp. 657-670.
- [29] Casagrande A. (1969). Participation in panel discussion on earth and rockfill dams. In: *Proc. 7th ICSMFE*, Mexico, Vol. 3, p. 301.
- [30] Whitman R.V. (1884). Evaluating calculated risk in geotechnical engineering. *JGED. ASCE*, Vol. 110, No. 2, pp. 145-188.
- [31] Vaniček I. (1988). Creation and behaviour of cracks in clay core of earth and rockfill dams. (In

Czech). SNTL - Publishing house of technical literature, Praha, 168 p.

- [32] Dunlop P, Duncan J.M. (1970). Development of failure in excavated slopes. JSMFED, ASCE, Vol.96, No SM 2.

OCENA PASIVNEGA PRITISKA NA KRAJNO PODPORO INTEGRALNEGA MOSTU OB UPOŠTEVANJU VPLIVA USLOČENJA

MOJTABA MOVAHEDIFAR IN JAFAR BOLOURI BAZAZ

o avtorjih

vodilni avtor

Mojtaba Movahedifar
Department of Civil Engineering,
Neyshabur Branch, Islamic Azad University
Neyshabur, Iran
E-pošta: m.movahedi@iau-neyshabur.ac.ir

Jafar Bolouri Bazaz
Department of Civil Engineering, Ferdowsi University of Mashhad
Mashhad, Iran
E-pošta: bolouri@um.ac.ir

izvleček

Večina inženirskih konstrukcij je v času uporabe podvržena cikličnim obremenitvam, kot npr. podporni zidovi, morske konstrukcije (valovanju), cestiča (prometnim obremenitvam) ter seizmičnim obremenitvam. V primeru integralnega mostu z oporniki (IMO) je zasipni granulatni material podvržen počasnim cikličnim spremembam napetosti in raztezka v dreniranih pogojih. Ti mostovi so zgrajeni tako, da je prekladna konstrukcija vzdolžno neprekinjena. Drugače povedano, IMO so brezstični mostovi, pri katerih je preklada povezana z opornikom. Togi stik omogoča, da opornik in preklada delujeta kot ena konstrukcijska enota, brez dilatacijskih stikov, ki so pogosti pri tradicionalnih mostovih. Vzrok za odsotnost dilatacij so večinoma visoki vzdrževalni stroški. Na obnašanje IMO vplivajo ciklične temperaturne spremembe cestišča. To privede do pojavljanja cikličnih horizontalnih premikov zasipnega materiala pri podporah. Pričujoča raziskava je poskus preučevanja nastalega pasivnega pritiska na gredni IMO z uporabo laboratorijskega modela in analitičnega pristopa. Rezultati kažejo, da je porazdelitev pasivnega pritiska nelinearna in da je njegova maksimalna vrednost vzdolž stene odvisna od velikine rotacije stene in števila ciklov. Izgleda, da za takšno obnašanje obstajata dva različna mehanizma. V zgornjem delu stene se pesek obnaša kot plastični material, upad pasivnega pritiska v spodnjem delu pa je posledica usločenja.

ključne besede

integralni most z oporniki, ciklični premiki, pasivni pritisk, usločenje

AN ESTIMATION OF THE PASSIVE PRESSURE AGAINST INTEGRAL BRIDGE ABUTMENTS CONSIDERING ARCHING EFFECTS

MOJTABA MOVAHEDIFAR and JAFAR BOLOURI BAZAZ

about the authors

corresponding author

Mojtaba Movahedifar
Department of Civil Engineering,
Neyshabur Branch, Islamic Azad University
Neyshabur, Iran
E-mail: m.movahedi@iau-neyshabur.ac.ir

Jafar Bolouri Bazaz
Department of Civil Engineering,
Ferdowsi University of Mashhad
Mashhad, Iran
E-mail: bolouri@um.ac.ir

abstract

Most civil engineering structures are subjected to cyclic loading during their service life, such as retaining walls, wave loading on offshore structures, seismic loading and the traffic loading of pavements. In the case of an integral abutment bridge (IAB), as an example, the backfill granular material is subject to slow cyclic stress and strain changes under drained conditions. These bridges are constructed so that the top deck is longitudinally continuous. In other words, IABs are joint-less bridges where the superstructure is connected with the abutment. The rigid connection enables the abutment and superstructure to act as a single structural unit, i.e., the expansion joints which are widely used in traditional bridges are removed in IABs. This removal is mainly due to the high costs of maintenance. The behavior of IABs is dominated by the cyclical temperature changes in the bridge deck. This results in the imposition of cyclical horizontal displacements to the backfill soil of the abutments. The present research is an effort to investigate the induced passive pressure on the IABs, using a laboratory model and an analytical approach. The results indicate that the passive pressure distribution is non-linear and its maximum value along the wall is dependent on the magnitude of the wall rotation and number of cycles. It seems that there are two different mechanisms for this behavior. In the above part of the wall, sand behaves as a plastic material. A decline in the passive pressure in the bottom part, however, is the result of arching.

keywords

integral abutment bridge, cyclic displacement, passive pressure, arching

1 INTRODUCTION

Integral abutments bridges can be categorized into three types: shallow abutments, full height frame abutments on spread footings, and full height embedded abutments. Shallow abutments and frame abutments (Fig. 1.a) normally retain granular backfill. Embedded abutments are typically constructed in-situ in clayey ground (Fig. 1.b) [1].

The abutment of the integral bridges is generally subjected to cyclic displacement. This is due to the omission of the joint between the deck and the abutment, i.e., the superstructure is connected monolithically with the abutment [2-6]. This rigid connection enables the abutment and the superstructure to act as a single structural unit, and ensures full moment transfer between the abutment and the slab [5]. The omission of the expansion joints results in a fluent traffic and reduces the maintenance costs [7, 8].

The behaviour of these structures is dominated by the cyclical temperature changes in the bridge deck. In other words, due to the daily and seasonal variations in temperature, the bridge deck experiences the movement of thermal expansion and contraction, resulting in the imposition of cyclical horizontal displacements to the backfill soil of the abutments [9], and this imposed cyclic movement will in turn cause changes in the behaviour of the backfill material behind the bridge abutment.

The most influential lateral loading on integral bridges is due to the daily and seasonal thermal expansions and contractions of the superstructure [5].

In these bridges, if the variation in the environment temperature and the coefficient of thermal expansion of

the bridge are δ_{TEB} ($^{\circ}\text{C}$) and α_t ($1/^{\circ}\text{C}$), respectively, the change in the length of the bridge due to temperature changes, d_0 , can be calculated as [3-5]:

$$d_0 = \alpha_t \cdot \delta_{TEB} \cdot L \quad (1)$$

in which L is the length of the bridge deck (Fig. 1).

In practice, the soil at the back of the bridge abutment would resist against the deck elongation. The actual bridge deck elongation is, therefore, less than d_0 . Dicleli showed that the actual bridge-deck elongation, d' , could be calculated as (Fig. 1):

$$d' = d_0 - d_c \quad (2)$$

In this relation, d_c is the amount of deck contraction due to the backfill material's resistance [10]. Obviously,

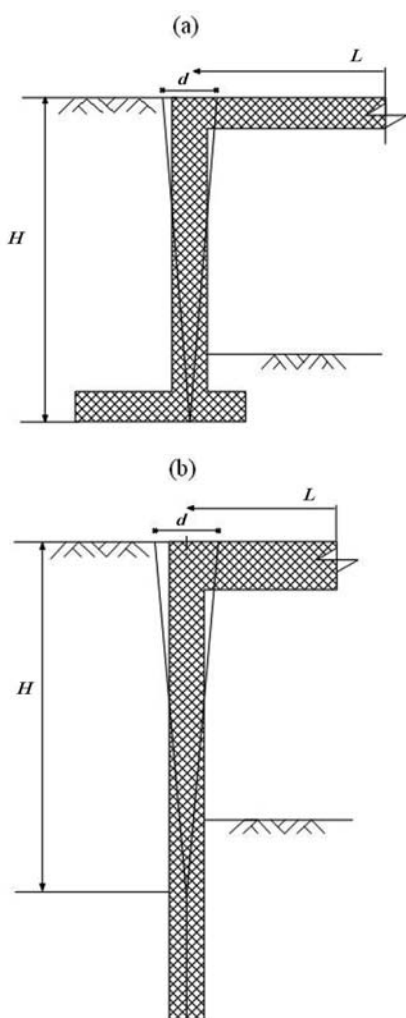


Figure 1. Imposed cyclic movement of the bridge deck to the retaining wall.

d_c depends on the bridge's axial stiffness. However, the effect of the backfill soil resistance on the behaviour of the abutment wall's movement is mostly neglected [11].

The effect of the soil-structure interaction of the integral bridges has been an interesting issue for many investigators. A wide range of experimental researches deals with investigations of the induced lateral earth pressure due to the cyclic movement of the bridge deck [1, 9, 12-19].

Springman et al., for example, performed a series of tests on a smooth and rigid wall that had the ability to rotate around a hinge located at its bottom. The induced stress on the face of the wall was measured using miniature pressure transducers. Their results indicate an increase in the maximum lateral earth pressure due to cyclic movements [18].

Barker and Carder performed a series of in-situ tests in which the pressure escalation was measured behind a bridge abutment. The length of the bridge was 40 m and the lateral movement and the stress behind the bridge abutment were evaluated. They observed a trend of pressure increase during the daily and seasonal temperature variations. Again, they evaluated the stress variations of a bridge abutment with a length of 50 m. The pressure and the movement of the abutment were recorded during the construction and the first year of operation. The results indicate that the lateral earth pressure during construction was about the at-rest pressure and gradually increased afterwards [13]. In addition, investigations indicate that the lateral earth pressure distribution is nonlinear and reaches its maximum value near the middle of the abutment [12]. More investigations indicate that the stress increases initially with depth and then decreases gradually in the region adjacent to the bottom of the wall. This phenomenon can be well interpreted by arch forming in this region. Many researchers have reported the stress reduction due to the arching effect [9, 17, 20-23].

The main objective of this paper is to investigate the influences of cyclic rotation on the behaviour of sandy soil behind the shallow abutment and frame abutments. To investigate these effects, a laboratory retaining wall was introduced. In this model, the wall itself was made from hard plastic material and stiffened by backing alloys in order to be sufficiently rigid.

Since the integral bridge abutments are generally analysed in the plane strain condition [1, 24], and in practice, the abutment is mostly built in reinforced concrete, it is relatively rigid [11], this is the reason that the retaining wall model was designed in such a way as to maintain the plane strain condition.

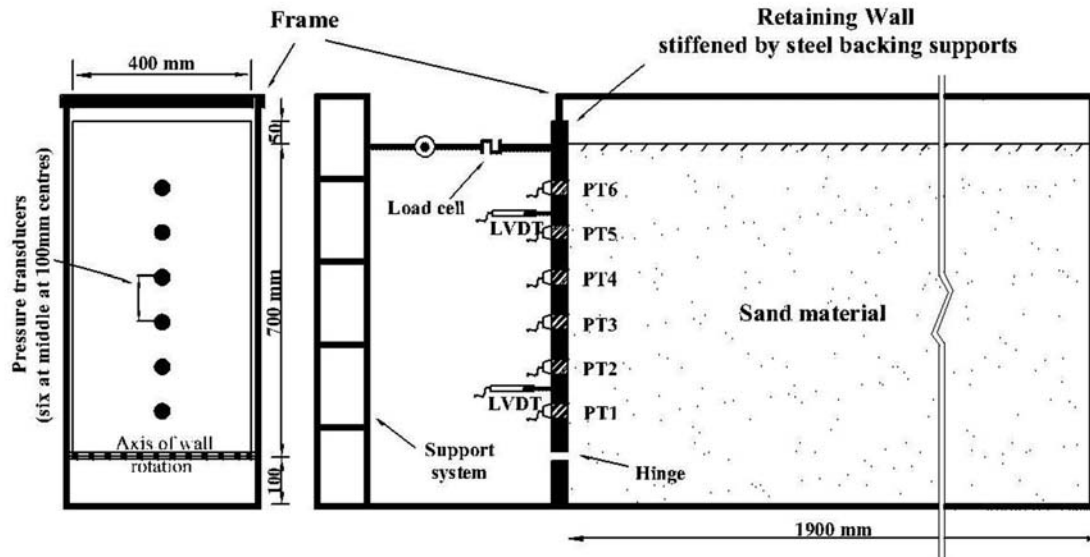


Figure 2. A schematic view of the retaining wall model apparatus.

The granular material placed behind any abutment is normally specified to be in a dense condition, achieved by mechanical compaction [25]. However, loose granular backfill has also been recommended behind the integral abutments as a possible means of avoiding high earth lateral pressures [25]. In this paper, the behaviour of sandy materials is loose conditions. The details of the model test, the loading condition and the material properties are presented in the following sections. Also, in order to interpret the laboratory model test results, an analytical model has been developed and the test results have been compared and validated.

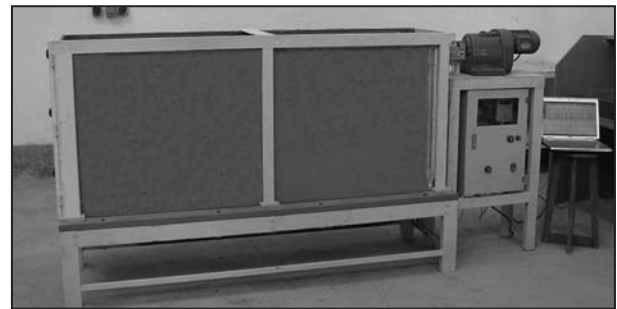


Figure 3. A general view of the laboratory model.

2 THE LABORATORY MODEL

In practice, the behaviour of the integral bridge abutment is in the plane strain condition [1, 24]. To maintain this condition in the laboratory model, the glassy side-walls (wing walls in practice) were fixed inside a frame. This prevented the lateral movement of sidewalls. It, in turn, results in the plane strain conditions to be maintained. In the laboratory model, the frame was made from steel with glass panels. Fig. 2 illustrates a schematic presentation of the apparatus. In order to observe the soil deformation during the tests, both longitudinal sides of the apparatus were made from thick (10 mm) glass panel. Shown in Fig. 3 is a general view of the laboratory model. The experimental device is 400 mm in width and 850 mm in height, allowing soil to be filled up to a depth of 800 mm. In this model, the rigid retaining wall itself was made from a hard plastic material and stiffened by backing alloys. It was able to rotate around its toe

by a hinge, which was installed in 100 mm, measured from the bottom of the apparatus. This resulted in up to 700 mm of soil depth to be contributed in the test. The friction between the wall and the glass panels was minimized by using PTFE sealing strips. In this model, the length of the apparatus was long enough to allow the rupture surface to be formed wholly. Based on the maximum friction angle of the backfill sand, which measured about 38.2° (Table 1), and assuming a plane rupture surface with an angle of $(45+\phi/2)^\circ$ with respect to the vertical, the length of the apparatus, l , was calculated as:

$$l = H \cdot \tan(45 + \phi/2) = 700 \times \tan(45 + 38.2/2) \approx 1450 \text{ mm} \quad (3)$$

Since the rupture surface is not completely plane and tends to be curvature, the length of the laboratory model was increased to 1900 mm. The friction angle between the sand and the wall was measured using direct shear test. Due to the smoothed face of the wall, the friction angle

between the walls and the sand, which was measured by direct shear device, was very low and close to zero. The lateral soil pressure measurements were made on the face of the wall using pressure transducers with a flat diaphragm that was very sensitive to the pressure. Six pressure transducers, PT1 to PT6, are installed at heights of $H=20, 30, 40, 50, 60$ and 70 cm, measured from the bed of the sand reservoir. These transducers measure the stress perpendicular to their face (i.e., the lateral earth pressure). The exact installation position of the pressure transducer on the rotatable wall is also shown in Fig. 2.

In this model, the top of the wall displacement is achieved using a mechanical motor. The driving shaft of the motor provides an inward and outward displacement to simulate the cyclic deformation. The model wall was equipped with a load cell to measure the applied load to the rotatable wall. This facilitated controlling the equilibrium of the applied load and the lateral earth pressure distribution on the wall face. In addition, the horizontal movements of the wall were captured using two LVDTs, installed both at the top and at the middle of the wall (Fig. 2). This made it possible to measure the horizontal movement of the wall and control its rigidity during the test. The reading of these LVDTs showed no wall bending in any test.

All the required data, including the wall displacement, soil pressures, and the applied loads, were captured as signals, using a data acquisition system. The data was then converted into digital numerical values based on calibration sheets.

3 BACKFILL MATERIAL PROPERTIES AND TEST PROGRAM

In the current research Firooz-Kouh sand with a similar texture to Leighton Buzzard sand was used. This sand, with a mean particle size (D_{50}) of 0.55 mm and a uniformity coefficient of 1.425 , was employed in the experiments. The friction angle, ϕ , of this sand and the friction angle between the sand and the wall using triaxial and direct shear tests, respectively. Due to the smoothed face of the wall, the friction angle between the walls and the sand, which was measured by direct shear device, was very low and close to zero. In addition, since the purpose of this study is to investigate the behaviour of sandy materials in loose conditions, the sand was rained from a constant drop height of 100 mm. This resulted in an initial sand relative density of $27\pm 2\%$ and unit weight of about 13.92 (kN/m^3). The corresponding internal friction angle was $\phi_{ini}=32.5^\circ$. Table 1 summarizes the properties of this sand.

Table 1. Specifications of Firooz-Kough sand.

Friction angle	ϕ_{max}	38.2°
	ϕ_{min}	30.0°
	ϕ_{ini}	32.5°
Void ratio	e_{min}	0.707
	e_{max}	1.040
	e_{ini}	0.95
Unit weight	γ	$13.92(\text{kN/m}^3)$
Grain density	γ_s	$26.58(\text{kN/m}^3)$
Relative density	D_r	$27\pm 2\%$
Specific gravity	G_s	2.71

4 TEST PROGRAM

In the present research, a wide range of experimental tests were carried out. Since the main objective of these series of tests was to evaluate the influence of the large amplitude [26] of wall rotation on the soil-wall interaction, the different amplitudes of the displacement at the top of the wall including $d/2=1.75, 2.45$ and 6.50 mm, equivalent to the wall rotation ($d/2H$) of $0.25, 0.35$ and 0.929% , are considered for these series of tests.

In these tests the retaining wall (totally smooth) was fixed in the vertical position and the LVDTs were set at zero. The subsequent readings indicated the forward and backward movements of the wall and these movements are repeated in the subsequent cycles.

These tests were terminated when no significant changes in the magnitude and distribution regime of passive pressure were observed. In addition, as we know, the rate of wall abutment of the integral bridges is significantly low (daily and seasonal variations of temperature). Movahedifar and Bolouri-Bazaz have shown the rate of wall movement (for low velocity magnitude) has no significant effect on the passive pressure magnitude [17]. Therefore, in these series of tests, the top of the wall movement velocity was constant and very low (0.015 mm/s). Fig. 4 depicts the induced passive pressure on the face of the wall for different wall movements including $(d/2)_{max}=1.75, 2.45$ and 6.50 mm.

When the test terminated, the settlement profile of the soil layers at different heights was determined by measuring the difference between the coloured sand layers and horizontal lines drawn initially on the glass panel. The settlement profiles for $(d/2)_{max}=1.75$ mm and 2.45 mm, for example, are shown in Fig. 5.

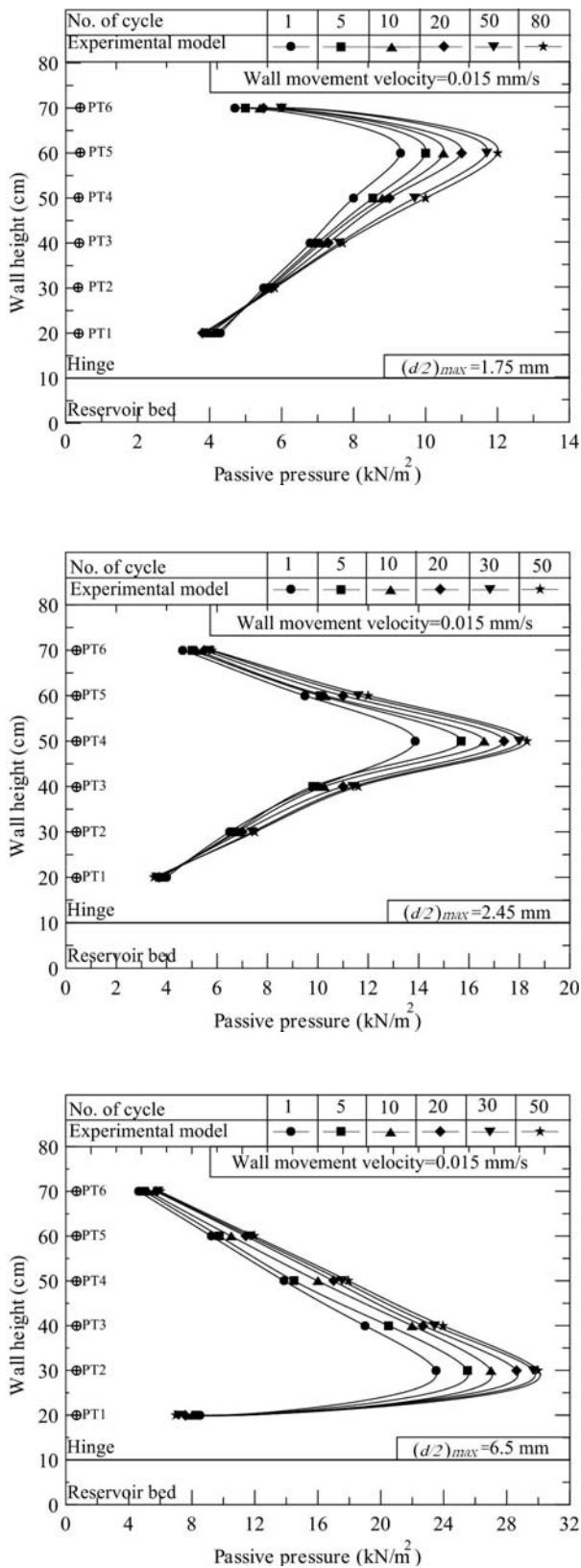


Figure 4. Induced passive pressure on the wall for different top of the wall movements.

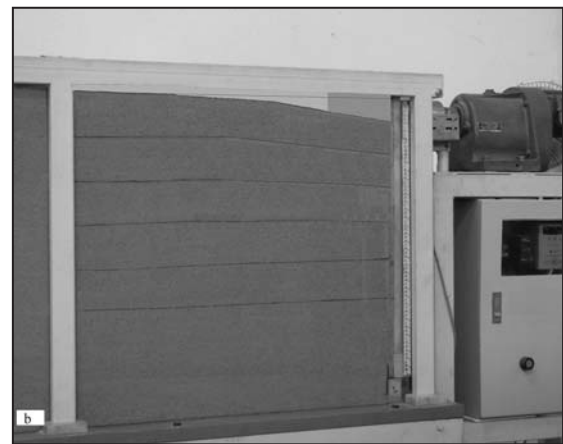
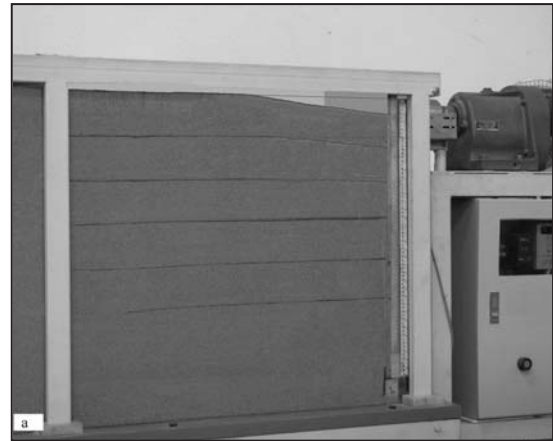


Figure 5. View of the settlement of the sand layers in the final cycles; a: $d/2=1.75$ mm and b: $d/2=2.45$ mm.

The settlement profile shown in Fig.5 is quantified and shown in Fig.6. This figure shows the settlement profiles in the vicinity of the rigid wall for $(d/2)_{max}=1.75$ mm (after 80 cycles), 2.45 mm (after 50 cycles) and 6.5 mm (after 50 cycles). This clearly indicates a huge decrease in void ratio of sand just close to the wall.

The following observations are based on Fig. 4, Fig. 5 and Fig. 6:

- The passive pressure distribution that is non-linear can be divided into two parts: above and below of the maximum point (see Fig. 4). It seems that the sand behaviour is different in these two parts. In the upper part the sand behaviour is plastic. In the lower part, however, a reduction in pressure can be observed. This imitates an arch formation, which tolerates some weight of sand. This results in a reduction in the vertical pressure and this, in turn, causes a reduction in the horizontal pressure.

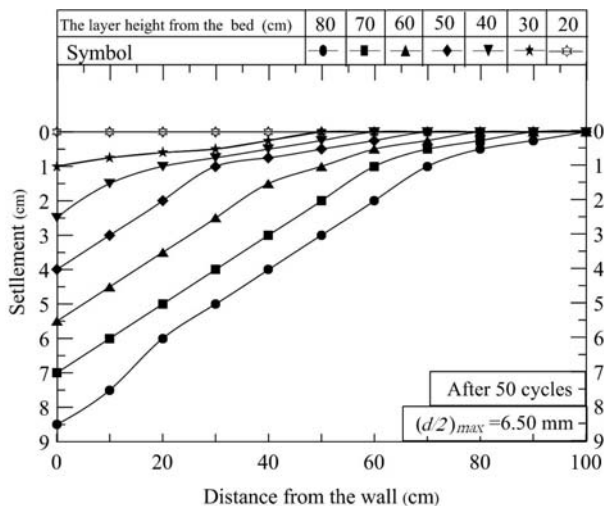
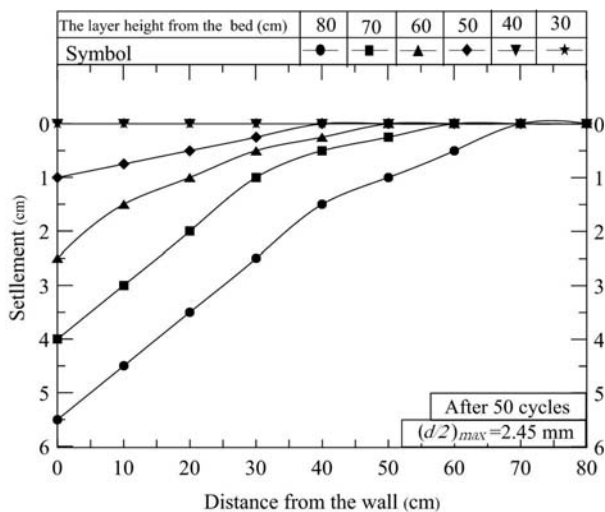
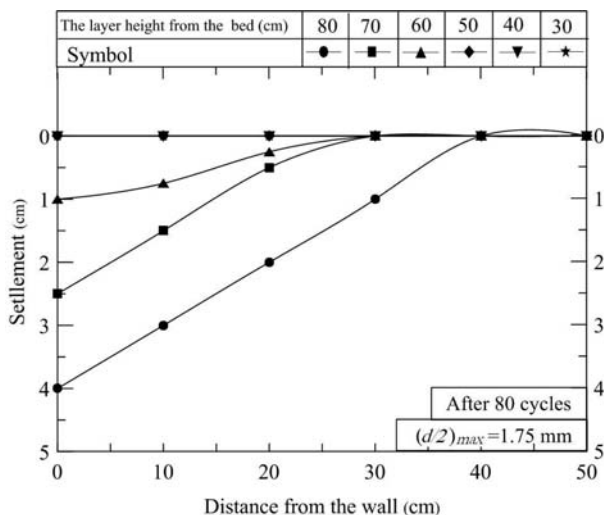


Figure 6. The settlement profile of the sand layers.

- The settlement profiles, shown in Fig. 6, indicate with increasing displacement amplitude, that more layers of soil are affected by the settlement. The heights of the sand layer measured from the top of the wall influenced by the settlement are 20, 30, and 50 cm for the range of 1.75, 2.45, and 6.50 mm displacements, respectively. The soil layers beyond these heights are not affected by the huge settlement on top of the wall. This is a clear indication of a reduction in the voids ratio and an increase in the friction angle in the upper part.

5 ESTIMATION OF THE ARCH ZONE

As shown in Fig. 4, when the wall is pushed inward to the fully passive condition, with an increase in the wall rotation amplitude, the passive pressure reaches a maximum value, after which it decreases gradually. This clearly indicates a decrease in the surcharge, i.e., a decrease in the vertical stress in the bottom part. This reduction is due to the arch forming between the wall and the material, leading to a reduction in the lateral passive pressure as well. If the wall starts to move back, the formed arch is suddenly destroyed, and the vertical stress and horizontal pressure in turn, must be increased. To investigate the process of arch formation, the variations of the passive pressure and the different magnitudes of the wall rotation are illustrated in Fig. 7. In this section, the wall starts from the at-rest condition (vertical position), and then the wall is pushed inward to the fully passive condition. It is then pulled back to the fully active condition and returned to the initial position.

The data taken from six pressure transducers, PT1 to PT6 (Fig. 2), are shown in Fig. 7. It should be noted that the captured data are pertained to the first half of a cycle, i.e., from at rest to the passive condition and just after returning back to the initial position.

Fig. 7 indicates for ($d/2$)_{max} = 1.75, 2.45 and 6.5 mm, when the wall resumes to move back, the pressure in the transducers PT1 to PT4 [for ($d/2$)_{max} = 1.75 mm] and PT1 to PT3 [for ($d/2$)_{max} = 2.45 mm] and finally just PT1 [for ($d/2$)_{max} = 6.5 mm] is increased and no significant increase for the remaining pressure transducers is observed. This means that with moving back the wall, the arch forming is destroyed, which results in an increase in the vertical stress. This, in turn, causes the lateral pressure to increase as well. In addition, it can be deduced that with increasing wall rotation amplitude, the height of the arch zone moves down. It is thought that if the wall rotation increases further (which is out of the

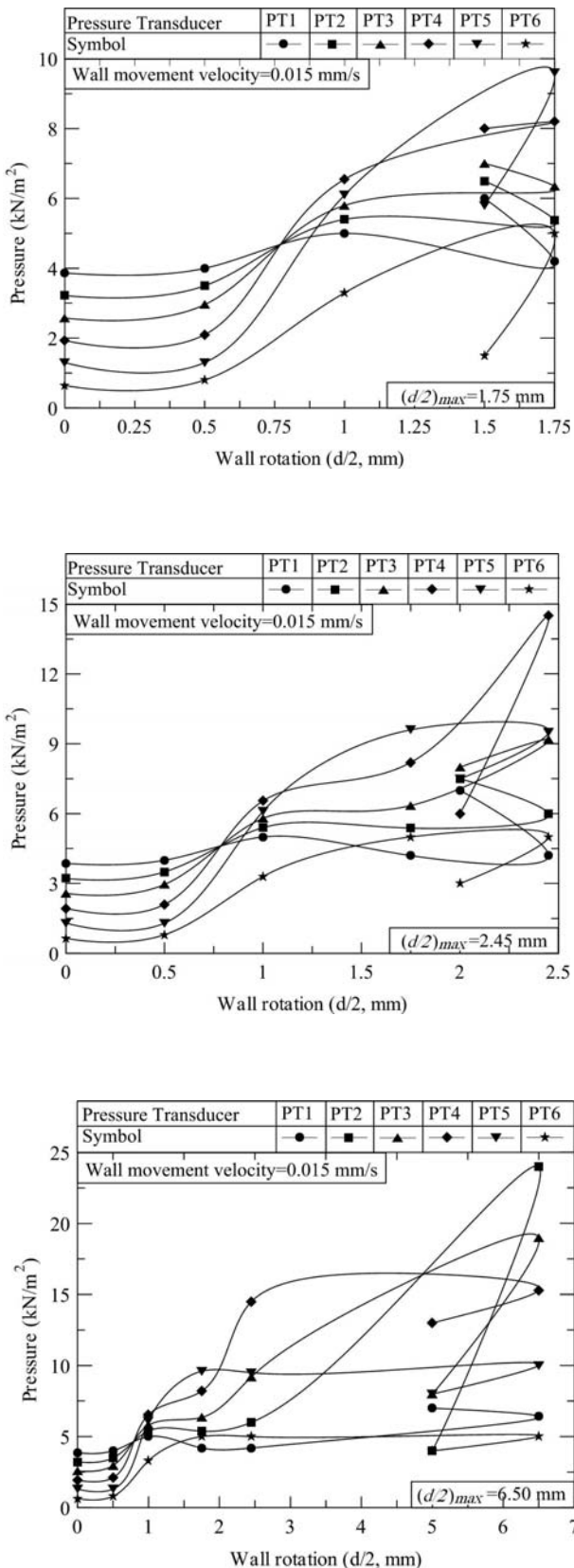


Figure 7. Passive pressure measured at various depths.

working range of the laboratory model) a fully passive condition is reached, i.e., the arch forming is (totally) destroyed. It is necessary to mention that the results for more cycles are similar to the first cycle, and that is why the results are reported only for the first cycle.

6 ANALYTICAL APPROACH FOR AN ESTIMATION OF THE PASSIVE PRESSURE

Although a wide range of experimental researches deals with investigations of the induced lateral earth pressure, regarding the cyclic movement of the bridge's deck, it is difficult to have an exact estimation of the passive pressure for IABs. In this section, based on an analytical approach, we attempt to estimate the passive pressure for shallow abutments and frame abutments.

It is known that the rupture surface in rigid retaining wall, rotating about a hinge located in the bottom of the wall, is mainly dependent on the friction between the wall and the soil. The rupture surface, however, is planar for the frictionless wall and curvature in the friction presence [21, 27, 28].

In addition, experimental and theoretical researches indicate that in active and passive conditions the soil failure wedge does not always cross the hinge. The height of the failure wedge depends on the wall rotation amplitude and with the increase in the rotation amplitude, the position of the bottom of the failure wedge approaches to the hinge [29, 30].

Based on the above observations, in order to interpret the interaction behaviour between the soil and the wall, a rigid retaining wall with a height of H is considered (Fig. 8). This wall, which is frictionless (friction angle between the walls and sand was very low and close to zero), is capable of rotating around a hinge located at the bottom of the wall. It is assumed that the failure wedge is forming at the height of H_p (from the top of the wall, Fig. 8) when the wall position is altered from the vertical position to the passive condition.

The angle of this failure wedge with the horizon is assumed to be θ . Consider the soil element ABCD in this wedge, which is called plastic zone. Also consider another soil element, EFGH, in the lower part of the wall with a height of H_e (the height of the arch zone), for which no failure wedge is formed. This element is located between the wall and a plane which forms an angle μ with the horizon and passes through the hinge. The formation of this hard bounding plane has also been reported by Tsang et al [9].

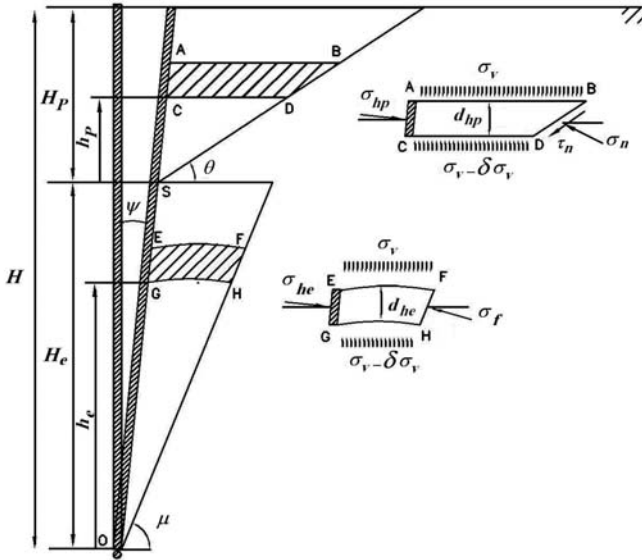


Figure 8. Wall analytical model.

Now, if we write the equilibrium equation for the element ABCD, we have:

$$\sigma_{hp} \cdot \cos \psi \cdot AC - \sigma_n \cdot BD \cdot \cos(\frac{\pi}{2} - \theta) - \tau_n \cdot BD \cdot \cos \theta = 0 \quad (4)$$

and:

$$\begin{aligned} &\sigma_{hp} \cdot \sin \psi \cdot AC + \sigma_v \cdot AB - (\sigma_v - \delta \sigma_v) \cdot CD \\ &+ [(CD - AC \cdot \sin \psi) + BD \cdot \cos \theta] \cdot \gamma \cdot d_{hp} \\ &+ \frac{1}{2} \gamma d_{hp} \cdot AC \cdot \sin \psi - \frac{1}{2} \gamma d_{hp} \cdot BD \cdot \cos \theta \\ &- \sigma_n \cdot BD \sin(\frac{\pi}{2} - \theta) + \tau_n \cdot BD \cdot \sin \theta = 0 \end{aligned} \quad (5)$$

Also, the following equations can be established for the SAB and SCD triangles and the element ABCD:

$$AC = d_{hp} / \cos \psi \quad (6)$$

$$BD = d_{hp} / \sin \theta \quad (7)$$

$$AB = (hp + d_{hp}) \cdot \tan(\frac{\pi}{2} - \theta) - (hp + d_{hp}) \cdot \tan \psi \quad (8)$$

$$CD = hp \cdot \tan(\frac{\pi}{2} - \theta) - hp \cdot \tan \psi \quad (9)$$

By substituting these equations into equations 4 and 5 we have:

$$\sigma_{hp} \cdot d_{hp} - \sigma_n \cdot d_{hp} - \tau_n \cdot d_{hp} \cdot \cot \theta = 0 \quad (10)$$

$$\begin{aligned} &\sigma_{hp} \cdot d_{hp} \cdot \tan \psi + \sigma_v [(hp + d_{hp}) \cdot \tan(\frac{\pi}{2} - \theta) - (hp + d_{hp}) \cdot \tan \psi] - (\sigma_v - \delta \sigma_v) (hp \cdot \tan(\frac{\pi}{2} - \theta) - hp \cdot \tan \psi) + \\ &[hp \cdot \tan(\frac{\pi}{2} - \theta) - hp \cdot \tan \psi - d_{hp} \cdot \tan \psi + d_{hp} \cdot \cot \theta] \cdot \gamma \cdot d_{hp} + \frac{1}{2} \gamma \cdot \tan \psi \cdot d_{hp}^2 - \frac{1}{2} \gamma \cdot d_{hp}^2 \cdot \cot \theta - \\ &\sigma_n \cdot d_{hp} \cdot \cot \theta + \tau_n \cdot d_{hp} = 0 \end{aligned} \quad (11)$$

The relationship between the shear and the normal stresses in the upper part of the wall and in the element ABCD can be stated as [31]:

$$\tau_n = \sigma_n \cdot \tan \varphi \quad (12)$$

Since equation 12 is valid in the plastic zone, by substituting equations 10 and 12 in equation 11 and ignoring (d_{hp}^2) and after simplification we have:

$$\sigma_{hp} = \frac{(\cot \theta - \tan \psi) (\sigma_v + \delta \sigma_v / d_{hp} \cdot hp + hp \cdot \gamma)}{\left(\frac{\cot \theta - \tan \varphi}{1 + \tan \varphi \cdot \cot \theta} - \tan \psi \right)} \quad (13)$$

Also, according to equations 14 and 15, the vertical stress and its variations can be calculated as:

$$\sigma_v = (H - H_e - hp) \cdot \gamma \quad (14)$$

$$\partial \sigma_v / d_{hp} = -\gamma \quad (15)$$

Substituting equation 14 and 15 into equation 13 leads to:

$$\sigma_{hp} = \sigma_v \cdot \frac{(\cot \theta - \tan \psi)}{\left(\frac{\cot \theta - \tan \varphi}{1 + \tan \varphi \cdot \cot \theta} - \tan \psi \right)} \quad (16)$$

In which K_p is the passive lateral earth pressure coefficient, i.e.:

$$K_p = \frac{(\cot \theta - \tan \psi)}{\left(\frac{\cot \theta - \tan \varphi}{1 + \tan \varphi \cdot \cot \theta} - \tan \psi \right)} \quad (17)$$

Fig. 9 illustrates a comparison of the above (K_p) and the Coulomb passive lateral earth pressure coefficient (C_o) for the condition of $\delta = \alpha = 0^\circ$, $\omega = (\psi + 90)^\circ$ and $\theta = (45 - \phi/2)^\circ$. It can be deduced by increasing the wall rotation; the difference becomes greater and greater, especially when the sand friction angle is relatively high. However, as seen in Fig. 9, even for $\phi = 45^\circ$ and $\psi = 10^\circ$ the maximum difference reaches up to about 6.5 percent.

Also, at the lower part of the wall, by writing the equilibrium for the element EFGH, we have:

$$\sigma_{he} \cdot EG \cdot \cos \psi = \sigma_f \cdot FH \cdot \cos(\frac{\pi}{2} - \mu) \quad (18)$$

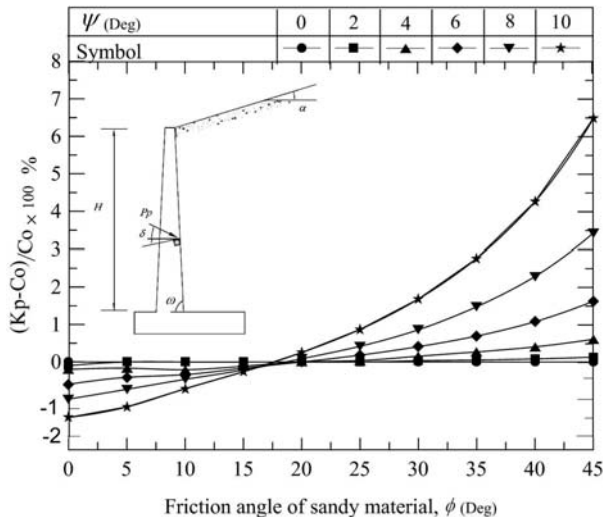


Figure 9. Comparison between the Coulomb coefficient (Co) and equation 17 (Kp).

$$\sigma_v \cdot EF - (\sigma_v - \delta\sigma_v) \cdot GH + \gamma \cdot d_{he} \cdot GH - \gamma \cdot EG \cdot \sin \psi \cdot d_{he} / 2 + \gamma \cdot FH \cdot \cos \mu \cdot d_{he} / 2 + \sigma_{he} \cdot EG \cdot \sin \psi - \sigma_f \cdot FH \cdot \sin(\pi/2 - \mu) = 0 \quad (19)$$

Also, in the element EFGH and the triangles OGH and OEF we have:

$$OG \cdot \cos \mu = OH \cdot \sin \mu = he \quad (20)$$

$$EG \cdot \cos \psi = FH \cdot \cos(\frac{\pi}{2} - \mu) = d_{he} \quad (21)$$

$$GH = OH \cdot \cos \mu - OG \cdot \sin \psi \quad (22)$$

$$EF = OH \cdot \cos \mu - OG \cdot \sin \psi - GE \cdot \sin \psi + FH \cdot \cos \mu \quad (23)$$

By substituting equations 18, 20, 21, 22 and 23 into equation 19, and after some simplification, the following equation is obtained.

$$\begin{aligned} & \sigma_v \cdot (he \cdot \cot \mu - he \cdot \sin \psi / \cos \mu - d_{he} \cdot \tan \psi + d_{he} \cdot \cot \mu) \\ & - (\sigma_v - \delta\sigma_v) \cdot (he \cdot \cot \mu - he \cdot \tan \psi) + \\ & \sigma_{he} \cdot d_{he} \cdot \tan \psi + \gamma \cdot d_{he} \cdot (he \cdot \cot \mu - he \cdot \tan \psi) \\ & - \gamma / 2 \cdot d_{he}^2 \cdot \tan \psi + \gamma / 2 \cdot d_{he}^2 \cdot \cot \mu - \sigma_{he} \cdot d_{he} \cdot \cot \mu = 0 \end{aligned} \quad (24)$$

If we ignore (d_{he}^2) and after the simplification, the following equation is obtained:

$$\sigma_v \cdot (\cot \mu - \tan \psi) + \partial \sigma_v / d_{he} \cdot he \cdot (\cot \mu - \tan \psi) + \gamma \cdot he \cdot (\cot \mu - \tan \psi) - \sigma_{he} \cdot (\cot \mu - \tan \psi) = 0 \quad (25)$$

Obviously, the arching phenomenon decreases the vertical stress. For the upper part of the wall no arching is formed, but for the lower part where the arch exists (Fig. 7), however, the vertical stress reduces and can be stated with the following relation:

$$\sigma_v = (H - he) \cdot \gamma \cdot \beta \quad 1 \geq \beta \geq 0 \quad (26)$$

β is a reduction coefficient and is considered to be a function of he (equation 27). It is always smaller than unity. For $he=He$, however, where the plastic zone starts, $\beta=1$.

$$\beta = f(he) \quad (27)$$

If we derive σ_v (equation 26) with respect to he is calculated we have:

$$\partial \sigma_v / d_{he} = H \cdot \gamma \cdot \partial \beta / d_{he} - (\gamma \cdot \beta + \gamma \cdot he \cdot \partial \beta / d_{he}) \quad (28)$$

By substituting equation 28 and equation 26 into equation 25 and after simplification equation 29 is obtained.

$$\sigma_{he} = H \cdot \gamma \cdot \beta + \gamma \cdot he - 2\beta \cdot \gamma \cdot he + \partial \beta / d_{he} \cdot he \cdot \gamma \cdot (H - he) \quad (29)$$

Equation 29 shows the horizontal stress in the lower part of the wall. With dividing σ_{he} (equation 29) to σ_v (equation 26), the lateral earth pressure coefficient in the lower part of the wall (Ke) can be calculated, i.e.:

$$Ke = \frac{H \cdot \gamma \cdot \beta + \gamma \cdot he(1 - 2\beta)}{(H - he) \cdot \gamma \cdot \beta} + \partial \beta / d_{he} \cdot he / \beta \quad (30)$$

Now, for $he=0$, (i.e., at the lowest part of the wall) $Ke=1$. In addition, Tsang et al. considered a linear variation for the lateral earth pressure coefficient in the lower part [9]. With this assumption, Ke (equation 30) increases from unity (at the lowest part of the wall) and approaches to Kp (at the start of plastic zone; equation 17). Therefore, we have:

$$Ke = 1 + he \cdot n \cdot (Kp - 1) / H \quad (31)$$

in which $n=H/He$.

With a comparison of equations 30 and 31 and after simplification we have:

$$\partial \beta / d_{he} = \beta \cdot n \cdot (Kp - 1) / H + \beta / he - \frac{H \cdot \beta + he \cdot (1 - 2\beta)}{he \cdot (H - he)} \quad (32)$$

With the proper integration and by applying the boundary condition of $he=H/n=He$, $\beta=1$, equation 33 leads to:

$$\begin{aligned} \beta = & (-1 / (Kp - 1) / n) \cdot H \cdot \exp(-n \cdot he \cdot (Kp - 1) / H) \\ & - \exp(1 / H \cdot n \cdot he \cdot Kp) / \exp(n \cdot he / H) / (he - H). \end{aligned} \quad (33)$$

$$H \cdot (Kp \cdot n - Kp - n) / \exp(-1) / n / \exp(Kp) / (Kp - 1)$$

By substituting equations 32 and 33 into equation 29, the lateral earth pressure on the lower part of the wall can be calculated. Now, for specific values of ψ and ϕ , according to equations 16 and 29, the lateral earth pressure on the upper and lower parts can be calculated.

Now, based on an analytical approach, the effect of different parameters, including the wall rotation (ψ) and friction angle (ϕ), on the lateral earth pressure can be investigated. Also, in order to study the accuracy of the proposed model just established, the experimental results are also included.

6.1 EFFECT OF WALL ROTATION ON THE PASSIVE PRESSURE

To investigate the effect of the wall rotation, the passive pressure escalation was calculated, using the analytical model. The results that are presented in Fig. 10 are for $\phi=32.5^\circ$. Also included in this figure, are the experimental results for the first cycle of movement (the initial friction angle). This also helped to evaluate the accuracy of the proposed analytical model. For this purpose, the maximum movements of the top wall including $(d/2)_{max}=1.75, 2.45$ and 6.50 mm, equivalent to the wall rotation of $\psi=0.143^\circ, 0.201^\circ$ and 0.532° , were considered.

The following observations are based on this figure:

- With increasing wall rotation, the magnitude of the passive pressure on the top of the wall increases, but the passive pressure in the bottom part and near the

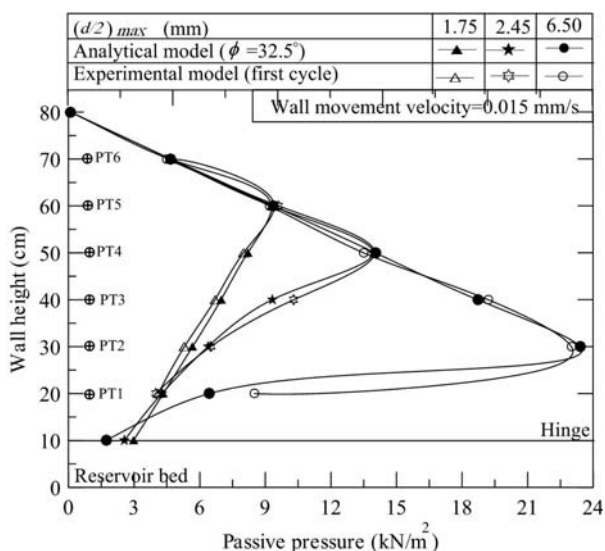


Figure 10. The effect of different wall rotations on the passive pressure escalation.

hinges decreases. Also, the location of the maximum pressure moves gradually from the top of the wall towards the lower region.

- Since the stress in the hinge decreases due to the arching phenomenon between the materials and the wall, it is concluded that by increasing the rotation of the wall, the arching effect increases in the bottom parts.
- Since the maximum pressure location separates the place of the upper and the lower parts of the wall, it can be deduced that by increasing the rotation wall, the height of the arch zone has been decreased. In other words, by increasing the rotation of the wall, the plastic deformation increases in the upper part and the height of the arch zone moves down.

6.2 THE EFFECT OF THE NUMBER OF CYCLES ON THE PASSIVE PRESSURE

Generally, when granular material is subjected to cyclic displacement, especially for loose and medium dense sand, the sand void decreases and it becomes increasingly dense, i.e., it tends to reach the densest possible state. This in turn results in an increase in the material friction angle during successive cycles [1, 20]. This fact was also observed for the sand just adjacent to the wall, which resulted in a markedly settlement in the upper region (see Fig. 6).

Now, based on the analytical model and by considering different angles of friction, the amount of passive

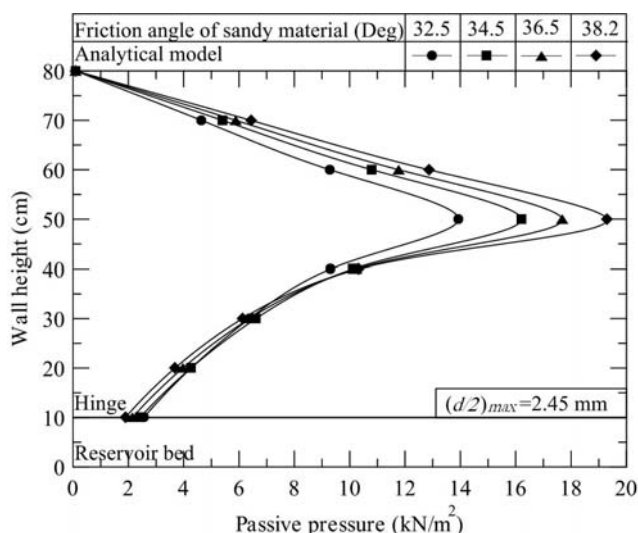


Figure 11. Calculation of the lateral passive pressure on the wall based on the analytical model.

pressure on the wall can be calculated. For example, for a $(d/2)_{\max}=2.45$ mm, equivalent to the wall rotation of $\psi=0.201^\circ$ and different friction angles (for example, $\phi=32.5, 34.5, 36.5$ and 38.2°), the passive earth pressure was calculated and shown in Fig. 11.

Since the initial angle of friction ($\phi_{\text{ini}}=32.5^\circ$) and the final angle of friction ($\phi_{\max}=38.2^\circ$) is known (Table 1) the analytical model has been established for these values of ϕ . The results of the model together with the experimental results for the first and the 50th cycle (for which no significant change in pressure is observed) are compared in Fig. 12. The same result has been observed between the analytical model and the experimental results.

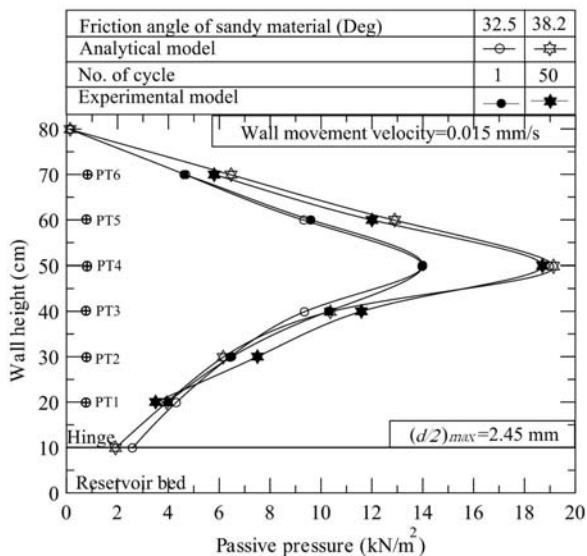


Figure 12. Comparison of tests results with analytical relations in the displacement range 2.45 mm.

In addition, it can be deduced that by increasing the number of cycles, the maximum magnitude of the passive pressure on the wall increases. The passive pressure, however, decreases in the lower part of the wall, which is due to the strengthening of the arch.

7 CONCLUSION

The present research focuses on evaluating the interaction between the soil and the rigid wall in large rotations. A model retaining wall apparatus was designed and constructed. In addition, an analytical model provided to imitate the cyclic behaviour of the granular material behind the rigid wall. For practical purposes

and loose sand, the wall displacements considered in this study were $d/2=1.75, 2.45$ and 6.50 mm. The most important points in this research are as follows:

- The distribution regime of the passive pressure is nonlinear. The passive pressure increases with depth, reaches a maximum, after which it decreases in the lower part of the wall.
- With an increase in the wall rotation amplitude, not only the amount of maximum pressure on the wall increases, but its location also moves gradually downwards. In other words, the plastic zone increases and the height of the arched zone decreases.
- For a specific wall rotation, as the number of cycles increases, the maximum passive pressure increases. After a limited number of cycles, the magnitude of the passive pressure remains roughly constant and no significant variation can be observed.
- In the lower part of the wall, by increasing the wall rotation amplitude and the number of cycles, the passive pressure tends to reduce. This is due to the increasing arch effect.
- It can be deduced that the magnitude of the passive pressure is not constant and depends on the magnitude of the wall rotation. In practice, it is not convenient to use the Coulomb theory for a lateral earth evaluation.

REFERENCES

- [1] Xu, M., Clayton, C.R., and Bloodworth, A.G. (2007). The earth pressure behind full-height frame integral abutments supporting granular fill. *Canadian Geotechnical Journal*, Vol. 44, No. 3, pp. 284-298.
- [2] Ahn, J.-H., Yoon, J.-H., Kim, J.-H., and Kim, S.-H. (2011). Evaluation on the behavior of abutment-pile connection in integral abutment bridge. *Journal of Constructional Steel Research*, Vol. 67, No. 7, pp. 1134-1148.
- [3] Dicleli, M. and Erhan, S. (2010). Effect of soil-bridge interaction on the magnitude of internal forces in integral abutment bridge components due to live load effects. *Engineering Structures*, Vol. 32, No. 1, pp. 129-145.
- [4] Hassiotis, S. and Xiong, K. (2007). Field measurements of passive pressures behind an integral abutment bridge. *Proceedings of the 7th International Symposium on Field Measurements in Geomechanics, Boston, MA, United states, American Society of Civil Engineers*.

- [5] Khodair, Y.A. and Hassiotis, S. (2005). Analysis of soil-pile interaction in integral abutment. *Journal of Computers and Geotechnics*, Vol. 32, No. 3, pp. 201-209.
- [6] Noorzai, J., Abdulrazeg, A.A., Jaafar, M.S. and Kohnehpooshi, O. (2010). Non-linear analysis of an integral bridge. *Journal of Civil Engineering and Management*, Vol. 16, No. 3, pp. 387 - 394.
- [7] Charuchaimontri, T., Senjuntichai, T., Ožbolt, J. and Limsuwan, E. (2008). Effect of lap reinforcement in link slabs of highway bridges. *Engineering Structures*, Vol. 30, No. 2, pp. 546-560.
- [8] Marques Lima, J. and de Brito, J. (2009). Inspection survey of 150 expansion joints in road bridges. *Engineering Structures*, Vol. 31, No. 5, pp. 1077-1084.
- [9] Tsang, N.C.M., England, G.L. and Dunstan, T. (2002). Soil/structure interaction of integral bridge with full height abutments. *Proc 15th ASCE Engineering Mechanics Conference, Columbia University, New York, NY, USA*.
- [10] Dicleli, M. (2000). A rational design approach for prestressed-concrete-girder integral bridges. *Engineering Structures*, Vol. 22, No. 3, pp. 230-245.
- [11] Alizadeh, M.H., Rashid, A.R.K., Chik, Z. and Mirhosseiny, S.M. (2010). Investigation of Abutment Displacement of a Full Height Integral Bridges in Dense Granule Backfill. *American Journal of Engineering and Applied Sciences*, Vol. 3, No. 4, pp. 749-756.
- [12] Barker, K.J. and Carder, D.R. (2001). Performance of an integral bridge over the M1-A1 Link Road at Bramham Crossroads. Transport Research Laboratory, Crowthorne, Berkshire, UK.
- [13] Barker, K.J. and Carder, D.R. (2000). Performance of the two integral bridges forming the A62 Manchester road over bridge. Transport Research Laboratory, Crowthorne, Berkshire, UK.
- [14] Cosgrove, E. and Lehane, B.H. (2003). Cyclic loading of loose backfill placed adjacent to integral bridge abutments. *International Journal of Physical Modelling in Geotechnics*, Vol. 3, No.3, pp. 9-16.
- [15] Darley, P., Carder, D.R. and Barker, K.J. (1998). Seasonal thermal effects over three years on the shallow abutments of an integral bridge in Glasgow. Transport Research Laboratory, Crowthorne, Berkshire, UK.
- [16] Goh, D. (2001). The behavior of shallow abutments of integral bridges. PhD Thesis, University of Birmingham, Birmingham.
- [17] Movahedifar, M. and Bolouri-Bazaz, J. (2011). An innovative apparatus to measure cyclic behavior of backfill granular material behind bridge abutment. in *The 14th Asian Regional Conference on Soil Mechanics and Geotechnical Engineering, Hong Kong*.
- [18] Springman, S.M., Norrish, A.R.M., and Ng, C.W.W. (1996). Cyclic loading of sand behind integral bridge abutment. Transport Research Laboratory
- [19] Tapper, L. and Lehane, B.M. (2004). Lateral stress development on integral bridge abutments. in *The Eighteenth Australasian Conference on Mechanics of Structures and Materials, Perth*.
- [20] England, G.L. and Bolouri-Bazaz, J. (1995). Ratcheting flow of granular materials. *Proceeding of Static and Dynamic Properties of Gravelly Soil, AISC, Geotechnical Division*.
- [21] Paik, K.H. and Salgado, R. (2003). Estimation of active earth pressure against rigid retaining walls considering arching effects. *Journal of Geotechnique*, Vol. 53, No. 7, pp. 643-653.
- [22] Roy, A. and Patra, N.R. (2009). Effect of arching on passive earth pressure for rigid retaining walls considering translation mode. *Proceedings of the 2009 Structures Congress, United states, American Society of Civil Engineers*.
- [23] Rupa, S.D. and Pise, P.J. (2008). Effect of arching on passive earth pressure coefficient. in *The 12th International Conference of International Association for Computer Methods and Advances in Geomechanics, Goa, India*.
- [24] Phillip, S.K.Ooi, Xiaobin, L. and Harold, S.H. (2010). Numerical Study of an Integral Abutment Bridge Supported on Drilled Shafts. *Journal of Bridge Engineering*, Vol. 15, No. 19, pp. 19-31.
- [25] Card, G.B. and Carder, D.R. (1993). A literature review of the geotechnical aspects of integral bridge abutments. Transport Research Laboratory, Crowthorne, Berkshire, UK.
- [26] Bayoglu Flener, E. (2004). Soil-Structure interaction for integral bridges and culverts. PhD Thesis, Royal Institute of Technology, Stockholm, Sweden.
- [27] Benmebarek, S., Khelifa, T., Benmebarek, N. and Kastner, R. (2008). Numerical evaluation of 3D passive earth pressure coefficients for retaining wall subjected to translation. *Computers and Geotechnics*, Vol. 35, No. 1, pp. 47-60.
- [28] Fang, Y.-S., Ho, Y.-C. and Chen, T.-J. (2002). Passive Earth Pressure with Critical State Concept. *Journal of Geotechnical and Geo-environmental Engineering, ASCE*, Vol. 128, No. 8, pp. 651-659.
- [29] James, R.G. and Bransby, P.L. (1970). Experimental and theoretical investigations of a passive earth pressure problem. *Journal of Geotechnique*, Vol. 20, No. 1, pp. 17-37.
- [30] Matsuzawa, H. and Hazarika, H. (1996). Analyses of active earth pressure against rigid retaining wall

subjected to different modes of movement. *Journal of Soil and Foundations*, Vol. 36, No. 3, pp. 51-65.

- [31] Das, B.M. (2002). Principles of foundation engineering. 4th Bill Stenquist, Virginia, USA.

SPREMEMBA VOLUMNA SLJUDASTIH PEŠČENIH TAL IZ STARE DELTE REKE GEDIZ PO LIKVIFAKCIJI

ENDER BASARI İN GURKAN OZDEN

o avtorjih

Ender Basari
Celal Bayar University,
Department of Civil Engineering
Manisa, Turčija
E-pošta: ender.basari@cbu.edu.tr

Gurkan Ozden
Dokuz Eylul University,
Department of Civil Engineering
Izmir, Turčija
E-pošta: gurkan.ozden@deu.edu.tr

izvleček

Posedanje sljudastega peska po likvifakciji ni dovolj raziskano. Trenutno so na voljo preglednice o volumskem raztezu čistega peska po likvifakciji v odvisnosti od relativne gostote. Ocena posedanja sljudastih tal po likvifakciji je zato negotova, ker obstajajo dokazi, da lahko sljudasta zrna povečajo tendenco po spremembi volumna. Članek preučuje vpliv vsebnosti sljude na volumski raztezek zmesi peska in sljude. Pripravili smo vzorce zemljin različne relativne gostote. Preučili so tudi vpliv vsebnosti prahu, ki je lahko prisoten na terenu, v zbitih naravnih vzorcih, pridobljenih na terenu iz vrtin v gosto naseljenem področju stare delte reke Gediz v Izmirju. Ugotovili so, da ima povečanje vsebnosti sljude pri določeni relativni gostoti posledično višji volumski raztezek v primerjavi s čistim peskom. Zaključek je pokazal, da je vpliv sljudastih zrn na obnašanje peska odvisen od začetnega količnika por v pesku. Vpliv zrn sljude se zmanjšuje s povečanjem relativne gostote. Empirično so izpeljali enostavne odnose med vsebnostjo sljude in relativno gostoto ter volumskim raztezkom. Opazili so tudi, da je vsebnost prahu pospešila in povečala volumski raztezek po likvifakciji.

ključne besede

pesek, sljuda, ne-plastični prašni delci, sprememba volumna po likvifakciji

POST-LIQUEFACTION VOLUME CHANGE IN MICA-CEOUS SANDY SOILS OF OLD GEDIZ RIVER DELTA

ENDER BASARI and GURKAN OZDEN

about the authors

Ender Basari
Celal Bayar University,
Department of Civil Engineering
Manisa, Turkiye
E-mail: ender.basari@cbu.edu.tr

Gurkan Ozden
Dokuz Eylul University,
Department of Civil Engineering
Izmir, Turkiye
E-mail: gurkan.ozden@deu.edu.tr

abstract

Post-liquefaction settlement characteristics of micaceous sands are not well investigated topic. Currently available charts relating post-liquefaction volumetric strain to relative density were developed for clean sand. Estimation of post-liquefaction settlement of micaceous sands, therefore, may stay on the unsafe side, since there is evidence indicating that mica grains could increase volume change tendency. Influence of mica content on post-liquefaction volumetric strain of sand-mica mixtures is studied in this article. Soil samples were prepared at various relative densities. Influence of fine content that could be present in the field was also investigated on tamped natural field samples recovered from boreholes drilled in a highly populated alluvial site known as the Old Gediz River Delta of Izmir. It was found that increasing mica content at a certain relative density resulted in higher volumetric strains as compared with the data on clean sands. It is deduced that influence of mica grains on sand behavior depends on initial void ratio of sand. Effects of mica grains decrease with increasing of relative density. Simple empirical relationships were derived relating mica content and relative density to volumetric strain. It was also noticed that fine content accelerated and increased post-liquefaction volumetric strains.

keywords

sand, mica, non-plastic fines, post-liquefaction volume change

1 INTRODUCTION

One of the consequences of seismic action on saturated sand deposits is post liquefaction settlement. The excess pore water pressure generated during earthquake loading dissipates as the ground motion ceases generating volumetric deformations of which magnitude depends on the severity of the loading, initial void ratio, grain size distribution, grain shape, depth, effective stress state, degree of saturation and fine content [1~6].

It was shown in previous studies that platy mica grains present in sandy soils affect mixture's packing and engineering characteristics [7~9]. Harris et al. (1984) [7] and Lee et al. (2007) [8] have revealed that platy mica grains would decrease shear strength and increase compressibility potential of sands. Harris et al. (1984) [7] showed that mica grains became more influential as their ratio in the mixture exceeded 10% by weight.

Lee et al. (2007) [8] studied influence of mica grain size on sand-mica mixture behavior in triaxial, direct shear and oedometer tests. They found that mica grains would increase global void ratio of the mixture when median mica grain size was equal to or larger than that of the sand. This was attributed to the bridging mechanism generated by the mica grains. This so called bridging effect was more pronounced with growing mica size resulting in a marked reduction in the stability and strength of the mixture. Knowledge on the dynamic behavior of silty sands involving platy grains such as mica flakes is limited. It can be said that it has not been systematically researched in the literature yet. Limited studies showed that mica grains could cause a considerable change in dynamic parameters of the sand such as shear modulus, damping ratio and shear wave velocity [8, 9].

Lee and Albesia (1974) [3] pioneered studies on post liquefaction volume change. In the last few decades, however, extensive experimental research was made regarding post-liquefaction volumetric strains of satu-

rated sands. It was stated that post-liquefaction volume change would attain a maximum value as the cyclic axial strain level exceeds 7~8% in cyclic triaxial tests [1, 3, 10~13]

It has long been known that fine grains were quite effective on liquefaction resistance of coarser soils [2, 4, 14]. The manner how plastic or non-plastic fines affect dynamic shear strength, however, has not been well understood yet. Although plastic fines contribute to the liquefaction resistance, there are cases where dynamic shear strength decreases at certain fine contents [4]. This is especially valid for low plasticity silts as they may separate sand grains enabling them to slide and roll over from each other more easily inside the mixture.

Findings on dynamic behavior of sandy and silty soils that contain platy grains (flake or plate shaped such as mica grain) are limited [8, 9]. In this study, effects of platy and non-plastic fine materials on post-liquefaction volume change of sandy soils are examined by means of a cyclic triaxial compression testing program.

Soil samples utilized throughout the study were obtained from a site well known with deep and saturated liquefiable soil deposits [2, 5]. The study area is located in northern Izmir Bay area on a Quaternary age old river delta (The Old Gediz River Delta). The Gediz River carried its sediments through valleys, which contain abundant amount of mica-schist rocks [15]. Disturbed sand samples from various depths were recovered down to 25 m below surface and transferred to the soil dynamics laboratory where artificial test specimens were prepared. Comprehensive liquefaction tests were made in cyclic triaxial testing device where post-liquefaction volumetric strains were measured at large axial strain levels (i.e. axial strains exceeding 8%) Influence of mica content on post-liquefaction volumetric strains was studied on test samples at different initial void ratios. The testing program also provided information regarding effect of non-plastic fines on post-liquefaction compressional behavior of sands with mica grains.

2 MATERIALS AND EXPERIMENTAL METHODS

Disturbed micaceous silty sand samples were recovered in eight engineering boreholes that were drilled down to ~25 m depth. Locations of the boreholes can be grouped into three sites as shown in Fig. 1. During drillings, Standard Penetration Test (SPT) was performed at 1.5 m depth intervals and test samples were obtained by means of SPT spoon.

Laboratory studies commenced with the physical separation of mica and sand grains in the field samples. Flotation technique as described by Geredeli et al. (1995) [16] was used for this purpose. Accordingly separated mica and sand portions can be seen in Fig. 2 where natural



Figure 1. Study area in the Old Gediz River Delta and locations of boreholes (modified from <http://maps.google.com>).

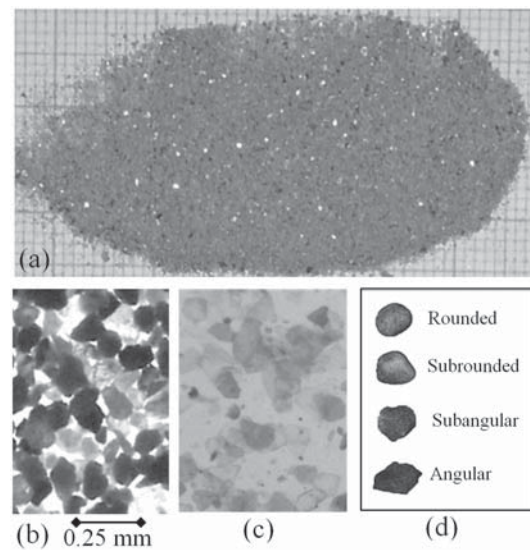


Figure 2. Images of test materials, (a) micaceous natural sand, (b) separated sand, (c) separated mica, (d) angularity chart.

micaceous sand is also given. One may notice in Fig. 2 that sand grains can be characterized as sub-angular.

X-Ray diffraction spectrometer (XRD) counts of artificial sand-mica mixtures were obtained in order to establish a correlation between XRD counts and mica portions. A sample XRD count plot is given in Fig. 3 where peaks

corresponding to mica grains at $2\theta=8.82^\circ$ are marked (2θ : angle of diffracted X-rays). The variation of XRD counts with respect to mica content is shown in Fig. 3. The procedure explained by Aydal (1990) [17] was utilized in order to establish the correlation. A simple linear regression that fit to the data yields Eq. 1:

$$M = (10.5 \times 10^{-3})X_{RD} - 3.7 \quad (1)$$

where M and X_{RD} stand for the mica content and XRD counts, respectively. Coefficient of correlation is equal to $(R^2) = 0.96$.

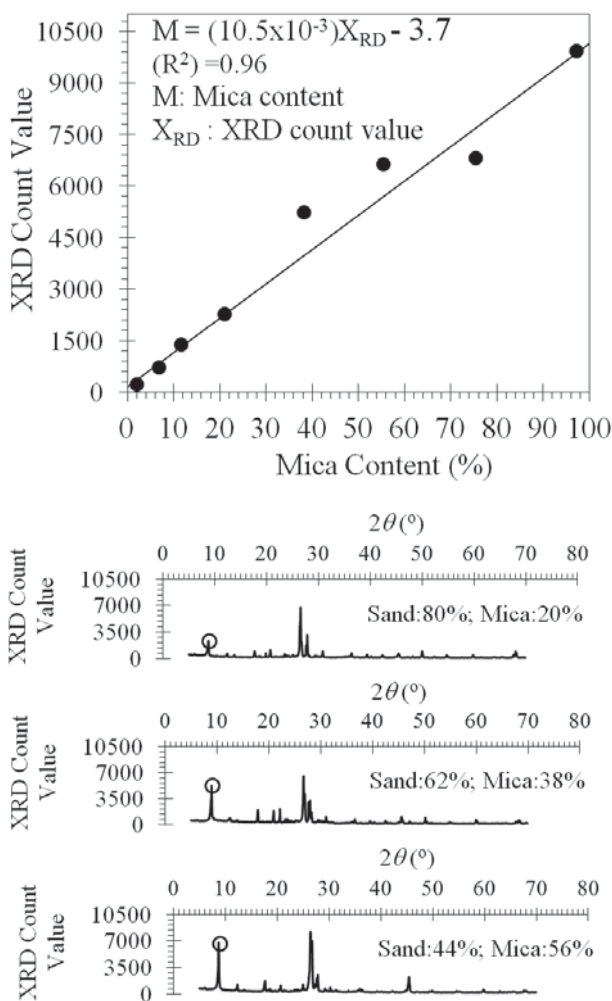


Figure 3. The relation between mica content by weight and XRD count values of test samples.

XRD values of field samples were also determined in order to obtain mica content variation with depth using Eq.1 (Fig. 4). As one can notice in Fig. 4, there is a slight increase in mica content with depth in Site-2 and Site-3 whereas variation is more remarkable to the depth of 12.4 m below ground surface in Site-1.

Fundamental characteristics of test soils were determined by means of standard index and classification tests. The maximum and minimum void ratios of artificially prepared sand-mica mixtures were found following the procedures of ASTM [18]. It can be

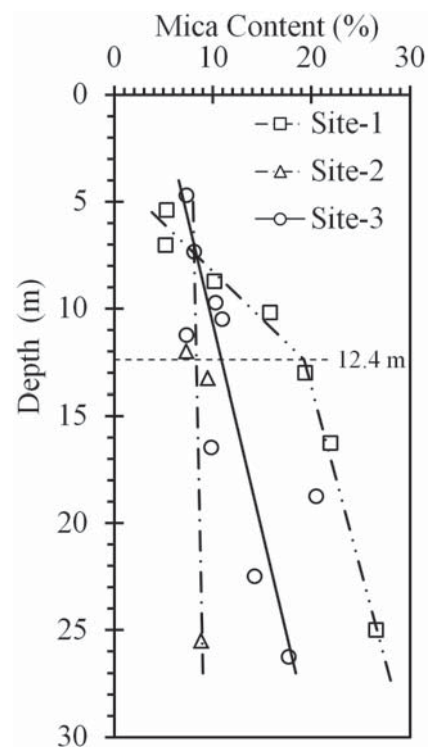


Figure 4. Variation of mica content of field samples with depth in Old Gediz River Delta.

followed in Fig. 5 and Table 1 that physically separated sand and mica samples are poorly graded. The natural field samples exhibit a rather wide variation range. Fig. 5 also contains liquefiable sands reported in the literature [19~23]. One should note that test materials of this study fall in the general range for liquefiable sands.

Great care was spend in order to obtain pure sand and mica samples by means of the floatation technique.

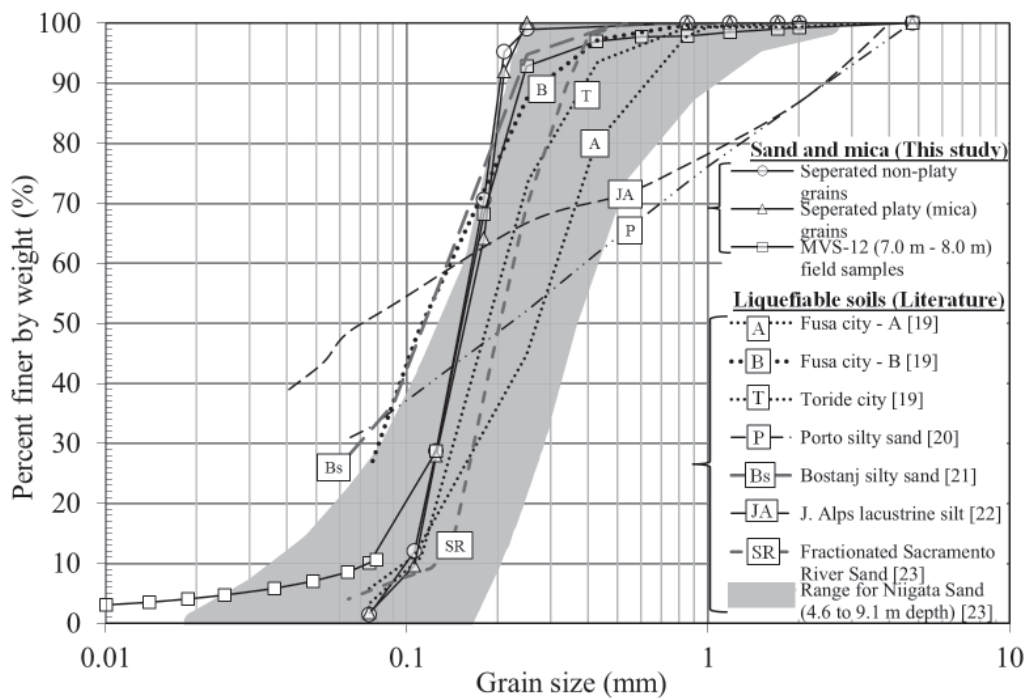


Figure 5. Grain size distribution for liquefiable soils including the test materials of this study.

However, a small amount of mica was left over in sand on the order of 1.5%. Mica grains in proportions of 5, 10 and 20% by weight were mixed with sand. These artificially prepared test mixtures were subject to undrained cyclic triaxial tests at varying relative densities (i.e. ~32%, ~47%, ~64 and ~79%). Similar

tests were also made on natural micaceous sand samples recovered 7.0~8.0 m below ground surface involving 10% non-plastic fine and 7.5% mica. Relative densities of the natural micaceous sand samples happened to be ~32%, ~52% and ~69% on the average.

Table 1. Physical characteristics and index properties of the test materials.

	Separated Sand (Non-platy grains)	Separated Platy Grains (Mica grains)	MVS-12 Borehole Sample (7.0 ^m -8.0 ^m)	Fine fraction of MVS- 12 Borehole Sample
Specific gravity, G	2.67	2.80	2.67	2.69
Coefficient of uniformity, c_u	1.67	1.64	2.30	39.70
Coefficient of curvature, c_c	0.98	0.89	1.33	2.70
Mean diameter, D_{50} (mm)	0.15	0.16	0.15	0.03
Maximum dry unit weight, γ_{dmax} (gr/cm ³)	1.54	1.23	1.75	1.17
Minimum dry unit weight, γ_{dmin} (gr/cm ³)	1.23	0.45	1.17	0.77
Minimum void ratio, e_{min}	0.74	1.28	0.53	1.28
Maximum void ratio, e_{max}	1.16	5.19	1.29	2.46
Fines Content, FC (%)	< 2.0	< 2.0	10.6	100.0
Plasticity Index, I_p	-	-	Non-Plastic	Non-Plastic

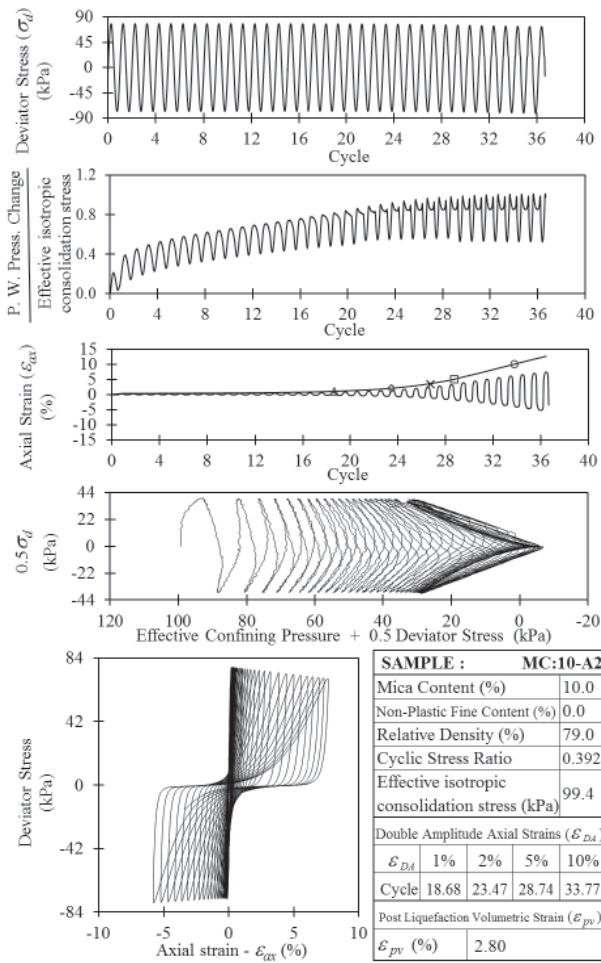


Figure 6. A typical liquefaction test for micaceous sand.

All of the 70 mm x 140 mm test samples were prepared in six layers using moist tamping method. In order to overcome saturation problem, carbon dioxide was circulated through the samples. Skempton's B value [24] was 0.975 or higher in the test. The loading frequency was 0.1 Hertz in cyclic undrained triaxial tests. The load was applied in terms of a sine wave. Samples were isotropically consolidated under 100 kPa prior to cyclic loading. Triaxial tests were terminated as the axial strain exceeded 8% and full liquefaction took place (Fig. 6). Following termination of the test, drainage was allowed and post-liquefaction volumetric strains (ε_{pv}) were measured. Axial strains (ε_{ax}) were transformed to shear strains (γ) by means of Eq. 2.

$$\gamma = (1 + \nu) \epsilon_{ax} \quad (2)$$

where Poisson's ratio (ν) is equal to 0.5 for undrained condition.

3 TEST RESULTS AND DISCUSSIONS

Post-liquefaction volumetric strains are plotted with respect to relative density in Fig. 7. The clean sand curve developed by Ishihara and Yoshimine (1992) [1] constitutes a lower bound for the results of this study. Multiple linear correlation study yields the following relationship among relative density (D_r), mica content (M), and post-liquefaction volumetric strain (ε_{pv}):

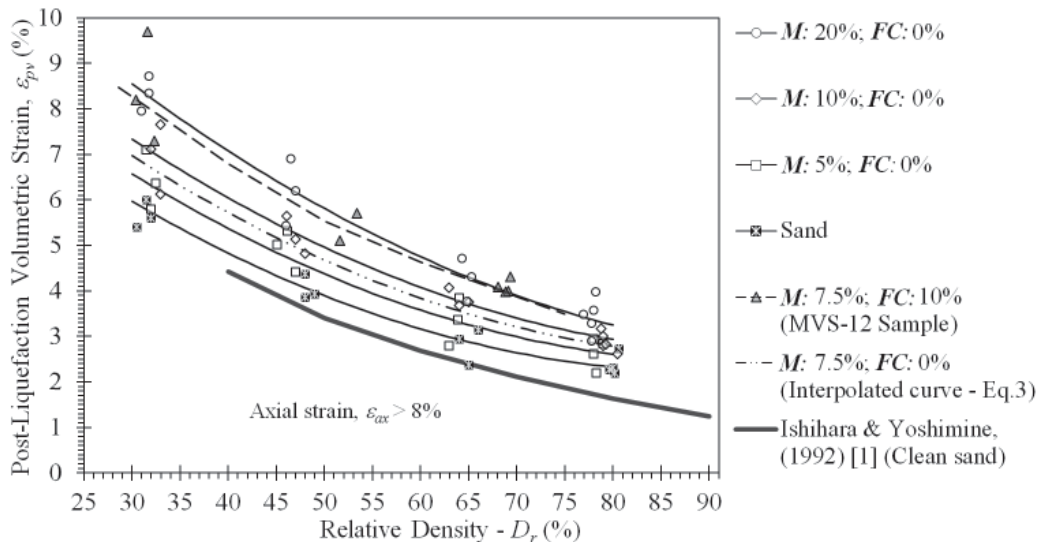


Figure 7. Post-liquefaction volumetric strain (ε_{pv}) of sand-mica mixtures and MVS-12 field sample which contains 7.5% mica and 10% non-plastic silt.

$$\varepsilon_{pv} = 10.28 - 0.1835D_r + 0.2387M + 0.00103D_r^2 - 0.0018D_r \times M - 0.0021M^2 \quad (3)$$

where D_r , M , ε_{pv} are expressed in percentage. Adjusted coefficient of correlation (R^2_{adj}) is found as 0.95.

Comparison of the volumetric strains of MVS-12 samples involving 7.5% mica and 10% non-plastic silt with the interpolated data using Eq. 3 corresponding to sand containing 7.5% mica with no fines shows that presence of non-plastic silts considerably increases post-liquefaction strains. One may note that the data obtained in this study are within the bounds of the literature. Influence of mica grains on volumetric strains is on the same order with that of the silt.

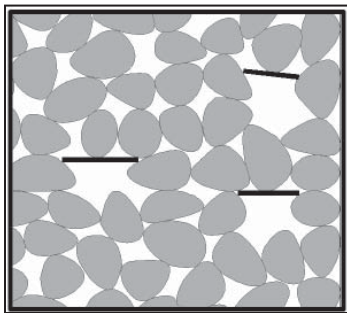


Figure 8. Bridging effect of the mica grains.

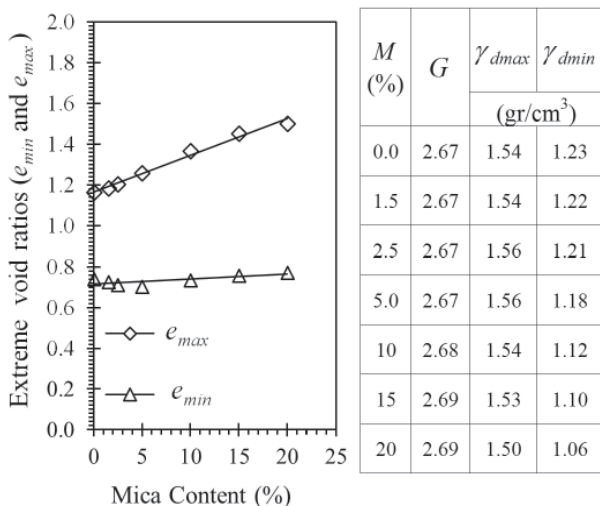


Figure 9. Maximum and minimum void ratios are plotted versus mica content with corresponding dry unit weights.

The fact that mica grains increase post-liquefaction volumetric strain at a certain relative density may be attributed to the bridging effect [8, 25] as shown in Fig. 8. It may be said that platy mica grains force the global void ratio to increase considerably by generating larger size voids inside the sand-mica mixture. This effect is more visible for loose samples. Larger number of bridges appears to collapse as compaction energy increases to form denser samples. This behavior may also be followed in Fig. 9.

Post-liquefaction volumetric strain of the Old Gediz River Delta sand sample containing non-plastic fine material is higher than that of the clean sand sample at same relative density containing same amount of mica. When post-liquefaction volumetric strain curve of clean sand for 7.5% mica content is compared with that of field samples containing 7.5% mica and 10% non-plastic fine material (Fig. 7), it can be seen that non-plastic fine material causes an increase in post-liquefaction volumetric strain. For instance, volumetric strains corresponding to relative density, $D_r = 40\%$ are determined as 5.7% and 6.8% for clean sand with 7.5% mica content (i.e., not including fine fraction) and MVS-12 field sample, respectively.

Fine material causes an increase in post-liquefaction volumetric strain potential and a decrease in stability of the sand. When grain size distributions of fine and coarse fractions are close to each other, fine grains may locate between contact points of coarse grains. Such fine grains at the contact points of coarse grains cause a decrease in the number of contact points. Therefore, stability of the materials decreases and compression potential of the materials increases. Consequently, fines may cause a decrease in stability and cause an increase in compressibility potential of coarse soils [26, 27]. Chien et al. (2000) [11] explored effects of fine content on post liquefaction settlement in an experimental study. In the study, it is reported that post liquefaction settlement increases with fine content for certain relative densities. This effect was also observed for the MVS-12 (7.0–8.0 m) sample containing 10% non-plastic fine materials.

Increasing trend due to mica content in extreme void ratio is more visible for e_{max} (Fig. 9). Same trend is also observed on variation of volumetric strain with respect to relative density (Fig. 7). These findings show that, mica grains become more effective on sand characteristics when the sample is loose. An increase in relative density reduces influence of mica grains on sand behavior. This indicates that bridging effect of mica grains is shaded with an increase in relative density of sand samples. In other words, in loose samples, more bridges are formed among sand grains by mica flakes.

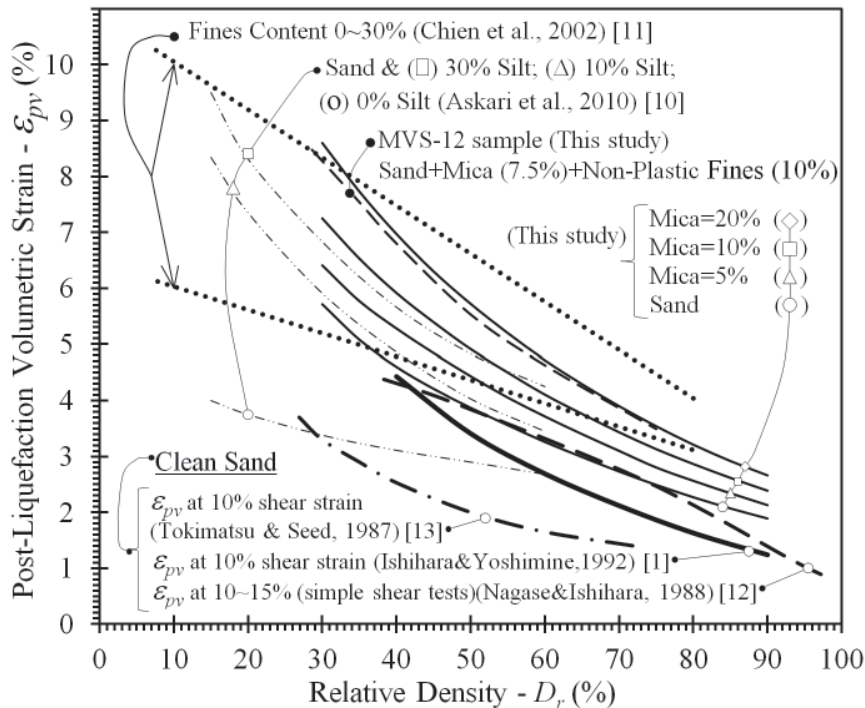


Figure 10. Comparison of test results with literature.

Non-plastic fines have a similar impact on volumetric strain as shown Fig. 7. Test results are plotted in Fig. 10 with the data available in the literature. One may note in Fig. 10 that post-liquefaction volumetric strain curve belonging to the clean sand sample of this study is in agreement with majority of data acquired from the literature. The curves pertaining to sands involving mica flakes demonstrate higher volumetric strains.

4 CONCLUSIONS

Platy mica grains and non-plastic fine materials cause a considerable increase in post-liquefaction volumetric strain of sandy soils. Test results of this study indicate that mica grains and fine materials have more effect on sand behavior for loose uniform fine sand. Mica influence on volumetric strain may be attributed to the formation of bridges among sand grains resulting in large size voids beneath platy mica grains. The effect of mica grains on sand behavior is less pronounced as relative density increases. It is thought that higher tamping effort applied to soil samples to increase the relative density results in smaller amount of mica bridges.

The relationship (Eq. 3) between relative density, mica content and post-liquefaction volumetric strain may be helpful in estimating such post-liquefaction settlement.

ACKNOWLEDGEMENTS

The authors are grateful to the support of The Scientific and Technological Research Council of Turkiye (TUBITAK) provided in the scope of research project 106G159 [28].

REFERENCES

- [1] Ishihara, K., Yoshimine, M. (1992). Evaluation of settlements in sands deposits following liquefaction during earthquakes. *Soils and Foundations*, Vol. 32, No. 1, pp. 173-188.
- [2] Youd, T. L., Idriss, I. M. (2001). Liquefaction resistance of soils: summary report from the 1996 NCEER and 1998 NCEER/NSF workshops on evaluation of liquefaction resistance of soils. *J. of Geotech. and Geoenviron. Eng.*, Vol. 127, No. 4, pp. 297-313.
- [3] Lee, K., Albesia, A. (1974). Earthquake induced settlements in saturated sands. *J. of ASCE*, Vol. 100, pp. 387-405.

- [4] Thevanayagam, S., & Martin, G. R. (2002). Liquefaction in silty soils—screening and remediation issues. *Soil Dynamics and Earthquake Eng.*, Vol. 22, pp. 1035-1042.
- [5] Seed, H. B. (1979). Soil liquefaction and cyclic mobility evaluation for level ground. *J. of the Geotechnical Eng. Division*, Vol. 105, No. GT2, pp. 201-254.
- [6] Žlender, B. and Trauner, L. (2007). The dynamic properties of the snail soil from the Ljubljana Marsh. *Acta Geotechnica Slovenica*, Vol. 4, No. 2, pp. 49-61.
- [7] Harris, W.G., Parker, J.C., Zelazny, L.W. (1984). Effects of mica content on engineering properties of sand. *Soil Science Soc. of America J.*, Vol. 48, pp. 501-505.
- [8] Lee, J. S., Guimaraes, M., Santamarina, J. C. (2007). Micaceous sands: Microscale mechanisms and macroscale response. *J. of Geotech. and Geoenviron. Eng.*, Vol. 133, pp. 1136-1143.
- [9] Cabalar, A. F., Cevik, A. (2009). Modeling damping ratio and shear modulus of sand-mica mixtures using neural networks. *Eng. Geology*, Vol. 104, pp. 31-40.
- [10] Askari, F., Dabiri, R., Shafiee, A., Jafari, M. K. (2010). Effect of non-plastic fines content on cyclic resistance and post liquefaction of sand-silt mixtures based on shear wave velocity. *J. of Seismology and Earthquake Eng., JSEE*, Vol. 12, No. 1, pp.13-24.
- [11] Chien, L. K., Oh, Y. N., Chang, C. H. (2000). Evaluation of liquefaction resistance and liquefaction induced settlement for reclaimed soil. *Twelfth World. Conf. on Earthquake Eng., Auckland*, Paper No. 0386.
- [12] Nagase, H., Ishihara, K. (1988). Liquefaction-induced compaction and settlement of sand during earthquakes. *Soils and Foundations*, Vol. 28, No. 1, pp. 65-75.
- [13] Tokimatsu, K., Seed, H. B. (1987). Evaluation of settlements in sands due to earthquake shaking. *Journal of Geotechnical Engineering*, Vol. 113, No. 8, pp. 861-878.
- [14] Prakash, S., Guo, T., Kumar, S. (1998). Liquefaction of silts and silt-clay mixtures. *Geotechnical Earthquake Engineering and Soil Dynamics III*, Vol. 75, pp. 337-348.
- [15] Bingol, E. (1977) Murat Dagi jeolojisi ve ana kayac birimlerinin petrolojisi. *TJK. Bulteni*, Vol. 20, pp. 12-66.
- [16] Geredeli, A., Ozbayoglu, G. (1995). Simav feldspatinin flotasyonu. *Industrial Raw Material Symposium, Izmir*, pp. 71-81.
- [17] Aydal, D. (1990). Cevherdeki toplam demir yuzdesinin XRD-floresans radyasyon siddeti yardimiyla kantitatif olarak bulunmasi. *Maden Tetkik ve Arama Dergisi*, Vol. 111, pp. 133-152.
- [18] ASTM (2005). Annual Book of ASTM Standards. *American Society for testing and materials*, Vol. 04.08, Philadelphia.
- [19] Lenart, S., Koseki, J. and Miyashita, Y. (2012). Soil liquefaction in the tone river basin during the 2011 Earthquake of the Pacific coast of Tohoku. *Acta Geotechnica Slovenica*, Vol. 12, No. 2, pp. 5-15.
- [20] Amaral, M.F., Rios, S. and Viana da Fonseca, A. (2012). Yielding in the isotropic compression of Porto silty sand. *Acta Geotechnica Slovenica*, Vol. 9, No. 1, pp. 30-45.
- [21] Lenart, S. (2008). The response of saturated soils to a dynamic load, *Acta Geotechnica Slovenica*, Vol. 5, No. 1, pp. 37-49.
- [22] Žlender, B. and Lenart, S. (2005). Cyclic liquefaction potential of lacustrine carbonate silt from Julian Alps, *Acta Geotechnica Slovenica*, Vol. 2, No. 1, pp. 23-31.
- [23] Seed, H. B. and Idriss I. M. (1967). Analysis of soil liquefaction: Niigata Earthquake. *Journal of the Soil Mechanics and Foundation Division Proceedings of the ASCE*. Vol. 93, No. SM3, pp. 83-108.
- [24] Skempton, A. W. (1954). The pore-pressure coefficients A and B. *Geotechnique*, Vol. 4 No. 4, pp. 143-147.
- [25] Santamarina, J. C., Cho, G. C. (2004). Soil behaviour: Role of particle shape. *Proceeding Skempton Conference. London*, pp. 1-14.
- [26] Monkul, M. M., Yamamuro, J. A. (2011). Influence of silt size and content on liquefaction behavior of sand. *Canadian Geotechnical Journal*, Vol. 48, pp. 931-942.
- [27] Lade, P. V., Liggio, C. D., Yamamuro, J. A. (1998). Effects of non-plastic fines on minimum and maximum void ratios of sand. *Geotechnical Testing Journal, GTJODJ*, Vol. 21, No. 4, pp. 336-347.
- [28] Modeling of Seismic Behavior of Soils for Safe Structural Design in Izmir Metropolitan Area and Aliaga, Menemen Towns. (2011). *Earthquake Research Center of Dokuz Eylul University (DAUM) and TUBITAK*. TUBITAK Project No: 106G159, Izmir, Turkiye.

EKSPERIMENTALNE IN NUMERIČNE ŠTUDIJE T-OBLIKOVANIH TEMELJEV

NIHAT KAYA İN MURAT ORNEK

o avtorjih

Nihat Kaya
Mustafa Kemal University,
Department of Civil Engineering
31200 Iskenderun / Hatay, Turčija
E-pošta: nihatkaya09@hotmail.com

Murat Ornek
Mustafa Kemal University,
Department of Civil Engineering
31200 Iskenderun / Hatay, Turčija
E-pošta: mornek@mku.edu.tr

izvleček

Temelji konstrukcij so podvrženi vertikalnim osnim obremenitvam, pogosto pa tudi ekscentričnim obremenitvam, ki jih povzročajo sile zemeljskega pritiska, potresov, vode, vetra itd. Zaradi ekscentričnih obremenitev se robova temelja posedata različno, kar povzroči nagibanje temelja in spremembo pritiska pod temeljem. Predlagana T-oblika temelja naj bi izboljšala nosilnost plitkih temeljev pri ekscentričnih obremenitvah. Pri vertikalni vstavitvi togih T-temeljev v nosilno zemljino pride do precejšnjega upora proti drsenju in prevrnjenju, ki je tako velik, da se nosilnost še zmanjša in posedanje poveča. V članku so predstavljeni številni eksperimentalni in numerični rezultati posedanja temeljev zaradi skrajnih obremenitev. Za preučevanje vplivov različnih parametrov, kot npr. problema geometrije in gostote zemljine, smo pripravili 48 modelnih preizkusov. Problem geometrije smo predstavili z dvema parametroma, ekscentričnostjo obremenitve (e) in globino vstavljanja (H) T-temelja v rahlo in gosto peščeno zemljino. Eksperimentalnemu delu so sledile še numerične analize, za katere smo uporabili računalniški program za ravninske deformacije z dvodimenzionalnimi končnimi elementi. Obnašanje T-temelja na peščenih posteljicah smo predstavili z modelom uterjevanja zemljine. Rezultati eksperimentalnih in numeričnih študij dokazujejo, da se lahko nosilnost temelja pri skrajnih ekscentričnih obremenitvah izboljša z vstavljanjem vertikalnega centralnega dela, ki se togo pritrdi na dno temelja. Krivulje posedanja zaradi obremenitve kažejo, da višja obremenitev privede do zmanjšanja nosilnosti pasovnega temelja. Dokazali so tudi, da se lahko glede na gostoto zemljine, v primerjavi z rahlim peskom, nosilnost temelja izboljša do štirikrat. Menimo, da je dala raziskava koristno osnovo za nadaljnje raziskovanje in omogočila boljše razumevanje T-temeljev.

ključne besede

modelni testi, metoda končnih elementov, T-temelj, ekscentrična obremenitev

EXPERIMENTAL AND NUMERICAL STUDIES OF T-SHAPED FOOTINGS

NIHAT KAYA and MURAT ORNEK

about the authors

Nihat Kaya
Mustafa Kemal University,
Department of Civil Engineering
31200 Iskenderun / Hatay, Turkey
E-mail: nihatkaya09@hotmail.com

Murat Ornek
Mustafa Kemal University,
Department of Civil Engineering
31200 Iskenderun / Hatay, Turkey
E-mail: mornek@mku.edu.tr

abstract

In addition to vertical axial loads, the footings of structures are often subjected to eccentric loads caused by the forces of earth pressures, earthquakes, water, wind, etc. Due to eccentric loading, the two edges settle by different amounts, causing the footing to tilt and then the pressure below the footing does not remain uniform. The T-shape is proposed as a footing shape for improving the bearing capacity of shallow footings against the action of eccentric loads. The vertical insertion of the rigid T-shaped footing, into the bearing soil, provides considerable resistance, against both of sliding and overturning, enough to regain the reduction in bearing capacity and increase in settlement. In this study, a series of experimental and numerical results from the ultimate loads and settlement of T-shaped footings are reported. A total of 48 model tests were conducted for investigating the effects of different parameters, such as the problem geometry and soil density. The problem geometry was represented by two parameters, the load eccentricity (e) and the insertion depth (H) of the T-shape into the loose and dense sand soil. After the experimental stage, the numerical analyses were carried out using a plane strain, two-dimensional, finite-element-based computer program. The behaviour of the T-shape footing on sand beds is represented by the hardening soil model. The results of the experimental and numerical studies proved that the ultimate bearing capacity of a footing under eccentric loads could be improved by inserting

a vertical central cut-off rigidly connected to the footing bottom. The load settlement curves indicate that the higher load eccentricity results in a decrease in the bearing capacity of the strip footing. It was also proved that the ultimate bearing capacity values can, depending on the soil density, be improved by up to four times that of the loose sand case. This investigation is considered to have provided a useful basis for further research, leading to an increased understanding of the T-shaped footing design.

keywords

model test, finite-element method, T-shaped footing, eccentric loading, sand

1 INTRODUCTION

Shallow footings are used to carry different types of structures. These structures may transfer concentric or eccentric loads to their footings, according to the acting case of the loading. Apart from the vertical axial loads, the footings of portal framed buildings are often subjected to eccentric loads caused by the forces of earth pressures, earthquakes, water, wind, etc. Sometimes the corner of the column of these portal-framed buildings is located very close to the property line, and hence subjected to eccentric loading. The eccentricity in a strip footing, e , is defined as the ratio of the moment (M) to the vertical load (Q). For designing footings subjected to earthquake forces, adopting appropriate values of the horizontal and vertical seismic coefficients, equivalent seismic forces can be conveniently evaluated. These forces in combination with static forces make the foundations subjected to eccentric and/or eccentric-inclined loads. The problems of footings subjected to eccentric loads are frequently encountered by an engineer in the case of the footings of the retaining wall, abutments, columns, stanchions, portal framed buildings, etc. Due to eccentric loading, the two edges settle by different amounts, causing the footing to tilt and the pressure

below the footing does not remain uniform. The amount of tilt and the pressure at the base depend on the value of the eccentricity width ratio.

The T-shape is a footing shape used to improve the bearing capacity of shallow footings against the action of eccentric loads. In addition to the vertical settlement, eccentrically loaded footings may also be affected from both horizontal displacement (and sliding) and/or rotation (or overturning), which are reasons that can reduce the ultimate bearing capacity and increase the settlement. The vertical insertion of the proposed rigid T-shaped footing, into the soil, provides considerable resistance, against both sliding and overturning, enough to regain the reduction in bearing capacity and the increase in settlement.

Experimental, numerical and theoretical studies of the bearing capacity of differently shaped footings under an eccentric load have been carried out by many researchers in the past. Patra et al. [1] conducted laboratory model tests to determine the ultimate bearing capacity of an eccentrically loaded strip foundation supported by geogrid-reinforced sand. Based on the laboratory test results, an empirical relationship, called the reduction factor, was suggested that correlates the ratio of the ultimate bearing capacity of an eccentrically loaded foundation with that for a foundation where the load is applied centrally. It is reported that the reduction factor is a function of the foundation depth and eccentricity. Singh et al. [2] presented the result of the laboratory model tests on the effect of soil confinement on the behaviour of a model footing resting on Ganga sand under an eccentric-inclined load. The results indicate that the ultimate bearing capacity of the square footing can be appreciably increased by soil confinement under axial load as well under an eccentric-inclined load. It has been observed that such a confinement resists the lateral displacement of the soil underneath the footing, leading to a significant decrease in the vertical settlement and hence improving the ultimate bearing capacity. Saleh et al. [3] performed tests with skirted foundations, in which a vertical or inclined wall surrounds one or more sides of the soil mass beneath the footing that is one of the recognized bearing capacity improvement techniques. Various load inclination angles, load eccentricities and skirt lengths were investigated. They found that sliding resistance is the most critical factor in the overall stability of the flat strip footing subjected to a high load inclination angle. Increasing the skirt inclination angle increases the ultimate bearing capacity and decreases the corresponding settlement. The rate of improvement increases with the increase of the load inclination angle. Sadoglu et al. [4] performed a series of tests with an eccentrically loaded model surface shallow strip footing

on reinforced, dense sand to investigate the decrease of the ultimate loads with increasing eccentricity. It is shown that the ultimate load decreases with increasing eccentricity. Joshi and Mahiyar [5] presented a new type of foundation that is very useful under the eccentric inclined loading conditions. The Angle Shaped Footing under the eccentric inclined load has been observed. This was after conducting a series of experiments and verifying the experimental results with the Ansys package that is based on the Finite-Element Technique. It has been observed that the angle-shaped footing becomes more effective when the angle of the projection with the vertical is in the range 150 to 300. The horizontal displacements in the footing due to the inclined eccentric loading are also reduced to large extent and have been found to be a maximum up to 1 to 2% of the width of the foundation. Musso and Ferlisi [6] investigated the behaviour of a model strip footing, resting on a saturated dense sandy soil, subjected to centred or eccentric vertical loading. Experimental tests, carried out on a small-scale physical model, are able to reproduce the effective stress levels equivalent to those prevailing in the prototype problems. The collapse mechanism is formed either by one or two sliding surfaces, depending on both the load eccentricities and the hydraulic gradient values. Significant differences were shown to occur between the centred and the eccentric loading footing response. Nawghare et al. [7] investigated the bearing capacity of the eccentrically loaded footing. Testing for the bearing capacity of the centrally loaded footing and then for the eccentrically loaded footing with a different e/B ratio was carried out. For every footing the bearing capacity and the settlement were found for the central as well as the eccentric loading. These results of the central and eccentric loading are compared with each other for the same footing. The results of the different footings are also compared for the central and eccentric loading. It is found that for the rectangular footing, as the size of the footing increased the bearing capacity has increased in the cases of the footing loaded centrally and the eccentrically loaded footings. For a square footing it is observed that there is no large difference in the bearing capacity of the footing for the central load ($e/B=0$) as well as in the eccentric loads, but a considerable difference is observed in the settlement of the footing. There are also researchers who studied the eccentric loading as numerical and theoretical perspectives. These include Taibeat and Carter [8], Taibeat and Carter [9], Hjiat et al. [10], Saran et al. [11] and Loukidis et al. [12]. Loukidis et al. [12] used the finite-element method for the determination of the collapse load of a rigid strip footing placed on a uniform layer of purely frictional soil subjected to inclined and eccentric loading. The footing was set on the free surface of the soil mass

with no surcharge applied. The soil was assumed to be elastic–perfectly plastic, following the Mohr–Coulomb failure criterion. Analyses for the associated and non-associated flow rules yielded essentially the same trends regarding the effective width, the inclination factor and the normalized vertical force–horizontal force–moment failure envelope. The results showed that the inclination factor depends on the value of the friction angle, whereas the effective width does not. Srinivasan and Ghosh [13] investigated the interaction between two nearby surface circular footings by conducting a number of laboratory-scale model tests on a dry, cohesionless Ennore sand bed. The interference effect between two closely spaced circular footings is obtained. They concluded that the bearing capacity of a single isolated footing on a double-layer soil deposit decreases with an increase in the depth of the top weak layer and a significant change in the bearing capacity and the settlement of the interfering footing is observed in a single- as well as double-layer soil deposit. Veiskarami and Kumar [14] computed the ultimate bearing capacity of strip foundations subjected to a horizontal groundwater flow using the stress-characteristics method. A numerical solution has been proposed both for smooth and rough footings placed on frictional soils. They found that the magnitude of f_y reduces continuously with an increase in the value of i . For a given hydraulic gradient, the value of f_y was found to reduce further with a decrease in the value of Φ . He [15] conducted a series of computational modelings using the mesh-free local Petrov-Galerkin (MLPG) method to evaluate the bearing capacity and response behaviour of extended-length piles. It is concluded that the MLPG gives better accuracy in the results and the optimal length of the pile is directly related to the stiffness of the soil, when compared to the finite-element method. Dash [16] performed a series of model tests to develop an understanding of the influence of the geo-cell material on the load-carrying mechanism of the geo-cell-reinforced sand foundations under strip loading. It is concluded that the performance of the reinforced-sand foundation bed is influenced by the strength, stiffness, aperture-opening size and the orientation of the rib of the geo-cell material.

In this study, experimental and numerical investigations into the ultimate loads of T-shaped footings are reported. A total of 48 model tests in two different series was carried out using the facility in the Geotechnical Laboratory of the Civil Engineering Department of the Mustafa Kemal University, Iskenderun, Hatay, Turkey. The effect of eccentricity and the effect of the insertion depths under vertical loadings were investigated in Series I and Series II, respectively. The experimental and numerical studies in every series were performed both for the loose

and the dense sand conditions. The problem geometry was presented using two parameters, the load eccentricity (e) and the insertion depth (H) of the T-shape footing into the loose and the dense sand soils. The findings will help in a better understanding of the T-shaped footings design with a different soil density and with a different footing geometry. It is expected that the information presented in this study will provide a contribution to the literature results and will be an alternative source for the design and applications for geotechnical engineers. This will result in a decrease in the cost of construction and save simplicity and time for the engineer, the contractor and the owner of the construction.

2 EXPERIMENTAL INVESTIGATIONS

2.1 GENERAL

The experimental program was carried out using the facility in the Geotechnical Laboratory of the Civil Engineering Department of the Mustafa Kemal University, Iskenderun, Hatay, Turkey. The facility and a typical model are shown in Figures 1 and 2.

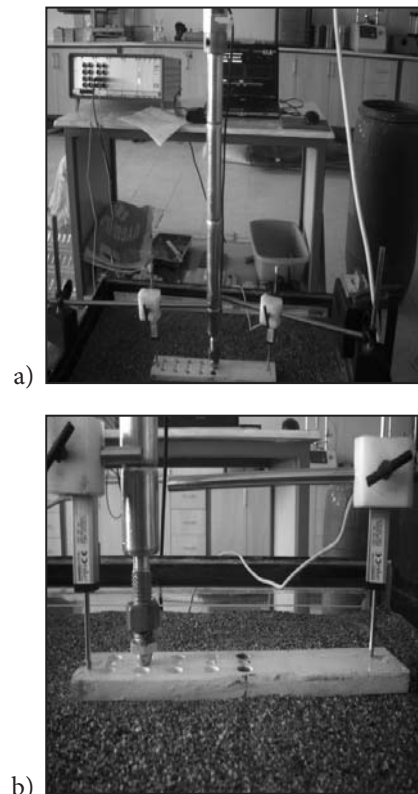


Figure 1. Test set-up: (a) overview; (b) footing.

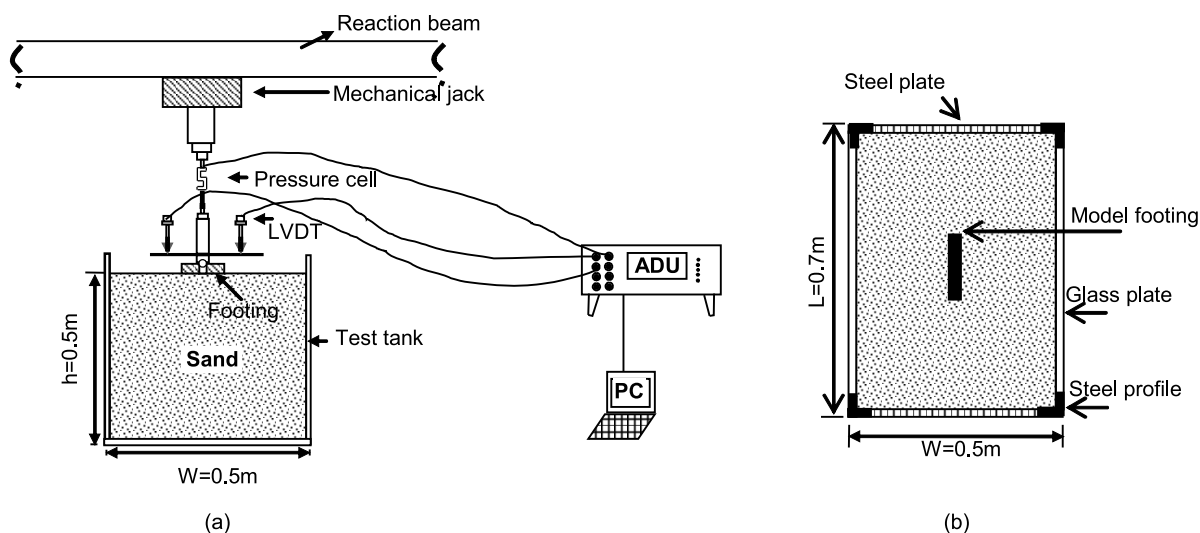


Figure 2. General layout of apparatus for the model test: (a) elevation; (b) plan view.

2.2 SOIL PROPERTIES

Uniform, clean, fine sand obtained from the Ceyhan River bed was used for the model tests. The laboratory tests were conducted on representative sand samples for the gradation, specific gravity, maximum and minimum densities and strength parameters. These properties are summarized in Table 1. The particle size distribution of this sand is shown in Figure 3. The model tests were conducted on loose sand and dense sand conditions. The angle of shearing resistances of the loose ($D_r=25\%$) and dense sand ($D_r=75\%$) at dry unit weights of 16.65kN/m^3 and 17.11kN/m^3 for normal pressures of 50, 100 and 200kPa were determined by direct-shear testing. The measured average peak friction angles were 36° and 42° for the loose and dense sands, respectively.

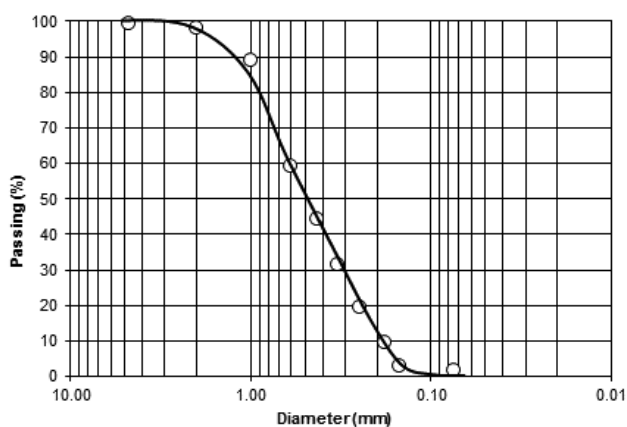


Figure 3. Particle size distribution of test sand.

Table 1. Properties of sand beds.

Property	Value
Coarse sand fraction (%)	0.00
Medium sand fraction (%)	65.00
Fine sand fraction (%)	35.00
D_{10} (mm)	0.16
D_{30} (mm)	0.28
D_{60} (mm)	0.58
Uniformity coefficient, C_u	3.63
Coefficient of curvature, C_c	0.84
Specific gravity	2.75
Maximum dry unit weight (kN/m^3)	17.11
Minimum dry unit weight (kN/m^3)	15.44
Dry unit weight of loose sand ($D_r=25\%$) (kN/m^3)	15.84
Dry unit weight of dense sand ($D_r=75\%$) (kN/m^3)	16.65
Cohesion, c (kPa)	0.00
The angle of shearing resistance of the sand, ϕ (degrees)	
Loose sand	36.00
Dense sand	42.00
Classification (USCS)	SP

Note: USCS = Unified Soil Classification System

2.3 MODEL FOOTINGS AND TEST TANK

Loading tests were carried out using a model rigid footing fabricated from mild steel, with a thickness of 15mm. The footing had a length of 30cm and a width

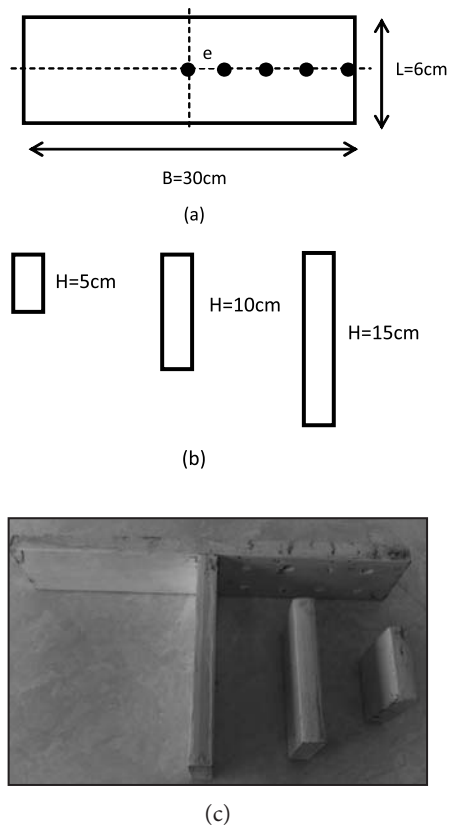


Figure 4. Strip footings: (a) plan view; (b) elevation; (c) photograph.

of 6cm. Figure 4 shows the geometry and the loading system of the model multi-edge footings considered in this investigation. The insertion depths are changed as 5, 10 and 15cm. The same footing ($L=6\text{cm}$ and $B=30\text{cm}$) was used and only the additional parts were assembled, respectively. The model test configurations were performed both for the loose and the dense sands.

Tests were conducted in a steel tank with dimensions of 0.7m (length), 0.5m (width) and 0.5m (depth). The bottom and vertical edges of the tank were stiffened using angle sections to avoid lateral yielding during the soil placement and loading of the model footing. The two side walls of the tank consist of 10-mm-thick glass plate and the other sides consist of 3-mm steel plate. Therefore, the inside walls of the tank were smooth enough to minimize the side friction. The boundary distances were greater than the footing length, the width and the depth, and during the tests it was observed that the extent of the failure zones was not more than the footing geometry, and the frictional effect was insignificant to affect the results of the model tests. Static vertical loads were applied to the model foundations using an electrically operated mechanical jack attached to a loading frame

located above the tank. Load and displacement measurements were taken using a pressure cell and two LVDTs installed between the jack and the model footing.

2.4 EXPERIMENTAL SETUP AND TEST PROGRAM

The sand bed was prepared up to the base level of the model footings in layers that were 50mm thick. Each layer was compacted by a hand-held vibratory compactor in the dense sand case. After the compaction of each sand layer, the next lift height was controlled using scaled lines on the glass plates of the test pit. After the bed's preparation, the sand was carefully levelled in the areas directly beneath the footing. This was to ensure that the model footing had full contact with the sand and that the load applied to the footing was vertical (normal). The model footing tests were performed with the sand at unit weights of 15.84kN/m^3 and 16.65kN/m^3 . To maintain the consistency of in-place density throughout the test pit, the same compactive effort was applied on each layer. The difference in the measured densities was found to be less than 1%. In all the tests the minimum depth of sand below the base of the model was 0.45 m. After the completion of each test, the test pit was excavated to a depth of $1.5B$ beneath the footing. This depth was chosen since the stress distribution calculated from the PLAXIS-2D computer program [17] dissipates to effectively zero at a depth of about $1.5B$ below the footing. That means that after the test was completed, only about the last 10 cm remained in the test box.

The model footing was placed on the surface of the sand bed at predetermined locations in the test pit. The vertical compressive load was gradually applied to the model footing by means of a mechanical jack supported against a reaction beam. Then the load was measured using a calibrated pressure cell. A ball bearing was positioned between the proving ring and the footing model to ensure that no extraneous moment was applied to the footing. A constant load increment was maintained until the footing settlement had stabilised. Settlements of the footing were measured using two calibrated LVDTs (Novotechnik TYP TR 50) placed on either side of the footing, as shown in Figure 2. For each test, the load-settlement readings were recorded with a sixteen-channel data-logger unit (MM700 series Autonomous Data Acquisition Unit) and converted to produce values of the settlement at ground level and load using Geotechnical Software-DS7 on a PC. The tests were continued until the applied vertical load was clearly reduced or a considerable settlement of the footing resulted from a relatively small increase in the vertical load. At the end of each test, the sand was carefully excavated.

Table 2. Details of model tests.

Test / Analysis Series	Soil Condition	Load Eccentricity	Insertion Depth	Number of Test or Analyses
I	Loose Dense	$e = 0 ; 0.1B ; 0.2B ; 0.3B ; 0.4B ; 0.5B$	$H = 0$	12
II	Loose Dense	$e = 0 ; 0.1B ; 0.2B ; 0.3B ; 0.4B ; 0.5B$	$H = 0.17B ; 0.33B ; 0.50B$	36

In this study, two series of experimental tests and numerical analyses were conducted on the T-shaped model footings. The details are given in Table 2.

3 FINITE-ELEMENT ANALYSIS

Numerical analysis is a powerful mathematical tool that makes it possible to solve complex engineering problems. The finite-element method is a well-established numerical analysis technique used widely in many civil-engineering applications, both for research and the solution of real engineering problems. The constitutive behaviour of the soils can be successfully modelled with numerical analyses. The finite-element method is one of the mathematical methods in which continuous media is divided into finite elements with different geometries. It provides the advantage of idealizing the material behaviour of the soil, which is non-linear with plastic deformations and is stress-path dependent, in a more rational manner. The finite-element method can also be particularly useful for identifying the patterns of deformations and stress distribution during deformation and at the ultimate state. Because of these capabilities of the finite-element method, it is possible to model the construction method and investigate the behaviour of shallow footings and the surrounding soil throughout the construction process, not just for the limit equilibrium conditions [18].

Numerical analyses were conducted using the program Plaxis 2D-V2011. It is a finite-element package that is specially developed for the analysis of deformation and stability in geotechnical engineering problems [17]. The stresses, strains and failure states of a given problem can be calculated.

The computer program used in this study incorporates a fully automatic mesh-generation procedure, in which the geometry is divided into elements of the basic element type, and compatible structural elements. Five different mesh densities are available in Plaxis, ranging from very coarse to very fine. In order to obtain the most suitable mesh for the present study, preliminary computations using the five available levels of global mesh coarseness

were conducted. Since there is not too much difference in the results for different mesh configurations, it was decided to use the fine mesh with a refinement around the footing in all the analyses. Plaxis generates full fixity at the base of the geometry and smooth conditions for the vertical sides, including the symmetric boundary. The modelled boundary conditions were assumed such that the vertical boundaries are free vertically and constrained horizontally, while the bottom horizontal boundary is fixed in both the horizontal and vertical directions. The soil medium was modelled using 15-node triangular elements. A typical graded finite-element mesh composed of the soil and footing, together with the boundary conditions and the geometry of the soil system used, is shown in Figure 5.

An elasto-plastic hyperbolic model called the hardening-soil model (HSM) was selected for the non-linear sand behaviour in this study. The HSM is an advanced model for simulating the behaviour of different types of soil, both soft and stiff. The HSM is formulated in the framework of the classical theory of plasticity and supersedes the hyperbolic model: first by using the theory of plastic-

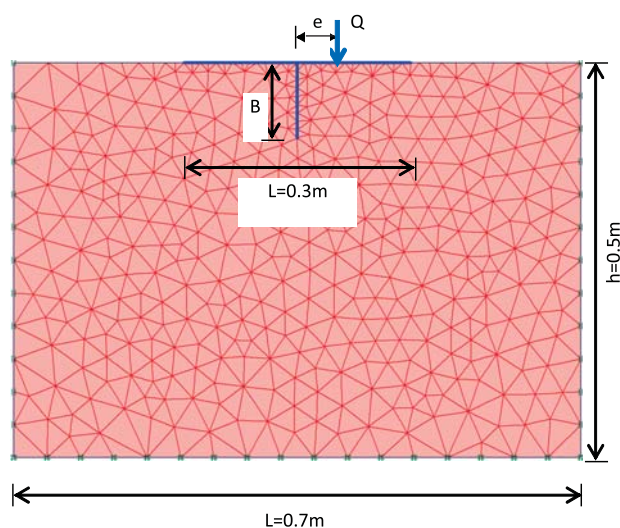


Figure 5. Typical mesh configurations in the numerical analyses.

ity rather than the theory of elasticity, second by including soil dilatancy, and third by introducing a yield cap [19]. The model T-shaped footing is modelled as a rigid plate, and is considered to be very stiff and rough in the analyses. Values of the Young's modulus and a Poisson's ratio of 207×10^6 kPa and 0.25, respectively, were assumed for the T-shaped footing. The number of triangular elements and nodal points varied with footing geometry arrangements, but the average numbers of triangular elements and nodal points in the mesh were 700 and 6000, respectively. The soil parameters in Table 3 represent the loose and dense sand used in the tests. Brinkgreve et al. [20] reported the following equations for calculating the HSM parameters. In the numerical parts of this study, the parameters for the sand soil were obtained using these equations.

$$E_{50}^{ref} = E_{oed}^{ref} = 6000 \cdot RD / 100 \quad (1)$$

$$E_{ur}^{ref} = 18000 \cdot RD / 100 \quad (2)$$

$$m = 0.7 - RD / 320 \quad (3)$$

$$R_f = 1 - RD / 800 \quad (4)$$

where E_{50}^{ref} , E_{oed}^{ref} , E_{ur}^{ref} are the stiffness parameters, RD is the relative density, m is the rate of the stress dependency. These parameters are proposed for considering, $p^{ref} = 100 \text{ kPa}$.

4 RESULTS AND DISCUSSION

4.1 GENERAL

Generally, the type of failure in sandy soil was observed as general shear failure. In this type of failure a peak value of Q_u is clearly defined in the curve of settlement against load (Figure 6).

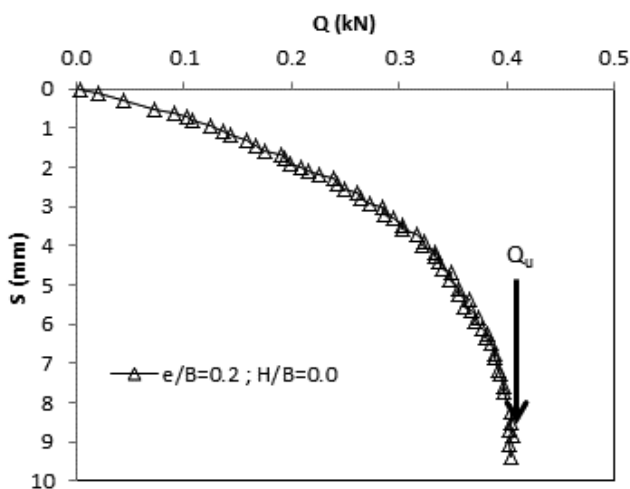


Figure 6. General shear failure.

Table 3. Model parameters for loose and dense sand soils.

HSM Parameters	Loose Sand	Dense Sand
p^{ref} (kPa)	100	100
γ_n (kN/m ³)	15.84	16.65
E_{50}^{ref} (kPa)	15000	45000
E_{ur}^{ref} (kPa)	45000	135000
E_{oed}^{ref} (kPa)	15000	45000
m	0.622	0.698
c (kPa)	0.1	0.1
ϕ (°)	36	42
Ψ (°)	6	12
ν	0.20	0.20
K_0	0.35	0.35
R_f	0.969	0.906

4.2 SERIES I: EFFECT OF LOAD ECCENTRICITY

Experimental and numerical studies were performed to investigate the effect of load eccentricity on the loose and the dense sand. A total of 12 tests and analyses were carried out using five different footing load eccentricities from $e/B=0.1$ to 0.5 and including the centric loading. The strip footing used in this series has a width of 0.3 m and length of 0.06 m (Figure 4). The load-settlement and bearing capacity-settlement curves of the loose sand case for different e/B ratios including centric loading are given in Figure 7. As seen from the figure the loads decrease with an increase in the load eccentricity. The settlement changes presented in Figure 7b are non-dimensional. The settlement ratio (S/L) is defined as the ratio of footing settlement (S) to footing length (L). Similar to the Q - S relations, the bearing capacity values decrease when the eccentricity ratio increases. For the case of $e/B > 0.3$, there is a dramatic decrease in the bearing capacity. Two examples for the loose sand ($e/B=0$ and $e/B=0.2$) are presented for a comparison of the experimental and numerical results in Figure 8. It is clear from the figure that the vertical displacements predicted by the numerical analysis are in good agreement with the experimental results for the centric loadings and an underestimation is observed for the eccentric loadings.

The relationships between the load-eccentricity ratio (e/B)-ultimate load (Q_u) and the load-eccentricity ratio (e/B)-ultimate bearing capacity (q_u), including the numerical results, are shown in Figure 9. The plots are given for both loose and dense sand. It is clear that the Q_u and the q_u values decrease with an increase in the load eccentricity in both the loose and

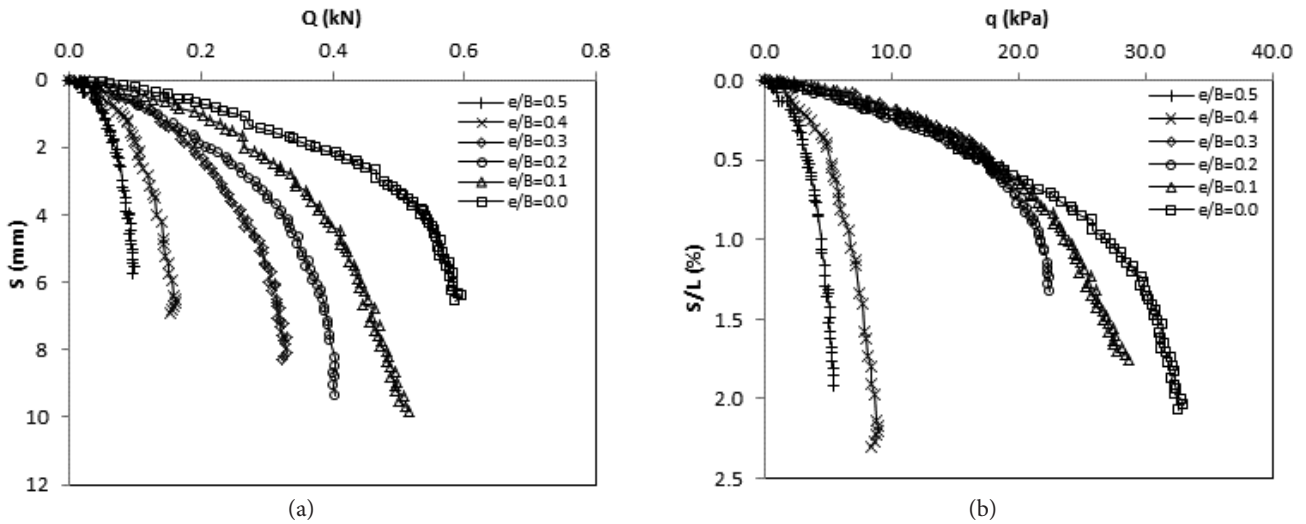


Figure 7. Load-settlement curves for load eccentricity ($H/B=0$).

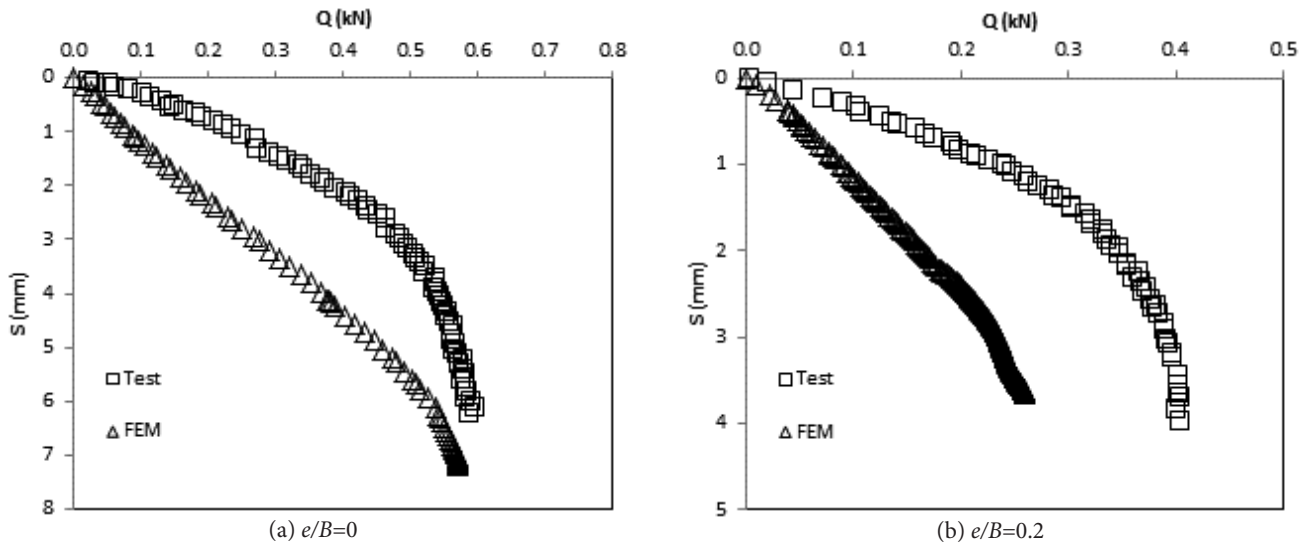


Figure 8. Comparison of test and numerical results for Series I.

dense sands. The test and numerical outcomes confirm the results from the literature [2; 4]. While the load eccentricity increases from 0 to 0.5, the ultimate load decreases by about 83% and 94% in loose and dense sands, respectively. For the same eccentricity ratio, the ultimate bearing capacity decreases by about 5.5 times and 16 times in loose and dense sand, respectively. For the numerical plots, similar behaviour was observed in both the loose and dense sands. The formation in the failure of eccentric footing occurs mainly at one side of the footing, in contrast to the symmetrical failure surfaces at both sides of the footing. This type of failure

mechanism for the eccentric footing loading was observed by many researchers [21–24]. Consequently, this failure mechanism causes less failure surface in the case of the eccentric footing than the same centric footing, since the ultimate load can be regarded as an effort to shear the soil mass along the potential failure surfaces. Due to the eccentric loading, the two edges settle by different amounts, causing the footing to tilt and the pressure below the footing does not remain uniform. The amount of tilt and the pressure at the base depend on the value of the eccentricity-width ratio.

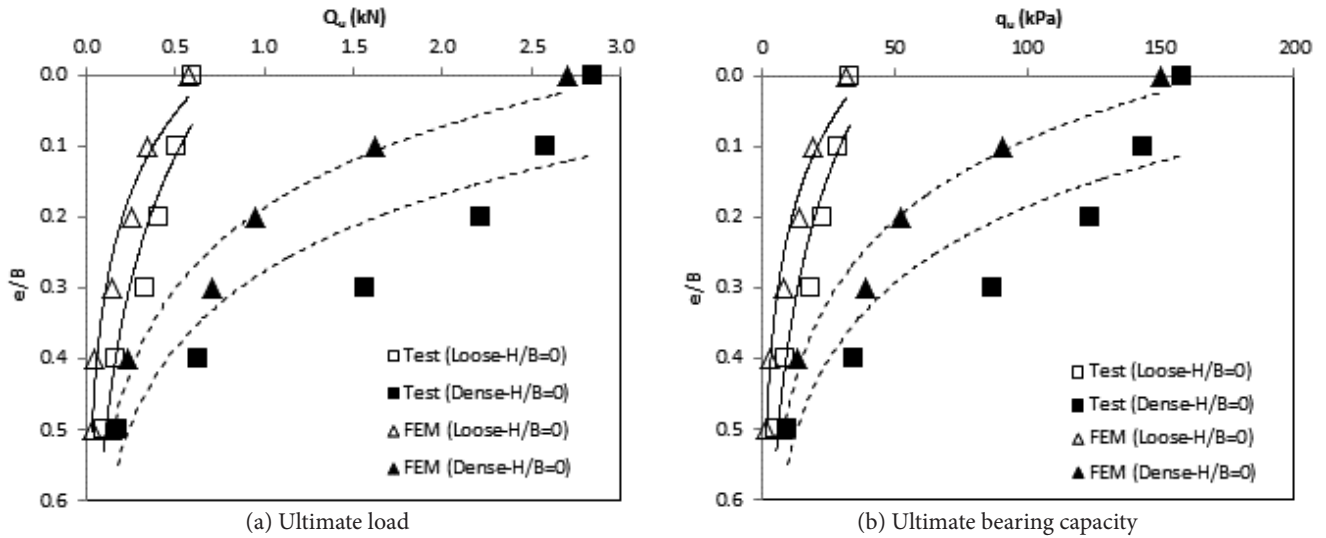
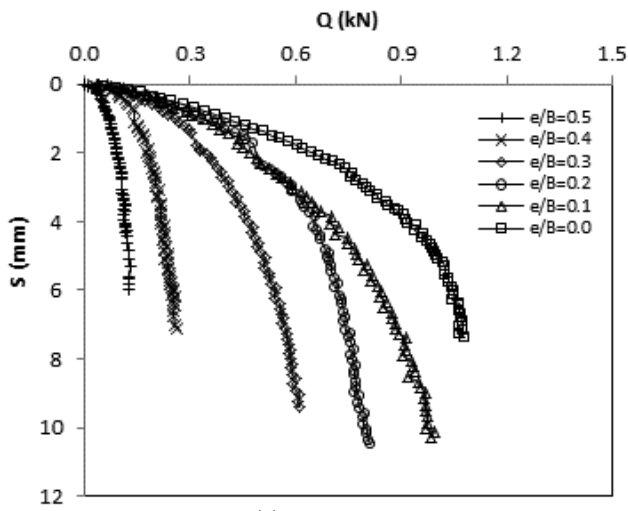
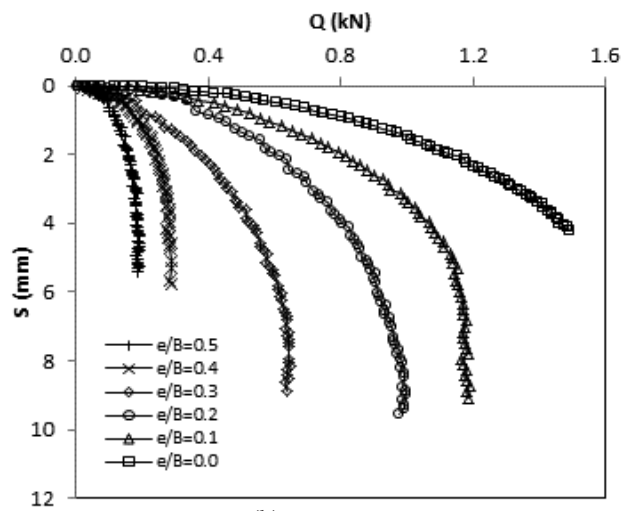


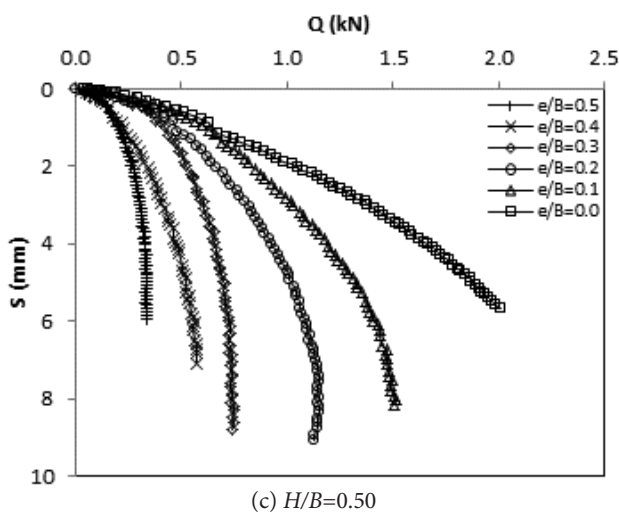
Figure 9. Effect of load eccentricity ($H/B=0$).



(a) $H/B=0.17$



(b) $H/B=0.33$



(c) $H/B=0.50$

Figure 10. Load settlement curves for different insertion depths.

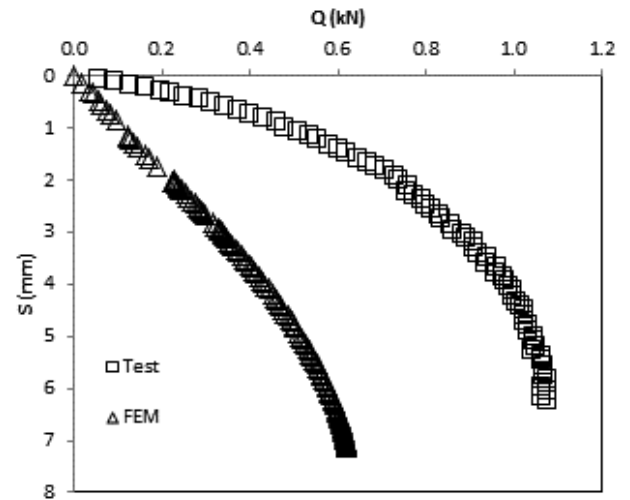


Figure 11. Comparison of test and numerical results for Series II.

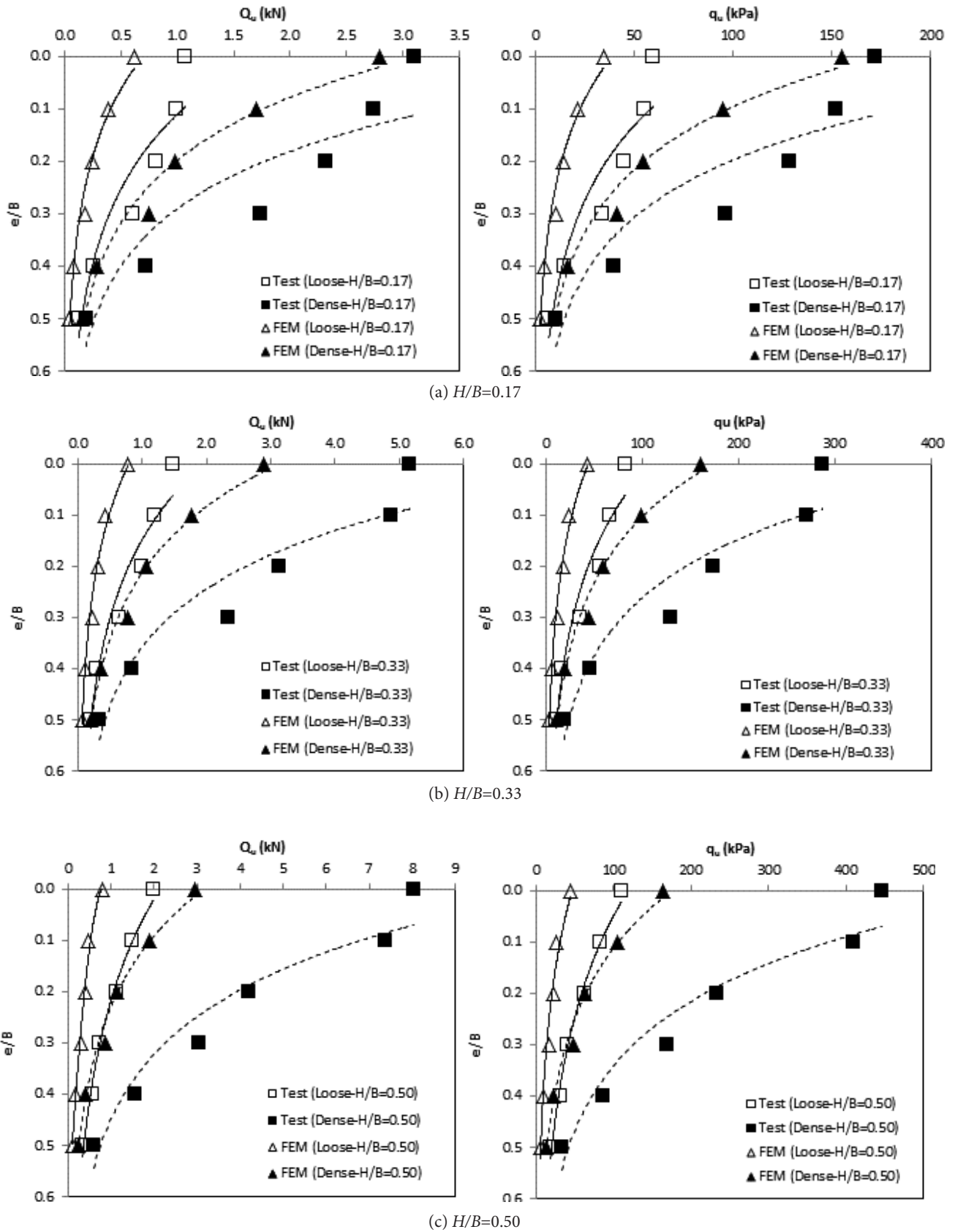


Figure 12. Ultimate values for different insertion depths.

4.3 SERIES II: EFFECT OF INSERTION DEPTH

In the previous series, the effect of eccentricity was examined. In this series (Series II), the disadvantages of the eccentricity are reduced or eliminated. For this purpose, the rigid T-shaped footing is inserted vertically into the bearing soil. This additional inserted part of the footing provides considerable resistance, against both the sliding and overturning, enough to regain a reduction in the bearing capacity and an increase in the settlement. A total of 36 tests and analyses were performed using three different insertion depths (H) of 5 cm, 10 cm, 15 cm and five different load eccentricities namely $e/B=0.1, 0.2, 0.3, 0.4$ and 0.5 , including the centric loading (i.e., $e/B=0.0$). The same footing ($L=6\text{cm}$ and $B=30\text{cm}$) is used and only the additional parts are assembled, respectively. The tests

and analyses are performed for both the loose and the dense sand conditions. Figure 10 shows the load-settlement plots for the inserted depths of $H=0.17B, 0.33B$ and $0.50B$ under the loose sand case. As seen from the figures, it is clear that the carrying loads decrease with an increase in the load eccentricity. It is also concluded that the depth-inserted part of the T-shaped footing has an important effect on the load-carrying capacity. For the same eccentricity ratio, the load increases when the inserted depth increases.

An example for the loose sand ($H=0.17B-e/B=0$) is presented for a comparison of the experimental and numerical results in Figure 11. Despite there being a similar tendency, the vertical displacements are underestimated by the numerical analysis when compared with the experimental results.

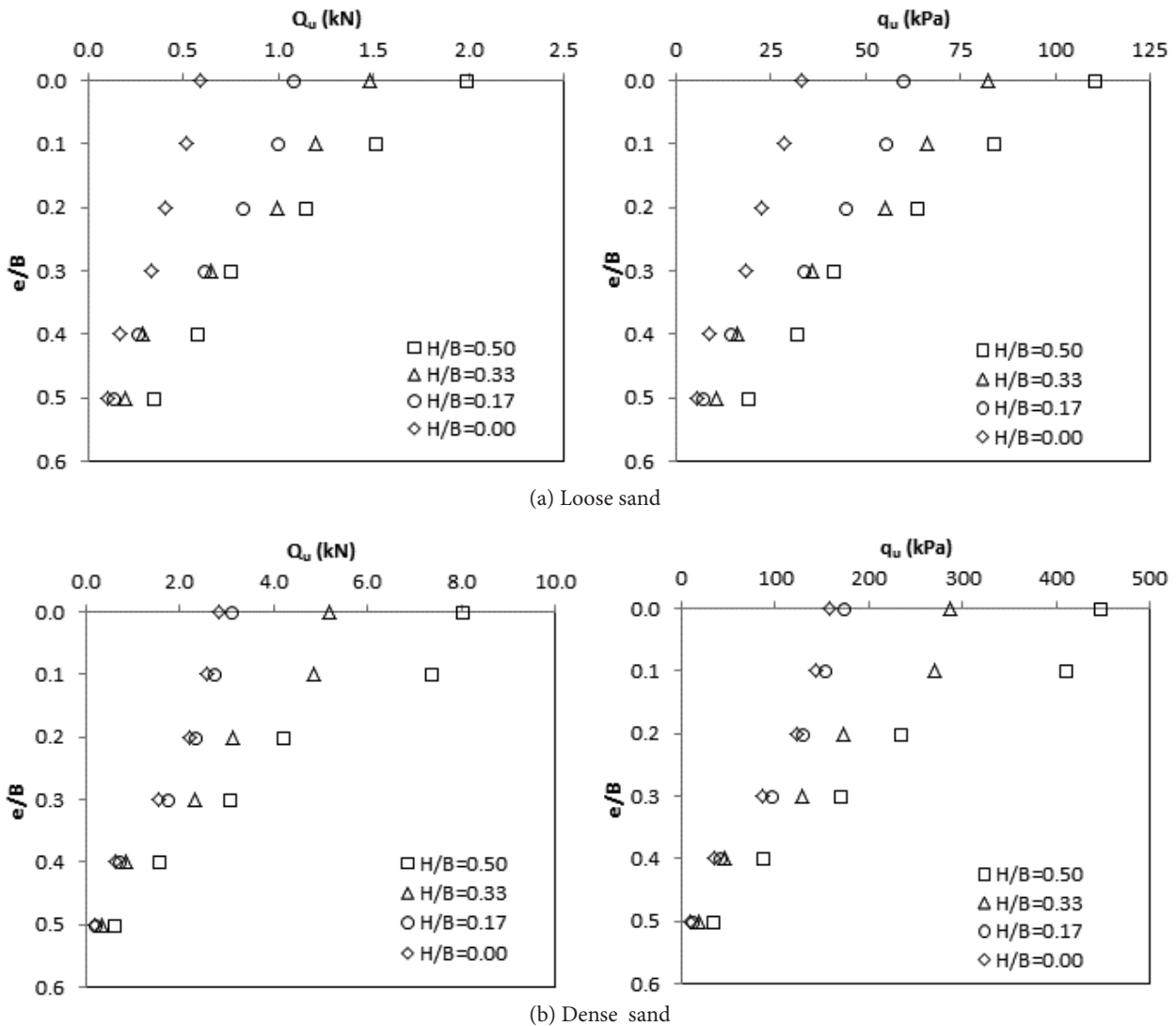


Figure 13. Effect of the insertion depths on the different soil densities.

The ultimate load (Q_u) and the ultimate bearing capacity (q_u) changes for the different e/B ratios, including the numerical results, are shown in Figure 12. These relations are presented for each H/B ratio and for both loose and dense sands. As seen from Figure 12 the ultimate values of Q_u and q_u decrease with an increase in the eccentricity ratio, e/B . Also, for the same eccentricity ratio, these ultimate values increase when the sand gets denser. It is expected that Q_u and q_u reach their maximum values at centric loading (i.e., $e/B=0$) both for loose and dense sand. From the lines in Figure 12a the ultimate load decreases about 16 times when the load eccentricity ratio increases from 0 to 0.5 for the dense sand. The similar logarithmic curves were obtained especially for the cases of $H=0.33B$ and $H=0.50B$. From the plots in Figure 12, similar tendencies are observed between the test and the numerical results. Generally, the finite-element method underestimates the ultimate values obtained from the experimental studies for both the loose and dense sands.

Figure 13 presents the Q_u and q_u relations with e/B ratios using another point of view. The plots are given for both loose and dense sands. As shown in the figures, the ultimate value increases when the insertion depth increases for each eccentric and centric loading. For example, for the loose sand under centric loading, the q_u value increases from 60kPa to 110kPa when the H value increases from $0.17B$ to $0.50B$. When the load is applied eccentrically (for example, $e=0.1B$, loose sand) the q_u values calculated are 55kPa and 84kPa for the H values $0.17B$ and $0.50B$, respectively. Similar behaviour is observed for both the loose and dense sands.

The effect of the inserted depth on the carrying load for the loose sand is investigated for the same eccentric ratio, in Figure 14. The graphs are given for the centric loading ($e/B=0.0$) and the eccentric loading (here, $e=0.2B$ is selected) conditions. As shown in the figures, the load increases when the insertion depth increases. The same phenomenon is observed for both the centric and eccentric loading conditions. For a constant settlement value, such as 5 mm, the measured centric loads are 0.56kN, 1.05kN, 1.44kN and 1.92kN, for $H=0$, $H=0.17B$, $H=0.33B$ and $H=0.50B$, respectively. Similarly, for the eccentric loadings, the measured values considering the settlement of 2.5 mm are 0.38kN, 0.78kN, 0.99kN and 1.15kN. There is also a difference in the settlement values for the centric and the eccentric loading cases. On the other hand, the effect of the eccentricity (as discussed earlier) is easily seen from the plots.

The expected failure patterns under the eccentric loading conditions are discussed in Figure 15. As investigated in Figure 15a, under the action of a vertical eccentric load (Q), the footing is settled vertically as S , and rotates with a definite rotation angle. When the failure stage occurs or the carrying load exceeds the ultimate value, a one sided failure pattern will occur in the soil, as pointed out in Figure 15b. Due to the rotation component, the bearing capacity is dramatically decreased, so that, preventing the rotation could help in improving the carrying capacity of the footings. Therefore, a T-shaped footing is used to improve the bearing capacity of these footings against the action of the eccentric loads. Figure 15c shows this mechanism, i.e., the failure pattern of a T-shaped footing under the eccentric loading. In this mechanism, rotation prevention could be attributed to the resistance of the created additional passive zone. It is observed from the experimental results that with the increase in the insertion depth (H), the rotation could be prevented.

The finite-element method generates an effective analysis and evaluation of the displacements, stresses and forces in and around the soil, the stabilized bodies and the

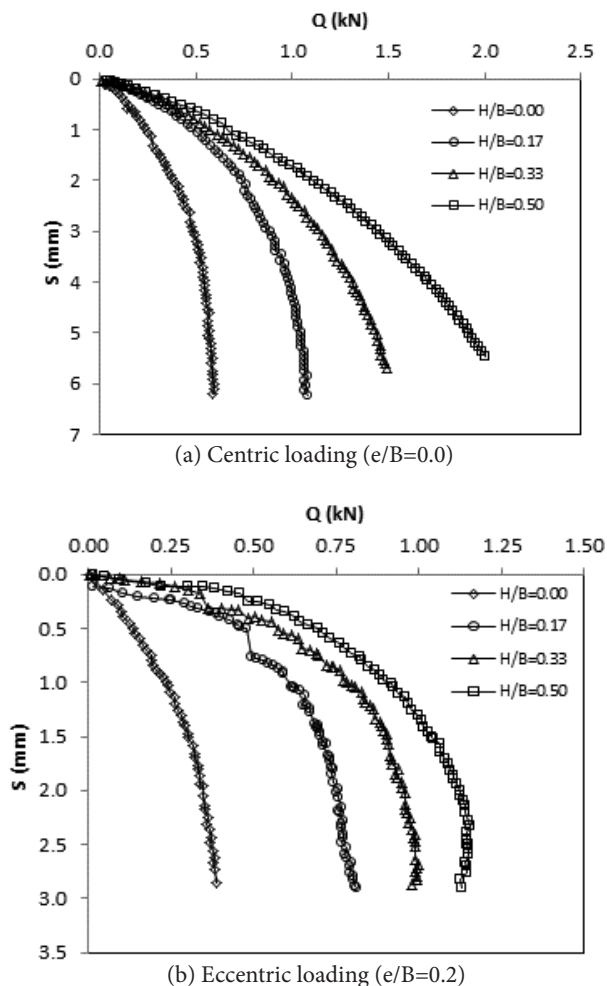


Figure 14. Effect of the insertion depths on the loading conditions.

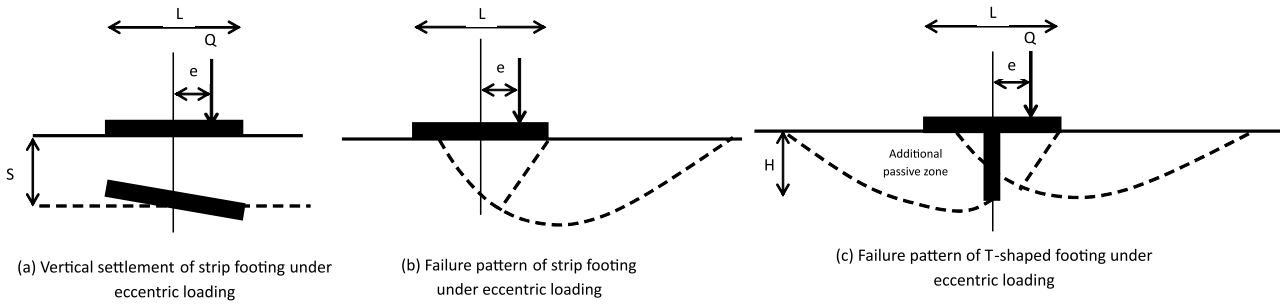


Figure 15. Collapse mechanism.

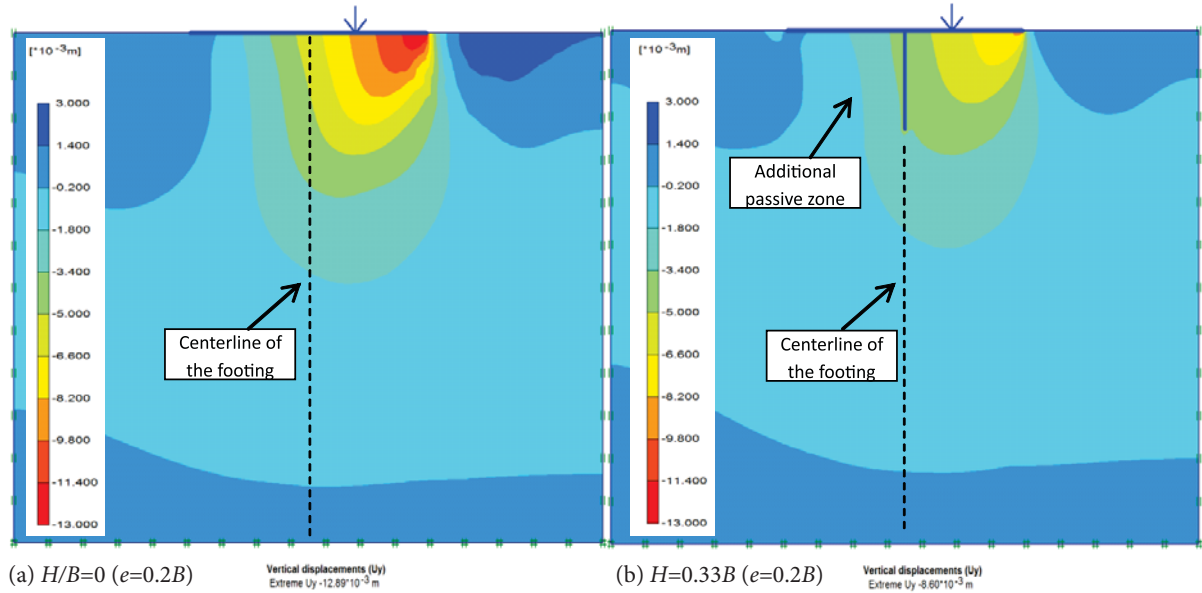


Figure 16. Vertical displacement fields below the T-shaped footings.

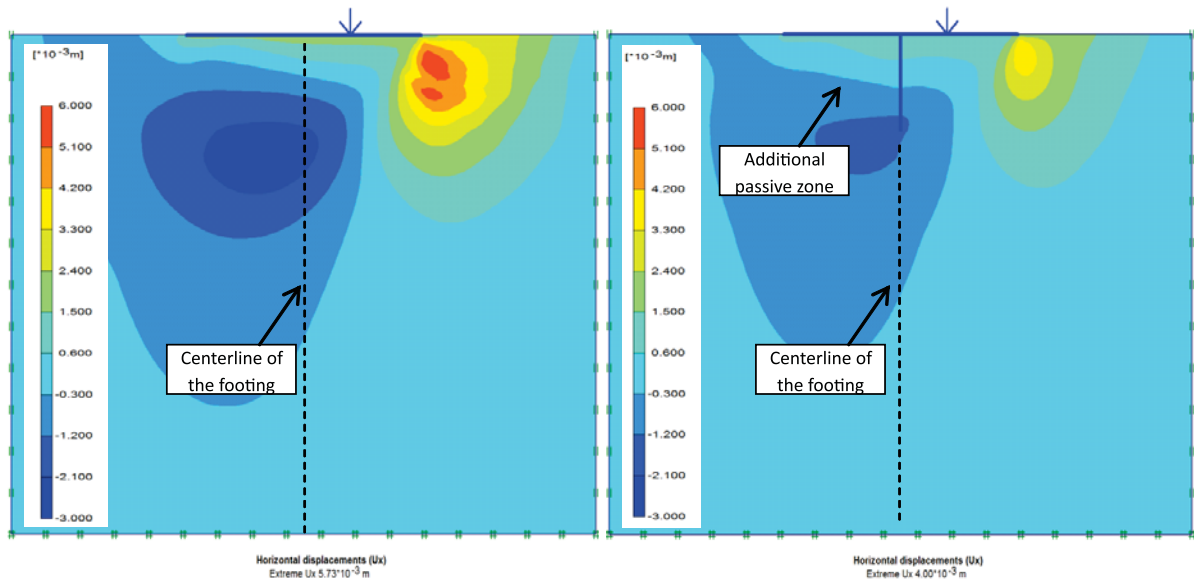


Figure 17. Horizontal displacement fields below the T-shaped footings.

footing. Figures 16 and 17 show some typical examples of the resultant vertical and horizontal displacement fields below the strip footing ($H/B=0$, $e=0.2B$) and the T-shaped footing cases ($H=0.33B$, $e=0.2B$) at the failure load of the strip footing. It can be seen that there is a clear reduction in the vertical and horizontal displacements for the T-shaped footing case compared with the strip footing case. A similar mechanism to that described in Figure 15 is observed numerically. In this mechanism, with the increase in the insertion depth (H), the rotation could be prevented. As seen from Figure 16, the maximum vertical displacement below the T-shaped footing decreases from 12.89×10^{-3} m to 8.60×10^{-3} m when the footing is supported by an insertion. In a similar manner, the maximum horizontal displacement values are 5.73×10^{-3} m and 4.00×10^{-3} m. The insertion part prevents the rotation of the footing by the additional passive zone.

Figure 18 shows the changes in the settlements along the length of the four different types (H/B ratio changes from 0 to 0.50) of footings. An eccentricity ratio of 0.2 is chosen. The horizontal axis represents the distances along the footings. The zero point refers to the centre of the footings. The settlement along the depth is seen in the vertical axis. These numerical data were obtained for the ultimate load of $H/B=0$ - $e/B=0.2$, i.e., for the strip footing condition. As seen from these numerical data, the settlement decreases when the H/B ratio increases. It is clear that there are heave zones in the

sand soil, well away from the application point of the load.

The maximum value for each footing type is obtained beneath the loading point. Similar findings were also obtained in the tests and the heave zones were visually observed.

5 LIMITATIONS

There are several limitations that should be mentioned. It is well known that full-scale loading test results are valid, especially for in-situ conditions and for soil properties in which the test was performed. However, a full-scale loading test is not economic, due to the expensive cost in terms of time and money that is required for the construction, instrumentation and testing. Therefore, small-scale model test studies are widely used as an alternative to full-scale loading tests, despite of their scale-errors [25]. Then, the tests were conducted on only one soil type. The results observed from this test program may be different for other soils. Additionally, only the model tests were introduced. The numerical analyses can also be included in future works, after some validation processes. The additional research using T-shaped footings with an angle and different geometries and soil beds is recommended as further investigations to improve the understanding of the bearing capacity and the settlement behaviour comprehensively, which may lead to developing a design method.

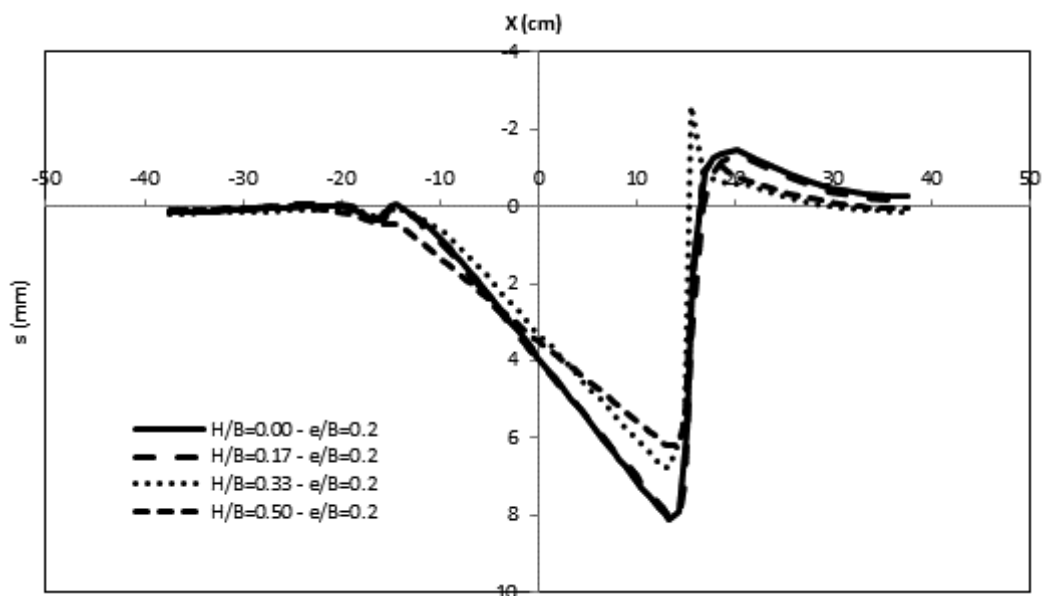


Figure 18. Settlement changes below the footings.

6 CONCLUSIONS

In this study, experimental and numerical investigations into the ultimate loads of T-shaped footings are reported. The effect of eccentricity and the effect of the insertion depths under vertical loadings were investigated in Series I and Series II, respectively. The studies in every test series were performed for both loose and dense sand conditions. At the end of the test and the numerical analysis, the load-settlement and bearing capacity-settlement curves were plotted. Based on the results of this investigation, the following main conclusions can be drawn:

- It is observed that the carrying loads and the bearing capacity of the strip footing decrease with an increase in the load eccentricity for both the loose and dense sands. There is a dramatic decrease in the bearing capacity, especially for the case of $e/B > 0.3$. The formation in the failure of the eccentric footing occurs mainly at one side of the footing, in contrast to the symmetrical failure surfaces on both sides of the footing.
- The ultimate loads and the ultimate bearing capacity values decrease with an increase in the load eccentricity. While the load eccentricity increases from 0 to 0.5, the ultimate loads decrease by about 83% and 94% in the loose and dense sand, respectively. For the same eccentricity ratios, the ultimate bearing capacity decreases about 5.5 times and 16 times in the loose and dense sand, respectively.
- The depth of the inserted part of the T-shaped footing has an important effect on the load-carrying capacity. For the same eccentricity ratio, the carrying load increases when the inserted depth increases.
- Similar to the strip footings, the ultimate values of the loads and the ultimate bearing capacities decrease with the increase in the eccentricity ratios for the T-shaped footings. And also, for the same eccentricity ratio, these ultimate values are increased when the sand gets denser.
- The ultimate loads and the ultimate bearing capacities reach their maximum values for the centric loading (i.e., $e/B=0$) both for loose and dense sand. The ultimate load decreases about 16 times when the load eccentricity ratio increases from 0 to 0.5 for the dense sand for the case of $H=0.17B$.
- The ultimate values increase when the insertion depth increases. For the loose sand under centric loading the q_u value increases from 60kPa to 110kPa when the H value increases from $0.17B$ to $0.50B$. When the load applied eccentrically (for example, $e=0.1B$) the q_u value increases are calculated as 55kPa and 84kPa for the H values $0.17B$ and $0.50B$. Similar

behaviour is observed both for the loose and dense sands.

- Numerical analyses, using an elasto-plastic hyperbolic model (Hardening Soil Model), gave results that have a similar tendency to those from physical model tests. Generally, the numerical model used in the analyses underestimates the test results. This means more conservative results are obtained with the numerical analyses.

Nevertheless, the investigation is considered to have provided a useful basis for further research leading to an increased understanding of the application of T-shaped footings to the ultimate bearing capacity and settlement problems.

REFERENCES

- [1] Patra, C.R., Das, B.M., Bhoi, M. and Shin, E.C. (2006). Eccentrically loaded strip foundation on geogrid-reinforced sand. *Geotextiles and Geomembranes*, Vol. 24, No. 4, pp. 254–259.
- [2] Singh, V.K., Prasad, A. and Agrawal, R.K. (2007). Effect of soil confinement on ultimate bearing capacity of square footing under eccentric–inclined load. *EJGE*, Vol. 12, Bund E.
- [3] Saleh, N.M., Alsaied, A.E. and Elleboudy, A.M. (2008). Performance of skirted strip footing subjected to eccentric inclined load. *EJGE*, Vol. 13, Bund F.
- [4] Sadoglu, E., Cure, E., Moroglu, B. and Uzuner, B.A. (2009). Ultimate loads for eccentrically loaded model shallow strip footings on geotextile-reinforced sand. *Geotextiles and Geomembranes*, Vol. 27, No. 3, pp. 176–182.
- [5] Joshi, D.P. and Mahiyar, H.K. (2009). Effectiveness of angle shaped footings resting on soil under eccentric inclined load. *International Journal of Theoretical Applied Mechanics*, Vol. 4, No. 1, pp. 95–105.
- [6] Musso, A. and Ferlisi, S. (2009). Collapse of a model strip footing on dense sand under vertical eccentric loads. *Geotechnical and Geological Engineering*, Vol. 27, No. 2, pp. 265–279.
- [7] Nawghare, S. M., Pathak, S. R. and Gawande, S. H. (2010). Experimental investigations of bearing capacity for eccentrically loaded footing. *International Journal of Engineering Science and Technology*, Vol. 2, No. 10, pp. 5257–5264.
- [8] Taiebat, H.T. and Carter, J.P. (2001). A semi-analytical finite element method for three-dimensional consolidation analysis. *Computers and Geotechnics*, Vol. 28, pp. 55–78.

- [9] Taiebat, H.A. and Carter, J.P. (2002). Bearing capacity of strip and circular foundations on undrained clay subjected to eccentric loads. *Geotechnique*, Vol. 52, No. 1, pp. 61–64.
- [10] Hjiiaj, M., Lyamin, A.V. and Sloan, S.W. (2004). Bearing capacity of a cohesive-frictional soil under non-eccentric inclined loading. *Computers and Geotechnics*, Vol. 31, No. 6, pp. 491–516.
- [11] Saran, S., Kumar, S., Garg, K.G. and Kumar, A. (2007). Analysis of square and rectangular footings subjected to eccentric-inclined load resting on reinforced sand. *Journal of Geotechnical and Geoenvironmental Engineering*, Vol. 25, No. 1, pp. 123–137.
- [12] Loukidis, D., Chakraborty, T. and Salgado, R. (2008). Bearing capacity of strip footings on purely frictional soil under eccentric and inclined loads. *Canadian Geotechnical Journal*, Vol. 45, No. 6, pp. 768–787.
- [13] Srinivasan, V. and Ghosh, P. (2012). Experimental investigation on interaction problem of two nearby circular footings on layered cohesionless soil. *Geomechanics and Geoengineering: An International Journal*, 1–10.
- [14] Veiskarami, M. and Kumar, J. (2012). Bearing capacity of foundations subjected to groundwater flow. *Geomechanics and Geoengineering: An International Journal*, Vol. 7, No. 4, pp. 293–301.
- [15] He, W. (2012). Application of the meshfree method for evaluating the bearing capacity and response behavior of foundation piles. *International Journal of Geomechanics*, Vol. 12, No. 2, pp. 98–104.
- [16] Dash, S. (2012). Effect of geocell type on load-carrying mechanisms of geocell-reinforced sand foundations. *International Journal of Geomechanics*, Vol. 12, No. 5, pp. 537–548.
- [17] Brinkgreve, R.B.J., Swolfs, W.M. and Engin, E. (2011). Plaxis Finite Element Code for Soil and Rock Analysis. *Plaxis 2D 2011*.
- [18] Laman, M. and Yildiz, A. (2007). Numerical studies of ring foundations on geogrid-reinforced sand. *Geosynthetics International*, Vol. 14, No. 2, pp. 52–64.
- [19] Schanz, T., Vermeer, P.A. and Bonnier, P.G. (1999). The hardening soil model: formulation and verification. *Beyond 2000 in Computational Geotechnics*, A. A. Balkema Publishers, Rotterdam, pp. 281–296.
- [20] Brinkgreve, R.B.J., Engin, E. and Engin, H.K. (2010). Validation of empirical formulas to derive model parameters for sands. *Knowledge Base Publications of Plaxis, Plaxis B.V., Delft, Netherlands*.
- [21] Meyerhof, G. G. (1953). The bearing capacity of foundations under eccentric and inclined loads. *In: Proceedings of the Third International Conference on Soil Mechanics and Foundation Engineering*, pp. 440–445.
- [22] Prakash, S. and Saran, S. (1971). Bearing capacity of eccentrically loaded footings. *Journal of SM and FE Division ASCE*, Vol. 97, No. 1, pp. 95–117.
- [23] Uzuner, B.A. (1975). Centrally and eccentrically loaded strip foundations on sand. PhD thesis, Strathclyde University, Glasgow, Scotland.
- [24] Moroglu, B. (2002). The bearing capacity of the eccentrically loaded model strip footing on reinforced sand. PhD thesis, Black Sea Technical University, Turkey.
- [25] Dickin, E.A. and Nazir, R. (1999). Moment-carrying capacity of short pile foundations in cohesionless soil. *Journal of Geotechnical and Geoenvironmental Engineering, ASCE*, Vol. 125, No. 1, pp. 1–10.

UPORABA ANFIS-A PRI STABILNOSTNIH ANALIZAH STEN Z ŽEBLJANO ZEMLJINO

PRIMOŽ JELUŠIČ IN BOJAN ŽLENDER

o avtorjih

vodilni avtor

Primož Jelusič

University of Maribor,

Faculty of Civil Engineering

Smetanova 17, 2000 Maribor, Slovenija

E-pošta: primoz.jelusic@um.si

Bojan Žlender

University of Maribor,

Faculty of Civil Engineering

Smetanova 17, 2000 Maribor, Slovenija

E-pošta: bojan.zlender@um.si

izvleček

V članku so izvedli optimiranje varnostnega faktorja sidrane stene. Optimiranje so izvedli s pristopom nelinearnega programiranja in v ta namen razvili optimizacijski model OPTINC. Varnostni faktor in optimalni nagib sidra od horizontalne smeri sta odvisna od tipa sidrane stene. Na osnovi dobljenih rezultatov so razvili ANFIS-INC model za napovedovanje optimalnega nagiba sider za poljubno sidrano steno. Razvili so tudi model ANFIS-SF za napovedovanje varnostnega faktorja za različne nagibe sten, kota nagiba brežine, dolžine sider in premera vrtine. Ugotovili so, da se mora nagib sidra prilagoditi nagibu stene, dolžini sidra, kotu nagiba brežine in premeru vrtine. S povečanjem nagiba stene, dolžine sidra in premera vrtine se varnostni faktor povečuje. Po drugi strani pa se varnostni faktor zmanjšuje s povečanjem kota brežine. Uporaba nelinearnega programiranja in metode ANFIS (Adaptive Network based Fuzzy Inference System) omogoča obsežno analizo geotehničnih problemov.

ključne besede

žebljana zemljina, stabilnost stene, optimizacija, NLP, ANFIS

SOIL-NAIL WALL STABILITY ANALYSIS USING ANFIS

PRIMOŽ JELUŠIČ and BOJAN ŽLENDER

about the authors

corresponding author

Primož Jelušič
University of Maribor,
Faculty of Civil Engineering
Smetanova 17, 2000 Maribor, Slovenia
E-mail: primoz.jelusic@um.si

Bojan Žlender
University of Maribor,
Faculty of Civil Engineering
Smetanova 17, 2000 Maribor, Slovenia
E-mail: bojan.zlender@um.si

abstract

We present the safety-factor optimization for a soil-nail wall. The optimization is performed using the non-linear programming (NLP) approach. For this purpose, the NLP optimization model OPTINC was developed. The safety factor and the optimal inclination of the soil nails from the horizontal direction depend on the design of the soil-nail wall. Based on these results the ANFIS-INC model was developed for the prediction of the optimal inclination of the soil nail for any design of soil-nail wall. Additionally, an ANFIS-SF model was developed to predict the safety factor for different inclinations of the wall, the slope angle of the terrain, the length of the nails, and the hole diameter. It was found that the inclination of the soil nail should be adjusted to the inclination of wall, the length of nail, the slope angle of the terrain and the hole diameter. With increasing inclination of the wall, the length of the soil nail and the hole diameter, the safety factor is increasing. On the other hand, the safety factor is decreasing with the increasing slope angle of the terrain. The use of nonlinear programming and an Adaptive Network Based Fuzzy Inference System allows a comprehensive analysis of the geotechnical problems.

keywords

soil-nail, wall stability, optimization, NLP, ANFIS

INTRODUCTION

The idea of combining passive steel reinforcement and shotcrete was first used as a support system for underground excavations in rock. This system is known as the New Austrian Tunneling Method [1,2,3]. The soil-nailing support technique relies on the mobilization of the tensile strength of the steel reinforcement at relatively small deformations in the surrounding soil. The soil-nailing system was first used in 1972 to support an 18-m-high cut-slope near Versailles [4]. Since then, soil nailing was used in many locations in France [5,6], Germany [7,8,9] North America [10] and other countries. The use of soil-nail walls has substantially increased, because it has been demonstrated that soil-nail walls are technically feasible and, in many cases, a cost-effective alternative to the conventional retaining walls used in top-to-bottom excavations in temporary and permanent applications [11].

This paper presents the design analysis of a soil-nail wall. The internal stability of the soil-nail wall was calculated using a plane slip surface. Based on the analytical solutions for the nailed slopes an ANFIS-SF model was built. The depth of the excavation, the material properties of the soil, the number of nails, and the vertical and horizontal spacing of nails are constants, while the inclination of the wall, the slope angle of terrain, the length of the nails and the hole diameter are variables. The ANFIS-SF model predicts a safety factor for the initial design of the soil-nail wall. The safety factor is calculated for each angle (from 1° to 89°) of the slip surface. The critical angle of the slip surface is the one that has the smallest safety factor and depends on the inclination of the soil nails. Non-linear programming (NLP) was used to calculate the optimal inclination of the nails from the horizontal direction for different inclinations of the wall, the slope angle of the terrain, the length of the nails and the hole diameter. Based on the results obtained with NLP an ANFIS-INC model was built that allows a calculation of the optimal inclination of the soil nails for the initial design of the soil-nail wall.

Adaptive network fuzzy inference systems (ANFIS) have been applied to many geotechnical engineering problems and have demonstrated some degree of success [12,13,14, 15,16,17]. For braced excavations in soft clay, Goh et al. [18] developed a neural network model to provide initial estimates of the maximum wall deflections. With an efficient mathematical technique two ANFIS models were developed to predict the safety factor (ANFIS-SF) and the optimal soil-nail inclination (ANFIS-INC).

2 SOIL NAILING

Soil nailing is a construction technique that has many advantages over conventional retaining walls used in top-to-bottom excavations. However, passive anchors are mainly used for the temporary protection of the excavation, and where the displacement of retaining structures are permitted. The soil-nailing technique is carried out in stages:

1. excavation,
2. installation of the nails,
3. installation of the steel reinforcing bars or mesh and drainage,
4. shotcreting,
5. installation of the bearing plates.

These stages are repeated until the bottom of the excavation. The typical spacing between the soil nails is 1-2 m in the vertical and horizontal directions. The inclination of the soil nails is 5-30° from the horizontal direction. The holes are either cased or uncased depending on the type of soil and are, on average, 50 to 150 mm in diameter [11,19].

Soil nailing is a cost-effective alternative to pre-stressed anchors [20]. Soil nails are cheaper, mainly because they are made from cheaper materials. The use of soil nails is not suitable when the soil properties are inappropriate and displacements of supporting wall are not permitted [21]. Suitable soil properties for the use of passive anchors are:

1. natural cohesive materials, such as silts and low plasticity clays not prone to creep,
2. glacial till,
3. cemented sand with little gravel,
4. fine-to-medium sand with silt to acts as a binder.

Passive anchors are not recommended for the following soil conditions:

1. materials without cohesion,
2. loose granular soils,
3. silt and clay of high plasticity,
4. soft, cohesive soils that will not provide a high pullout resistance,
5. expansive clays,
6. the presence of groundwater.

The corrosion protection in aggressive soils has to be examined very closely in the soil-nailing system. The standard EN 14490:2010 (Execution of special geotechnical works - Soil nailing) establishes general principles for the execution, testing, supervision and monitoring of soil nailing. In aggressive soils, fully encapsulated nails are recommended.

The ultimate limit state (ULS) and serviceability limit state (SLS) are considered in the design and analysis of soil-nail walls. Three ULSs must be verified:

1. the external failure mode,
2. the internal failure mode,
3. the facing failure mode.

The major SLS is excessive wall deformation. According to Byrne [10], the external failure modes are those where failure surface do not intersect the nails and the internal failure modes intersect the nails. The external failure modes are:

1. global stability failure,
2. sliding stability failure,
3. bearing failure.

The internal failure modes are:

4. nail-soil pullout failure,
5. bar-grout pullout failure,
6. nail tensile failure,
7. nail bending failure.

The facing failure modes are:

8. facing flexure failure,
9. facing punching shear failure,
10. headed-stud failure.

Soil-nailed walls can withstand large deformation in all directions; therefore, they perform well during an earthquake. When large wall deformations are not permitted, soil nailing is not an appropriate retaining wall system.

3. PLANE SLIP SURFACE MODEL

An internal stability of soil nail wall could be calculated with different types of slip surface, such as plane slip surface, broken slip surface, parabolic slip surface, circular slip surface and logarithmic spiral slip surface. In this paper, the plane slip surface was used to calculate the safety factor. The geometry and geo-mechanics of the model are presented. The model is designed so that it is possible to change the geometric and geo-mechanical parameters. After determining the geometric design, the safety factor is calculated for each angle (from 1° to 89°) of the slip surface ϑ . The critical angle of the slip surface is the one that has the smallest safety factor.

3.1 GEOMETRY OF THE SOIL-NAIL WALL

The geometry of the soil-nail wall is shown in Fig. 1. In this model the depth of the excavation wall (H) and the spacings of the soil nails in the vertical direction (s_v) and the horizontal direction (s_h) were determined. The typical spacing between the anchors is 1–2 m and this is the same in the horizontal direction and the vertical direction. Based on these data it is possible to determine the number of anchors (N_0).

The geometry is designed so that it is possible to change the inclination of the wall (α), the slope angle of the terrain (β), the length of the nails (l), the inclination of

the soil nails (η), the spacing of the soil nails in the vertical direction (s_v) and the horizontal direction (s_h).

3.2 GEO-MECHANICAL MODEL OF SOIL-NAIL WALL

In the soil-nailing system for each nail, three bearing capacities are calculated:

1. tensile strength of the nail,
2. pull-out nail-bearing capacity,
3. nail-cap bearing capacity.

The strength characteristics of a nail represent the basic parameters to calculate the actual force in a nail. The tensile strength [11] of the nail is calculated with Eq. (1):

$$R_{1t} = \frac{\pi \cdot d_n^2 \cdot f_y}{4 \cdot SF_T} \quad (1)$$

where:

- R_{1t} is the strength against breaking (kN),
- d_n is the nail diameter (mm),
- f_y is the strength of the nail material (MPa),
- SF_T is the safety factor against breaking.

The pull-out resistance [11] is calculated with Eq. (2):

$$T_{1p} = \frac{\pi \cdot d \cdot q_s}{SF_p} \quad (2)$$

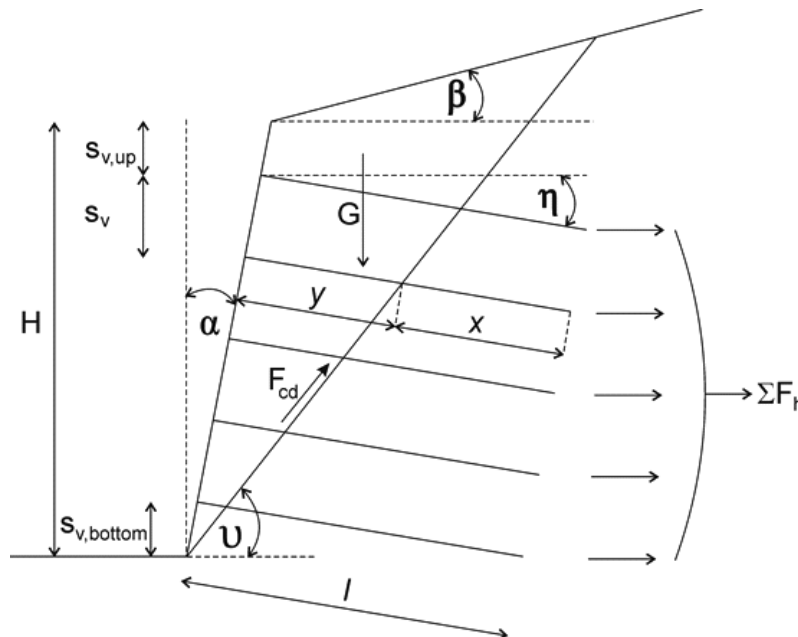


Figure 1. Internal stability analysis of a soil-nail wall using a plane slip surface.

where:

- T_{1p} is the pull-out nail bearing capacity (kN/m),
- d is the hole diameter (mm),
- q_s is the ultimate bond strength (kPa),
- SF_p is the safety factor against pull-out.

The nail head strength [11] is calculated with Eq. (3):

$$R_{1f} = \text{Min}(R_{1t}, T_{1p} \cdot l) \cdot ((0.6 + 0.2 \cdot (s_{\max} - 1))) \quad (3)$$

where:

- R_{1f} is the nail-cap bearing capacity (kN),
- l is the length of the soil nail (m),
- s_{\max} is the spacing of the soil nails in the horizontal or vertical direction, whichever is greater (m).

In plane slip a specific slip surface is examined for a variation of the angle ϑ . In an optimization analysis the calculation is carried out for different angles of the slip surface (From 1° to 89°). The safety factor is calculated for each angle of the slip surface. The ratio of resisting and shear (driving) forces acting on a slip surface should be greater than the minimum safety factor.

The forces acting on a slip surface are:

1. gravitational force parallel to the slip surface,
2. active earth pressure acting on the vertical part of the structure and parallel to the slip surface.

The resisting forces are:

3. the soil friction and cohesion along the slip surface,
4. the sum of the forces transmitted by the nails.

The nail force is determined based on the location of its intersection with the slip surface (see Fig. 1). If a nail is completely in front of the slip surface, then it does not enter the calculation. If a nail crosses the slip surface, then its force is determined with Eq. (4):

$$F = \text{Min}(T_{1p} \cdot x, R_{1t}, R_{1f} + T_{1p} \cdot y) \quad (4)$$

where:

- x is the nail length behind the slip surface in the direction of the soil body (m),
- y is the nail length in front of the slip surface (m),
- R_{1f} is the nail cap bearing capacity (kN),
- R_{1t} is the strength against breaking (kN),
- T_{1p} is the pull-out nail-bearing capacity (kN/m).

For the design, the tensile force distribution along the nail can be simplified, as shown in Fig. 2. The tensile force in the nail increases at a constant slope T_{1p} (equal to the pullout capacity per unit length), reaches a maximum value, R_{1t} , and then decreases at the rate T_{1p} to the value R_{1f} at the nail head.

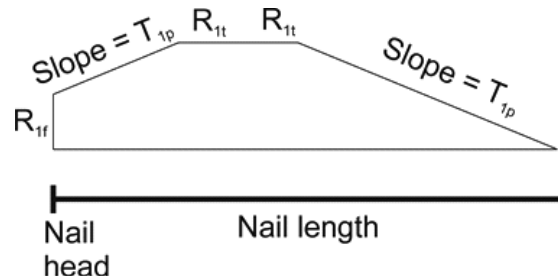


Figure 2. Distribution of the tensile force along the nail.

The safety factor [11] against global failure SF is expressed as the ratio of the resisting and driving forces, which act at a tangent to the potential failure plane:

$$SF = \frac{F_h \cdot \cos(\vartheta + \eta) + F_{cd}}{(G + S_{a,sv}) \cdot \sin(\vartheta) + S_{a,vod} \cdot \cos(\vartheta)} \quad (5)$$

$$F_h = \sum F_{h,n} \quad (6)$$

$$F_{cd} = \sum \frac{d_i}{d} (G \cdot \cos(\vartheta) + F_h \cdot \sin(\vartheta + \eta)) \cdot \tan(\varphi_i) + \sum d_{i,slip} \cdot c_i \quad (7)$$

where:

- G is the gravitational force (kN/m),
- $S_{a,sv}$ is the vertical component of active pressure (kN/m),
- $S_{a,vod}$ is the horizontal component of active pressure (kN/m),
- $d_{i,slip}$ is the length of the i^{th} section slip surface (m),
- d_{slip} is the length of the slip surface (m),
- $F_{h,n}$ is the bearing capacity of the n^{th} nail behind slip surface (kN/m),
- c_i is the cohesion of the i^{th} soil layer (kPa),
- φ_i is the angle of the internal friction of the i^{th} layer (°),
- ϑ is the inclination of the slip surface (°),
- η is the inclination of the nails from the horizontal direction (°).

The active earth pressure (the Coulomb theory) is given by Eq. (8)

$$\sigma_a = \sigma_z \cdot K_a - 2c_{ef} \cdot K_{ac} \quad (8)$$

where:

σ_z is the vertical geostatic stress (kPa),
 K_a is the coefficient of active earth pressure (-),
 K_{ac} is the coefficient of active earth pressure due to cohesion (-),

The horizontal and vertical components of the active earth pressure are:

$$S_{a,vod} = \sigma_a \cdot \cos(\alpha + \delta) \cdot \frac{H}{2} \quad (9)$$

$$S_{a,sv} = \sigma_a \cdot \sin(\alpha + \delta) \cdot \frac{H}{2} \quad (10)$$

where:

δ is the angle of the friction structure – soil (°).

3.3 OPTIMIZATION MODEL OPTINC

As the optimization problem of the soil-nail wall is non-linear, e.g., the objective function and the (in)equality constraints are non-linear, the non-linear programming (NLP) optimization approach is used and described in the paper. The retaining wall optimization using the NLP approach was presented by several authors [22, 23]. The general NLP optimization problem can be formulated as follows:

$$\text{Max } z = f(x)$$

subjected to:

$$\begin{aligned} h(x) &= 0 \\ g(x) &\leq 0 \\ x \in X &= \left\{ x \mid x \in R^n, x^{Lo} \leq x \leq x^{Up} \right\} \end{aligned}$$

where x is a vector of the continuous variables defined within the compact set X . The functions $f(x)$, $h(x)$ and $g(x)$ are nonlinear functions involved in the objective function z , equality and inequality constraints, respectively. All the functions $f(x)$, $h(x)$ and $g(x)$ must be continuous and differentiable. In the context of structural optimization, the variables include dimensions, cross-section characteristics, strains, materials, stresses, etc. The equality and inequality constraints and the bounds of the variables represent a rigorous system

of the design, loading, stress and resistance functions taken from the structural analysis and dimensioning. The optimization of the structures may include various objectives worthy of consideration. In this paper, a geo-mechanical objective function is proposed to maximize the safety factor of the soil-nail wall.

3.3.1 input data

Input data represent the design data (constants) for the optimization. The design data (constants) comprise the height of the soil-nail wall H (m), the vertical s_v (m) and the horizontal s_h (m) spacing of the nails, the number of nails N_o (-), the inclination of the wall α (°), the slope angle of the terrain β (°), the length of the nails l (m) and the hole diameter d (mm). In addition, the geo-mechanical data comprise the soil properties, such as the unit weight γ (kN/m³), the angle of the internal friction φ_{ef} (°), the cohesion of the soil (kPa), the ultimate bond strength of the soil nails in the soil q_s (kPa) and the structure-soil angle of friction δ (°).

3.3.2 variable

The inclination of the soil nails η (°) is declared as a variable in this optimization model (see Fig. 1).

3.3.3 geo-mechanical objective function

The objective function is defined with equation Eq. (11):

$$SF = \text{Max}(SF_{crit}) \quad (11)$$

The objective function SF includes the gravitational force G (kN/m), the vertical component of the active pressure $S_{a,sv}$ (kN/m), the horizontal component of the active pressure $S_{a,vod}$ (kN/m), the bearing capacity of the nails behind the slip surface F_h (kN/m), the resisting forces acting on a slip surface F_{cd} (kN/m).

3.3.4 geo-mechanical equality constraint

The critical angle of the slip surface ϑ_{crit} (°) is the one that has the smallest safety factor and depends on the inclination of the soil nails.

$$SF_{crit} = \text{Min} \left(\frac{F_h \cdot \cos(\vartheta + \eta) + F_{cd}}{(G + S_{a,sv}) \cdot \sin(\vartheta) + S_{a,vod} \cdot \cos(\vartheta)} \right) \quad (12)$$

3.3.5 design (in)equality constraint

The design (in)equality constraint determines the inclination of the soil nails from the horizontal direction η (°) to be calculated inside the defined limits.

$$\eta^{Lo} \leq \eta \leq \eta^{Up} \quad (13)$$

3.3.6 result of the optimization model

In order to interpret the proposed optimization approach, the paper presents a numerical example. The soil properties of silty sand are given in Table 1.

Table 1. Soil properties of silty sand.

Unit weight	γ	kN/m ³	18
Angle of internal friction	φ_{ef}	°	30
Cohesion of soil	c_{ef}	kPa	5
Angle of friction structure - soil	δ	°	20
Ultimate bond strength	q_s	kPa	100

The design data (constants), the initial values, and the lower and upper bounds of the design variable are given in Table 2.

Table 2. Design data, initial values, lower and upper bounds of the design variable (see Fig. 1).

Height of wall	H	m	8
Vertical spacing	s_v	m	1,5
Horizontal spacing	s_h	m	1,5
Inclination of wall	α	°	0
Slope angle of terrain	β	°	0
Length of nail	l	m	6
Hole diameter	d	mm	100
	Lower bound	Initial value	Upper bound
Inclination of nails η (°)	5	10	35

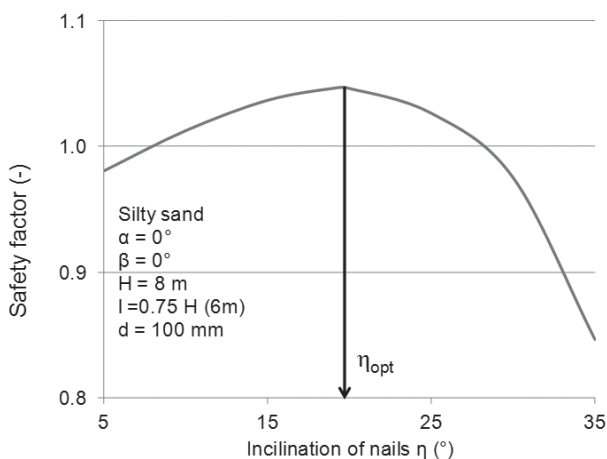


Figure 3. Optimal inclination of the soil nails from the horizontal direction η_{opt} .

The value of the safety factor is changing with the inclination of the nails η . The optimal inclination of the soil nails from the horizontal direction η_{opt} is defined with the maximum safety factor (see Fig. 3). In this numerical example the optimal inclination of the soil nails from the horizontal direction is $\eta_{opt} = 19.1^\circ$.

4 ADAPTIVE-NETWORK-BASED FUZZY INFERENCE SYSTEM

The basic structure of the fuzzy inference system (FIS) was introduced by Zadeh [24]. In this type of FIS it is essential to predetermine the rule structure and the membership functions. Human-determined membership functions are subjective and are different from person to person. Standard methods that transform human knowledge or experience into fuzzy rules and membership functions do not exist. Usually, there is a collection of input/output data, which we would like to use to construct the FIS model. The effective method for tuning the membership functions and minimizing the output error measure is the Adaptive-Network-Based Fuzzy Inference System (ANFIS). The ANFIS [25] uses given input/output data to construct a FIS, whose membership function parameters are tuned (adjusted) using either a back-propagation algorithm alone or in combination with a least-squares type of method. This adjustment allows fuzzy systems to learn from the data they are modelling. ANFIS only supports Sugeno-Takagi-Kang [26] identification models, which should

Table 3. Input and output data for two ANFIS models.

	ANFIS-SF	ANFIS-INC
Constants		
Height of wall H (m)	8	8
Vertical spacing s_v (m)	1.5	1.5
Horizontal spacing s_h (m)	1.5	1.5
$s_{v,up}$ (m)	1	1
$s_{v,bottom}$ (m)	1	1
Number of nails N_o (-)	5	5
Inclination of soil nail η (°)	10	-
Input data		
Inclination of wall α (°)	0, 10, 20	0, 10, 20
Slope angle of terrain β (°)	0, 15, 30	0, 15, 30
Length of nail l (m)	4, 6, 8	4, 6, 8
Hole diameter d (m)	50, 100, 150	50, 100, 150
Output data		
	Safety factor SF (-)	Inclination of soil nail η (°)

have only one output parameter. The adaptive network is a superset of all kinds of feedforward neural networks with a supervised learning capability [27]. ANFIS is a fuzzy inference system implemented in the framework of adaptive networks and uses the advantages of neural networks and fuzzy logic.

The safety factor SF and the optimal inclination of the soil nails from the horizontal direction η_{opt} depend on the design of the soil-nail wall. Therefore, the optimal inclination was calculated with the optimization model OPTINC for a different inclination of the wall α ($^\circ$), the slope angle of terrain β ($^\circ$), the length of the nails l (m) and the hole diameter d (mm). Based on these results the ANFIS-INC model was developed for the prediction

of the optimal inclination of the soil nail for any design of soil-nail wall. Additionally, the ANFIS-SF model was developed to predict the safety factor for different inclinations of the wall α ($^\circ$), the slope angle of terrain β ($^\circ$), the length of the nails l (m) and the hole diameter d (mm).

4.1 RESULTS OF GEO-MECHANICAL AND OPTIMIZATION MODEL

The soil properties of the geo-mechanical model are given for silty sand (see Table 1). The design data (constants) are given in Table 3. The series of calculations for the safety factor SF (-) and the optimal inclination soil nails η ($^\circ$) are given in Table 4. Table 4

Table 4. Output data for different combinations of input data.

Input				Output		Input				Output		Input				Output	
l (m)	α ($^\circ$)	β ($^\circ$)	d (mm)	SF (-)	η_{opt} ($^\circ$)	l (m)	α ($^\circ$)	β ($^\circ$)	d (mm)	SF (-)	η_{opt} ($^\circ$)	l (m)	α ($^\circ$)	β ($^\circ$)	d (mm)	SF (-)	η_{opt} ($^\circ$)
4	0	0	50	0.69	5.00	4	0	15	50	0.62	5.00	4	0	30	50	0.53	5.00
6	0	0	50	0.89	5.53	6	0	15	50	0.78	5.00	6	0	30	50	0.66	5.00
8	0	0	50	1.09	5.00	8	0	15	50	0.94	5.00	8	0	30	50	0.77	5.00
4	0	0	100	0.85	9.54	4	0	15	100	0.76	8.02	4	0	30	100	0.64	5.00
6	0	0	100	1.17	14.98	6	0	15	100	1.00	13.99	6	0	30	100	0.82	11.20
8	0	0	100	1.51	13.85	8	0	15	100	1.24	13.85	8	0	30	100	0.97	12.57
4	0	0	150	0.98	14.03	4	0	15	150	0.86	14.03	4	0	30	150	0.72	10.05
6	0	0	150	1.39	20.57	6	0	15	150	1.16	19.47	6	0	30	150	0.92	16.75
8	0	0	150	1.80	18.94	8	0	15	150	1.43	20.19	8	0	30	150	1.07	20.19
4	10	0	50	0.85	11.69	4	10	15	50	0.77	9.99	4	10	30	50	0.66	6.55
6	10	0	50	1.07	10.17	6	10	15	50	0.95	8.96	6	10	30	50	0.80	5.54
8	10	0	50	1.29	9.55	8	10	15	50	1.11	9.55	8	10	30	50	0.91	6.80
4	10	0	100	1.02	14.94	4	10	15	100	0.92	12.99	4	10	30	100	0.78	9.06
6	10	0	100	1.36	19.06	6	10	15	100	1.17	18.68	6	10	30	100	0.96	15.82
8	10	0	100	1.71	18.04	8	10	15	100	1.42	18.85	8	10	30	100	1.09	17.60
4	10	0	150	1.16	19.88	4	10	15	150	1.02	18.36	4	10	30	150	0.86	15.14
6	10	0	150	1.58	24.31	6	10	15	150	1.33	24.12	6	10	30	150	1.05	21.51
8	10	0	150	2.02	22.83	8	10	15	150	1.61	24.12	8	10	30	150	1.16	25.41
4	20	0	50	1.03	17.52	4	20	15	50	0.95	15.76	4	20	30	50	0.82	12.02
6	20	0	50	1.28	15.63	6	20	15	50	1.14	14.81	6	20	30	50	0.96	11.73
8	20	0	50	1.51	14.70	8	20	15	50	1.31	14.34	8	20	30	50	1.06	11.86
4	20	0	100	1.22	19.97	4	20	15	100	1.10	18.36	4	20	30	100	0.94	19.27
6	20	0	100	1.57	23.80	6	20	15	100	1.36	22.32	6	20	30	100	1.10	20.84
8	20	0	100	1.94	21.79	8	20	15	100	1.61	23.01	8	20	30	100	1.19	23.01
4	20	0	150	1.37	24.72	4	20	15	150	1.21	23.15	4	20	30	150	1.02	19.97
6	20	0	150	1.80	28.17	6	20	15	150	1.52	28.17	6	20	30	150	1.17	26.72
8	20	0	150	2.26	24.36	8	20	15	150	1.79	28.39	8	20	30	150	1.21	24.36

shows that the calculations were made for 81 different combinations of design data.

4.2 ANFIS STRUCTURE

For a Sugeno fuzzy model ANFIS-SF, a rule set with n fuzzy “If-then” is as follows:

Rule 1: If l is $In1MF_1$ and α is $In2MF_1$ and β is $In3MF_1$ and d is $In4MF_1$ then

$$SF_1 = k_1^1 \cdot l + k_2^1 \cdot \alpha + k_3^1 \cdot \beta + k_4^1 \cdot d + k_0^1 \quad (14)$$

Rule 2: If l is $In1MF_2$ and α is $In2MF_2$ and β is $In3MF_2$ and d is $In4MF_2$ then

$$SF_2 = k_1^2 \cdot l + k_2^2 \cdot \alpha + k_3^2 \cdot \beta + k_4^2 \cdot d + k_0^2 \quad (15)$$

where $k_0^1, k_1^1, k_2^1, k_3^1, k_4^1, k_0^2, k_1^2, k_2^2, k_3^2, k_4^2$ are the consequent parameters and l, α, β and d are the input variables. The sign $In1MF_1$ stands for the membership function 1 in input 1. The output of each rule is equal to a constant and the final output is the weighted average of each rule's output.

$$SF = \sum_{i=1}^n \bar{w}_i \cdot SF_i \quad (16)$$

$$\eta_{opt} = \sum_{i=1}^n \bar{w}_i \cdot \eta_{opt,i} \quad (17)$$

The weights are obtained from the Gaussian membership function.

$$\mu_A(x) = \exp \left[- \left(\frac{x-c}{\sqrt{2} \sigma} \right)^2 \right] \quad (18)$$

where c is the position of the centre of the curve's peak and σ is the width of the curve. The parameters c and σ are the premise parameters. The first membership grade of a fuzzy set ($In1MF_i, In2MF_i, In3MF_i, In4MF_i$) is calculated with the following equations:

$$\mu_{In1MF_i}(l) = \exp \left[- \left(\frac{l - c_{In1MF_i}}{\sqrt{2} \sigma_{In1MF_i}} \right)^2 \right] \quad (19)$$

$$\mu_{In2MF_i}(\alpha) = \exp \left[- \left(\frac{\alpha - c_{In2MF_i}}{\sqrt{2} \sigma_{In2MF_i}} \right)^2 \right] \quad (20)$$

$$\mu_{In3MF_i}(\beta) = \exp \left[- \left(\frac{\beta - c_{In3MF_i}}{\sqrt{2} \sigma_{In3MF_i}} \right)^2 \right] \quad (21)$$

$$\mu_{In4MF_i}(d) = \exp \left[- \left(\frac{d - c_{In4MF_i}}{\sqrt{2} \sigma_{In4MF_i}} \right)^2 \right] \quad (22)$$

where l, α, β and d are the inputs to the Gaussian membership function. Next, the product of the membership function for every rule is calculated:

$$w_i = \mu_{In1MF_i}(l) \cdot \mu_{In2MF_i}(\alpha) \cdot \mu_{In3MF_i}(\beta) \cdot \mu_{In4MF_i}(d) \quad (23)$$

where w_i represents the fire strength of the rule i . The ratio of the i^{th} rule's firing strength to the sum of all the rules' firing strengths is defined with:

$$\bar{w}_i = \frac{w_i}{w_1 + \dots + w_i + \dots + w_n}, \text{ for } i = 1, 2, \dots, n. \quad (24)$$

The input data represents a node on the left, and the right node represents the output data (Fig. 4).

In order to achieve the desired input-output mapping, the consequent and premise parameters are updated according to the given training data (Table 4) and the hybrid learning procedure. This hybrid learning procedure [25] is composed of a forward pass and a backward pass. In the forward pass, the algorithm uses the least-squares method to identify the consequent parameters. In the backward pass the errors are propagated backwards and the premise parameters are updated with the gradient descent. The premise (σ_i, c_i) and the consequent (k_i) parameters of the ANFIS-SF model and ANFIS-INC model are given in Table 5. By setting the premise and consequent parameters, the space of four variables is described.

4.3 TESTING THE ANFIS MODELS

To test and validate the ANFIS models, a data set was selected that was not used during the training of the network (Table 6).

The coefficient of determination (R-square) and the root-mean-squared error (RMSE) between the predicted and the calculated values is taken as a measure of the performance. The calculated and predicted safety factors SFs for the model ANFIS-SF are shown in Fig. 5.

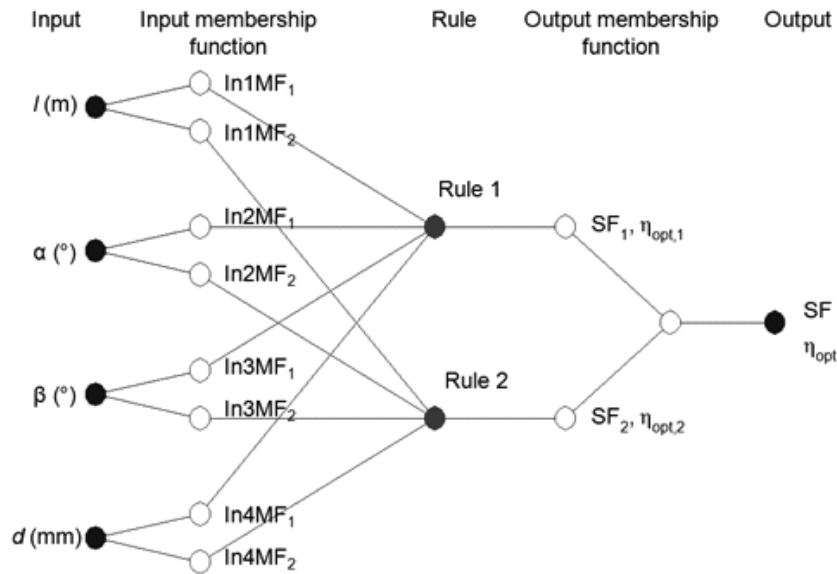


Figure 4. Structure of ANFIS-SF and ANFIS-INC model.

Table 5. The premise and consequent parameter for the ANFIS-SF and ANFIS-INC model.

ANFIS-SF	In1MF ₁	In1MF ₂	In2MF ₁	In2MF ₂	In3MF ₁	In3MF ₂	In4MF ₁	In4MF ₂
<i>c</i>	3.229	10.554	11.334	14.691	16.367	5.660	61.041	109.767
<i>σ</i>	2.523	11.309	11.792	17.988	18.558	9.861	48.925	136.300
	<i>k</i> ₁	<i>k</i> ₂	<i>k</i> ₃	<i>k</i> ₄	<i>k</i> ₀			
Rule 1	0.022	0.015	-0.005	0.001	0.485			
Rule 2	-0.090	-0.006	-0.082	-0.002	5.079			
ANFIS-INC	In1MF ₁	In1MF ₂	In2MF ₁	In2MF ₂	In3MF ₁	In3MF ₂	In4MF ₁	In4MF ₂
<i>c</i>	2.488	7.787	12.256	5.282	17.411	21.318	43.831	99.530
<i>σ</i>	2.572	5.583	11.995	4.191	18.402	25.186	54.367	50.416
	<i>k</i> ₁	<i>k</i> ₂	<i>k</i> ₃	<i>k</i> ₄	<i>k</i> ₀			
Rule 1	-6.552	0.175	0.199	0.004	86.382			
Rule 2	-3.885	0.449	-0.058	-0.355	27.041			

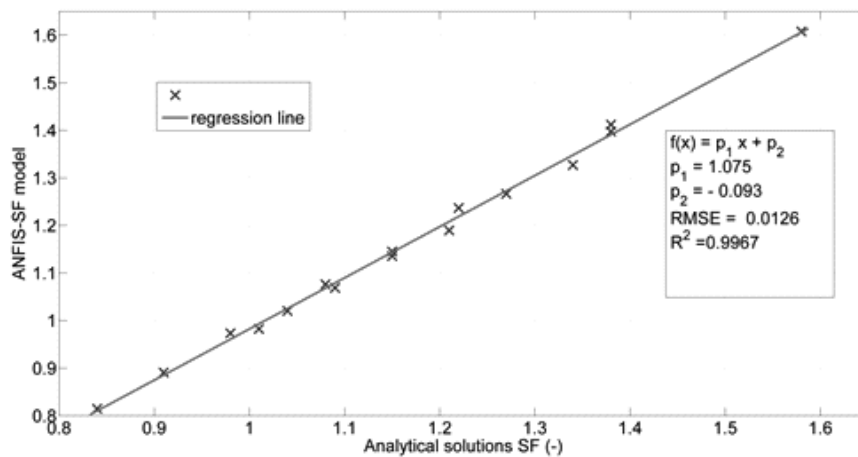


Figure 5. Calculated versus predicted safety factor *SF*.

Table 6. Testing data compared to ANFIS models.

l (m)	α (°)	β (°)	d (mm)	SF (-)	ANFIS-SF (-)	Error (%)	OPTINC (°)	ANFIS-INC (°)	Error (%)
5	5	10	75	0.91	0.89	2.1	11.1	10.2	8.1
7	5	10	75	1.15	1.14	1.2	12.0	12.3	2.8
5	5	10	125	1.08	1.08	0.3	16.2	17.8	10.0
7	5	10	125	1.38	1.41	2.3	19.1	20.6	7.9
5	15	10	75	1.09	1.07	1.9	17.3	15.2	12.1
7	15	10	75	1.34	1.33	1.0	17.0	16.8	1.1
5	15	10	125	1.27	1.27	0.3	21.7	22.7	4.6
7	15	10	125	1.58	1.61	1.8	23.7	24.6	3.7
5	5	20	75	0.84	0.81	3.0	10.1	8.9	11.5
7	5	20	75	1.04	1.02	1.9	12.0	11.5	4.0
5	5	20	125	0.98	0.97	0.7	15.5	16.6	6.9
7	5	20	125	1.22	1.24	1.4	18.7	20.3	8.2
5	15	20	75	1.01	0.98	2.7	14.5	14.0	3.4
7	15	20	75	1.21	1.19	1.7	16.9	16.1	4.6
5	15	20	125	1.15	1.15	0.4	23.4	21.6	8.0
7	15	20	125	1.38	1.40	1.3	23.9	24.4	1.8

The comparison between the optimal inclination of the soil nail calculated with the optimization model OPTINC and the ANFIS-INC model is shown in Fig. 6.

The higher coefficient of determination means that the correlation between the monitored and predicted data is high; it does not mean that the monitored data are close to the predicted data. To estimate the error of each model we used RMSE.

5 DISCUSSION

The presented ANFIS models are able to predict the safety factor SF (-) and the optimal inclination of the soil nails η (°) for different inclinations of the wall α (°), the slope angle of the terrain β (°), the length of the nails l (m) and the hole diameter d (mm). Fig. 7 shows the safety factor depending on the length of the soil nails and the inclination of the wall. With increasing inclination of

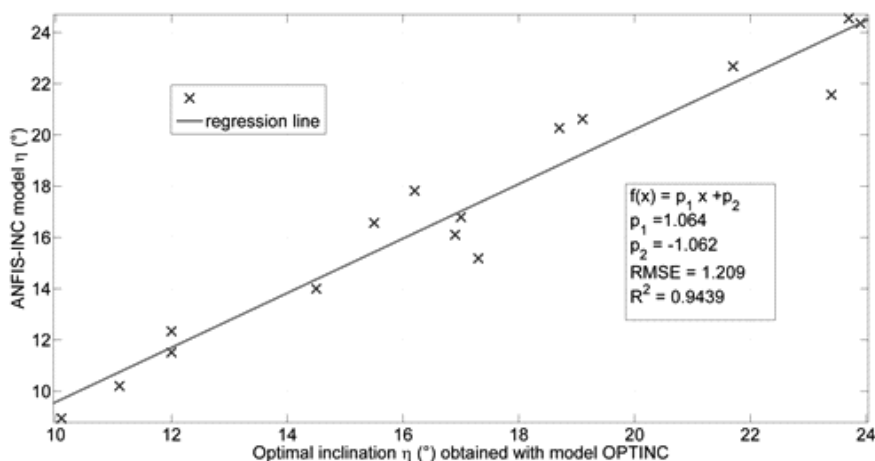


Figure 6. Calculated versus predicted optimal inclination of soil nails η .

the wall, the length of the soil nail and the hole diameter, the safety factor is increasing. On the other hand, the safety factor is decreasing with the increasing slope angle of the terrain. The larger hole diameter increases the pull-out resistance; therefore, the safety factor is larger.

Fig. 8 shows the optimal inclination of the soil nails depending on the length of the soil nails and the inclination of the wall. With increasing inclination of the wall, the optimal inclination of the soil nails increases. The lengths of the soil nails have a small influence on the optimal inclination of the soil nail in comparison with the inclination of the wall.

6 CONCLUSIONS

The paper presents the safety-factor optimization for a soil-nail wall. The optimization is performed using

the non-linear programming (NLP) approach. For this purpose, the NLP optimization model OPTINC was developed. The model comprises the safety-factor objective function, which is subjected to geo-mechanical and design constraints. As the model was developed in a general form, the optimization of the system can be performed for different heights of the wall, spacings of the nails as well as for different soil environments. The output of the OPTINC model is an optimal inclination of the soil nails.

The safety factor and the optimal inclination of the soil nails from the horizontal direction depends on the design of the soil-nail wall. Therefore, the safety factor SF (-) and the optimal inclination of the nails η ($^{\circ}$) were calculated for different inclinations of the wall α ($^{\circ}$), the slope angle of the terrain β ($^{\circ}$), the length of the nails l (m) and the hole diameter d (mm). Based on these results two ANFIS models were developed. The ANFIS-

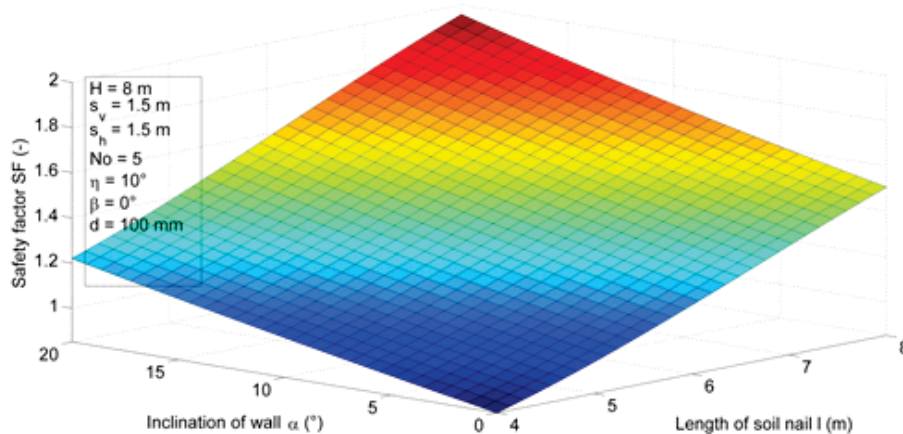


Figure 7. Graphical representation of ANFIS-SF model for safety-factor prediction.

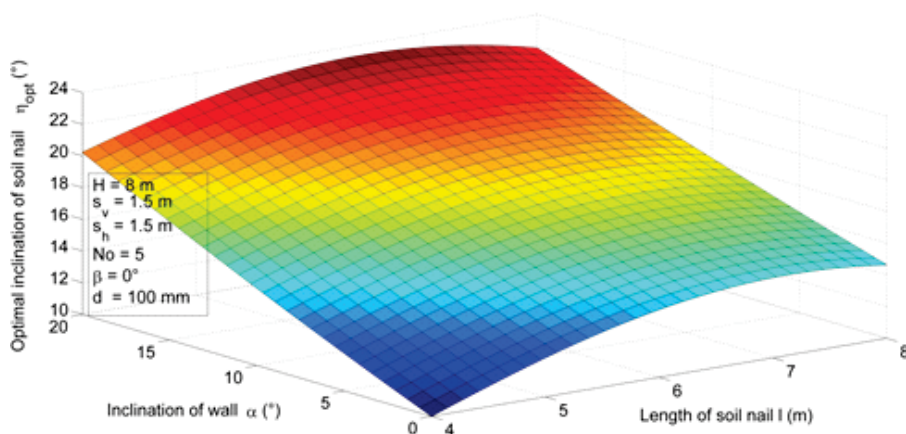


Figure 8. Graphical representation of ANFIS-INC model for the optimal inclination of the soil-nail prediction.

SF model is used to predict the SF factor and the ANFIS-INC model is used to predict the optimal inclination of the nails for different design data.

In the present study only a plane slip surface is used to calculate the internal stability, while other types of slip surface, such as a broken slip surface, parabolic slip surface, circular slip surface and logarithmic spiral slip surface, should also be calculated. It was found that the inclination of soil nail should be adjusted to the inclination of the wall, the length of the nail, the slope angle of the terrain and the hole diameter.

REFERENCES

- [1] Rabcewicz, L.V. (1964). The New Austrian Tunneling Method. Part 1, *Water Power*, Vol. 16, pp 453-457.
- [2] Rabcewicz, L.V. (1964). The New Austrian Tunneling Method. Part 2, *Water Power*, Vol. 16, pp 511-515.
- [3] Rabcewicz, L.V. (1965). The New Austrian Tunneling Method. Part 3, *Water Power*, Vol. 17, pp 19-24.
- [4] Rabejac, S., Toudic, P. (1974). Construction d'un mur de soutènement entre Versailles-Chantiers et Versailles-Matelots. Trans.: Construction of a retaining wall between Versailles-Chantiers and Versailles-Matelots, *Revue générale des chemins de fer*, Vol. 93, pp. 232-237.
- [5] Schlosser, F. (1983). Analogies et différences dans le comportement et le calcul des ouvrages de soutènement en Terre Armée et par clouage des sols. (Trad.: Similarities and differences in the behavior and design of retaining structures of reinforced earth and soil nailing). *Annales de L'Institut Technique de Batiment et des Travaux Publics*, No. 418, Series: Sols et Fondations.
- [6] Schlosser, F. (1991). Soil nailing recommendations for designing, calculating, constructing and inspecting earth support systems using soil nailing. US Department of transportation, Federal highway administration, Washington, D.C.
- [7] Stocker, M.F., Korber, G.W., Gässler, G., Gudehus, G. (1979). Soil Nailing. *International Conference on Soil Reinforcement I*, Vol. 2, pp. 469-474.
- [8] Gässler, G., Gudehus, G., (1981). Soil Nailing-Some Aspects of a New Technique. *10th International Conference on Soil Mechanics and Foundation Engineering*, Vol. 3., pp. 665-670.
- [9] Schlosser, F. and Unterreiner, P. (1990). Soil Nailing in France: Research and Practice. *Proceeding of 1st International Seminar on Soil Mechanics and Foundation Engineering of Iran*, Iran, pp. 436-468.
- [10] Byrne, R.J., Cotton, D., Porterfield, J., Wolschlag, C., Ueblacker, G. (1998). Manual for Design and Construction Monitoring of Soil Nail Walls. Report FHWA-SA-96-69R, Federal Highway Administration, Washington, D.C.
- [11] Lazarte, C.A., Elias, V., Espinoza, R.D., Sabatini, P.J. (2003). Geotechnical engineering circular No. 7 Soil Nail Walls. Report FHWA0-IF-03-017, Federal Highway Administration, Washington, D.C.
- [12] Faravelli, L., Yao, T., (1996). Use of Adaptive Networks in Fuzzy Control of Civil Structures. *Computer-Aided Civil and Infrastructure Engineering*, Vol. 11, No. 1, pp. 67-76.
- [13] Provenzano, P., Ferlisi, S., Musso, A. (2004). Interpretation of a model footing response through an adaptive neural fuzzy inference system. *Comput. and Geotech.*, Vol 31, No. 3, pp. 251-266.
- [14] Gokceoglu, C., Yesilnacar, E., Sonmez, H., Kaya-basi, A.A. (2004). A Neuro-fuzzy model for modulus of deformation of jointed rock masses. *Comput. and Geotech.*, Vol. 31, No. 5, pp. 375-383
- [15] Rangel, J.L., Iturraran-Viveros, U., Ayala, A.G., Cervantes, F. (2005). Tunnel stability analysis during construction using a neuro-fuzzy system. *Int. J. Numer. and Anal. Methods. in Geomech.*, Vol. 29, No. 15, pp. 1433-1456.
- [16] Kayadelen, C., Gunaydin, O., Fener, M., Demir, A., Ozvan A. (2009). Modeling of the angle of shearing resistance of soils using soft computing systems. *Expert Syst. with Appl.*, Vol. 36, No. 9, pp. 11814-11826.
- [17] Žlender B., Jelušič P., Boumezerane D. (2013). The feasibility analysis of underground gas storage caverns. *Eng. Struct.*, Available online 1 March 2013.
- [18] Goh, A. T. C., Wong, K. S., Broms, B. B. (1995). Estimation of lateral wall movements in braced excavation using neural networks. *Canadian Geotech. J.*, Vol. 32, No. 6, pp. 1059-1064.
- [19] Tuozzolo, T.J. (2003). Soil nailing: where, when and why – a practical guide. *Presented at the 20th Central Pennsylvania Geotechnical Conference*, Hershey, PA, 2003.
- [20] Sabatini, P.J. (1999). Ground Anchors and Anchored Systems, Geotechnical Engineering Circular No. 4, Publication FHWA-IF-99-015, Federal Highway Administration, Washington, D.C.
- [21] Žlender, B., Trauner, L., Lenart, S. (2011). The response modeling of the dynamically loaded silty sand. *13th International conference of the International Association for Computer Methods and Advances in Geomechanics (IACMAG)*, Melbourne, Australia. pp. 608-613.

- [22] Vrecl-Kojc, H., Trauner, L. (2010). Upper-bound approach for analysis of cantilever retaining walls. *Can. Geotech. J.*, Vol. 47, No. 9, pp. 999-1010.
- [23] Vrecl-Kojc, H. (2005). The anchored pile wall optimization using NLP approach. *Acta geotech. Slov.*, Vol. 2, No. 2, pp. 5-11.
- [24] Zadeh, L. (1965). Fuzzy sets. *Information and Control*, Vol.8, No. 3, pp. 338-353.
- [25] Jang, J.S.R. (1993). ANFIS: Adaptive-Network-Based Fuzzy Inference System. *IEEE Transactions on Systems, Man and Cybernetics*, Vol. 23, No. 3, pp. 665-685.
- [26] Sugeno, M. (1985). Industrial applications of fuzzy control. Elsevier Science pub. Co., Amsterdam.
- [27] Rumelhart, D.G. (1986). Learning representations by back-propagating errors. *Nature*, Vol. 323. pp. 533-536.

NAVODILA AVTORJEM

VSEBINA ČLANKA

Članek naj bo napisan v naslednji obliki:

- Naslov, ki primerno opisuje vsebino članka in ne presega 80 znakov.
- Izvleček, ki naj bo skrajšana oblika članka in naj ne presega 250 besed. Izvleček mora vsebovati osnove, jedro in cilje raziskave, uporabljeno metodologijo dela, povzetek izidov in osnovne sklepe.
- Največ 6 ključnih besed, ki bi morale biti napisane takoj po izvlečku.
- Uvod, v katerem naj bo pregled novejšega stanja in zadostne informacije za razumevanje ter pregled izidov dela, predstavljenih v članku.
- Teorija.
- Eksperimentalni del, ki naj vsebuje podatke o postavitvi preiskusa in metode, uporabljene pri pridobitvi izidov.
- Izidi, ki naj bodo jasno prikazani, po potrebi v obliki slik in preglednic.
- Razprava, v kateri naj bodo prikazane povezave in posplošitve, uporabljene za pridobitev izidov. Prikazana naj bo tudi pomembnost izidov in primerjava s poprej objavljenimi deli.
- Sklepi, v katerih naj bo prikazan en ali več sklepov, ki izhajajo iz izidov in razprave.
- Vse navedbe v besedilu morajo biti na koncu zbrane v seznamu literature, in obratno.

Dodatne zahteve

- Vrstice morajo biti zaporedno oštevilčene.
- Predložen članek ne sme imeti več kot 18 strani (brez tabel, legend in literature); velikost črk 12, dvojni razmik med vrsticami. V članek je lahko vključenih največ 10 slik. Isti rezultati so lahko prikazani v tabelah ali na slikah, ne pa na oba načina.
- Potrebno je priložiti imena, naslove in elektronske naslove štirih potencialnih recenzentov članka. Urednik ima izključno pravico do odločitve, ali bo te predloge upošteval.

ENOTE IN OKRAJŠAVE

V besedilu, preglednicah in slikah uporabljajte le standardne označbe in okrajšave SI. Simbole fizikalnih veličin v besedilu pišite poševno (npr. v , T itn.). Simbole enot, ki so sestavljene iz črk, pa pokončno (npr. Pa, m itn.). Vse okrajšave naj bodo, ko se prvič pojavijo, izpisane v celoti.

SLIKE

Slike morajo biti zaporedno oštevilčene in označene, v besedilu in podnaslovu, kot sl. 1, sl. 2 itn. Posnete naj

bodo v katerem koli od razširjenih formatov, npr. BMP, JPG, GIF. Za pripravo diagramov in risb priporočamo CDR format (CorelDraw), saj so slike v njem vektorske in jih lahko pri končni obdelavi preprosto povečujemo ali pomanjšujemo.

Pri označevanju osi v diagramih, kadar je le mogoče, uporabite označbe veličin (npr. v , T itn.). V diagramih z več krivuljami mora biti vsaka krivulja označena. Pomen oznake mora biti razložen v podnaslovu slike.

Za vse slike po fotografskih posnetkih je treba priložiti izvirne fotografije ali kakovostno narejen posnetek.

PREGLEDNICE

Preglednice morajo biti zaporedno oštevilčene in označene, v besedilu in podnaslovu, kot preglednica 1, preglednica 2 itn. V preglednicah ne uporabljajte izpisanih imen veličin, ampak samo ustrezne simbole. K fizikalnim količinam, npr. t (pisano poševno), pripišite enote (pisano pokončno) v novo vrsto brez oklepajev. Vse opombe naj bodo označene z uporabo dvignjene številke¹.

SEZNAM LITERATURE

navedba v besedilu

Vsaka navedba, na katero se sklicujete v besedilu, mora biti v seznamu literature (in obratno). Neobjavljeni rezultati in osebne komunikacije se ne priporočajo v seznamu literature, navedejo pa se lahko v besedilu, če je nujno potrebno.

oblika navajanja literature

V besedilu: Navedite reference zaporedno po številkah v oglatih oklepajih v skladu z besedilom. Dejanski avtorji so lahko navedeni, vendar mora obvezno biti podana referenčna številka.

Primer: »..... kot je razvidno [1,2]. Brandl and Blovsky [4], sta pridobila drugačen rezultat...«

V seznamu: Literaturni viri so oštevilčeni po vrstnem redu, kakor se pojavijo v članku. Označimo jih s številkami v oglatih oklepajih.

Sklicevanje na objave v revijah:

- [1] Desai, C.S. (2007). Unified DSC constitutive model for pavement materials with numerical implementation. *Int. J. of Geomech.*, Vol. 7, No. 2, pp. 83-101.

Sklicevanje na knjigo:

- [2] Šuklje, L. (1969). Rheological aspects of soil mechanics. Wiley-Interscience, London

Sklicevanje na poglavje v monografiji:

- [3] Mettam, G.R., Adams, L.B., 1999. How to prepare an electronic version of your article, in: Jones, B.S., Smith, R.Z. (Eds.), *Introduction to the Electronic Age*. E-Publishing Inc., New York, pp. 281–304.

Sklicevanje na objave v zbornikih konferenc:

- [4] Brandl, H. and Blovsky, S. (2005). Slope stabilization with socket walls using the observational method. *Proc. Int. conf. on Soil Mechanics and Geotechnical Engineering, Bratislava*, pp. 2485-2488.

Sklicevanje na spletne objave:

- [5] Kot najmanj, je potrebno podati celoten URL. Če so poznani drugi podatki (DOI, imena avtorjev, datumi, sklicevanje na izvirno literaturo), se naj prav tako dodajo.

PODATKI O AVTORJIH

Članku priložite tudi podatke o avtorjih: imena, nazive, popolne poštno naslove, številke telefona in faksa,

naslove elektronske pošte. Navedite kontaktno osebo.

SPREJEM ČLANKOV IN AVTORSKE PRAVICE

Uredništvo si pridržuje pravico do odločanja o sprejemu članka za objavo, strokovno oceno mednarodnih recenzentov in morebitnem predlogu za krajšanje ali izpopolnitev ter terminološke in jezikovne korekture. Z objavo preidejo avtorske pravice na revijo ACTA GEOTECHNICA SLOVENICA. Pri morebitnih kasnejših objavah mora biti AGS navedena kot vir.

Vsa nadaljnja pojasnila daje:

Uredništvo
ACTA GEOTECHNICA SLOVENICA
Univerza v Mariboru,
Fakulteta za gradbeništvo
Smetanova ulica 17, 2000 Maribor, Slovenija
E-pošta: ags@uni-mb.si

INSTRUCTIONS FOR AUTHORS

FORMAT OF THE PAPER

The paper should have the following structure:

- A Title, which adequately describes the content of the paper and should not exceed 80 characters;
- An Abstract, which should be viewed as a mini version of the paper and should not exceed 250 words. The Abstract should state the principal objectives and the scope of the investigation and the methodology employed; it should also summarise the results and state the principal conclusions;
- Immediately after the abstract, provide a maximum of 6 keywords;
- An Introduction, which should provide a review of recent literature and sufficient background information to allow the results of the paper to be understood and evaluated;
- A Theoretical section;
- An Experimental section, which should provide details of the experimental set-up and the methods used to obtain the results;
- A Results section, which should clearly and concisely present the data, using figures and tables where appropriate;
- A Discussion section, which should describe the relationships shown and the generalisations made possible by the results and discuss the significance of the results, making comparisons with previously published work;

- Conclusions, which should present one or more conclusions that have been drawn from the results and subsequent discussion;
- A list of References, which comprises all the references cited in the text, and vice versa.

Additional requirements for manuscripts

- Use double line-spacing.
- Insert continuous line numbering.
- The submitted text of Research Papers should cover no more than 18 pages (without Tables, Legends, and References, style: font size 12, double line spacing). The number of illustrations should not exceed 10. Results may be shown in tables or figures, but not in both of them.
- Please submit, with the manuscript, the names, addresses and e-mail addresses of four potential referees. Note that the editor retains the sole right to decide whether or not the suggested reviewers are used.

UNITS AND ABBREVIATIONS

Only standard SI symbols and abbreviations should be used in the text, tables and figures. Symbols for physical quantities in the text should be written in *Italics* (e.g. *v*, *T*, etc.). Symbols for units that consist of letters should be in plain text (e.g. Pa, m, etc.).

All abbreviations should be spelt out in full on first appearance.

FIGURES

Figures must be cited in consecutive numerical order in the text and referred to in both the text and the caption as Fig. 1, Fig. 2, etc. Figures may be saved in any common format, e.g. BMP, JPG, GIF. However, the use of CDR format (CorelDraw) is recommended for graphs and line drawings, since vector images can be easily reduced or enlarged during final processing of the paper.

When labelling axes, physical quantities (e.g. v , T , etc.) should be used whenever possible. Multi-curve graphs should have individual curves marked with a symbol; the meaning of the symbol should be explained in the figure caption. Good quality black-and-white photographs or scanned images should be supplied for the illustrations.

TABLES

Tables must be cited in consecutive numerical order in the text and referred to in both the text and the caption as Table 1, Table 2, etc. The use of names for quantities in tables should be avoided if possible: corresponding symbols are preferred. In addition to the physical quantity, e.g. t (in Italics), units (normal text), should be added on a new line without brackets.

Any footnotes should be indicated by the use of the superscript¹.

LIST OF REFERENCES

citation in text

Please ensure that every reference cited in the text is also present in the reference list (and vice versa). Any references cited in the abstract must be given in full. Unpublished results and personal communications are not recommended in the reference list, but may be mentioned in the text, if necessary.

reference style

Text: Indicate references by number(s) in square brackets consecutively in line with the text. The actual authors can be referred to, but the reference number(s) must always be given:

Example: "... as demonstrated [1,2]. Brandl and Blovsky [4] obtained a different result ..."

List: Number the references (numbers in square brackets) in the list in the order in which they appear in the text.

Reference to a journal publication:

- [1] Desai, C.S. (2007). Unified DSC constitutive model for pavement materials with numerical implementation. *Int. J. of Geomech.*, Vol. 7, No. 2, pp. 83-101.

Reference to a book:

- [2] Šuklje, L. (1969). Rheological aspects of soil mechanics. Wiley-Interscience, London

Reference to a chapter in an edited book:

- [3] Mettam, G.R., Adams, L.B. (1999). How to prepare an electronic version of your article, in: Jones, B.S., Smith, R.Z. (Eds.), *Introduction to the Electronic Age*. E-Publishing Inc., New York, pp. 281–304.

Conference proceedings

- [4] Brandl, H. and Blovsky, S. (2005). Slope stabilization with socket walls using the observational method. *Proc. Int. conf. on Soil Mechanics and Geotechnical Engineering, Bratislava*, pp. 2485-2488.

Web references:

- [5] As a minimum, the full URL should be given and the date when the reference was last accessed. Any further information, if known (DOI, author names, dates, reference to a source publication, etc.), should also be given.

AUTHOR INFORMATION

The following information about the authors should be enclosed with the paper: names, complete postal addresses, telephone and fax numbers and E-mail addresses. Indicate the name of the corresponding author.

ACCEPTANCE OF PAPERS AND COPYRIGHT

The Editorial Committee of the Slovenian Geotechnical Review reserves the right to decide whether a paper is acceptable for publication, to obtain peer reviews for the submitted papers, and if necessary, to require changes in the content, length or language.

On publication, copyright for the paper shall pass to the ACTA GEOTECHNICA SLOVENICA. The AGS must be stated as a source in all later publication.

For further information contact:

Editorial Board
ACTA GEOTECHNICA SLOVENICA
University of Maribor,
Faculty of Civil Engineering
Smetanova ulica 17, 2000 Maribor, Slovenia
E-mail: ags@uni-mb.si

NAMEN REVIJE

Namen revije ACTA GEOTECHNICA SLOVENICA je objavljavanje kakovostnih teoretičnih člankov z novih pomembnih področij geomehanike in geotehnike, ki bodo dolgoročno vplivali na temeljne in praktične vidike teh področij.

ACTA GEOTECHNICA SLOVENICA objavlja članke s področij: mehanika zemljin in kamnin, inženirska geologija, okoljska geotehnika, geosintetika, geotehnične konstrukcije, numerične in analitične metode, računalniško modeliranje, optimizacija geotehničnih konstrukcij, terenske in laboratorijske preiskave.

Revija redno izhaja dvakrat letno.

AVTORSKE PRAVICE

Ko uredništvo prejme članek v objavo, prosi avtorja(je), da prenese(jo) avtorske pravice za članek na izdajatelja, da bi zagotovili kar se da obsežno razširjanje informacij. Naša revija in posamezni prispevki so zaščiteni z avtorskimi pravicami izdajatelja in zanje veljajo naslednji pogoji:

fotokopiranje

V skladu z našimi zakoni o zaščiti avtorskih pravic je dovoljeno narediti eno kopijo posameznega članka za osebno uporabo. Za naslednje fotokopije, vključno z večkratnim fotokopiranjem, sistematičnim fotokopiranjem, kopiranjem za reklamne ali predstavitvene namene, nadaljnjo prodajo in vsemi oblikami nedobičkonosne uporabe je treba pridobiti dovoljenje izdajatelja in plačati določen znesek.

Naročniki revije smejo kopirati kazalo z vsebino revije ali pripraviti seznam člankov z izvlečki za rabo v svojih ustanovah.

elektronsko shranjevanje

Za elektronsko shranjevanje vsakršnega gradiva iz revije, vključno z vsemi članki ali deli članka, je potrebno dovoljenje izdajatelja.

ODGOVORNOST

Revija ne prevzame nobene odgovornosti za poškodbe in/ali škodo na osebah in na lastnini na podlagi odgovornosti za izdelke, zaradi malomarnosti ali drugače, ali zaradi uporabe kakršnekoli metode, izdelka, navodil ali zamisli, ki so opisani v njej.

AIMS AND SCOPE

ACTA GEOTECHNICA SLOVENICA aims to play an important role in publishing high-quality, theoretical papers from important and emerging areas that will have a lasting impact on fundamental and practical aspects of geomechanics and geotechnical engineering.

ACTA GEOTECHNICA SLOVENICA publishes papers from the following areas: soil and rock mechanics, engineering geology, environmental geotechnics, geosynthetic, geotechnical structures, numerical and analytical methods, computer modelling, optimization of geotechnical structures, field and laboratory testing.

The journal is published twice a year.

COPYRIGHT

Upon acceptance of an article by the Editorial Board, the author(s) will be asked to transfer copyright for the article to the publisher. This transfer will ensure the widest possible dissemination of information. This review and the individual contributions contained in it are protected by publisher's copyright, and the following terms and conditions apply to their use:

photocopying

Single photocopies of single articles may be made for personal use, as allowed by national copyright laws. Permission of the publisher and payment of a fee are required for all other photocopying, including multiple or systematic copying, copying for advertising or promotional purposes, resale, and all forms of document delivery.

Subscribers may reproduce tables of contents or prepare lists of papers, including abstracts for internal circulation, within their institutions.

electronic storage

Permission of the publisher is required to store electronically any material contained in this review, including any paper or part of the paper.

RESPONSIBILITY

No responsibility is assumed by the publisher for any injury and/or damage to persons or property as a matter of product liability, negligence or otherwise, or from any use or operation of any methods, products, instructions or ideas contained in the material herein.